MODELING OF PIPE FRICTION AND SMEAR EFFECT IN DRILLING OPERATIONS

A Thesis

Presented to

the Faculty of the Department of Chemical Engineering

University of Houston

In Partial Fulfillment

of the Requirements for the Degree

Master of Science

in Petroleum Engineering

by

Aniket

August 2012

MODELING OF PIPE FRICTION AND SMEAR EFFECT IN DRILLING OPERATIONS

Aniket

Approved:

Chair of the Committee,
Dr. Michael Nikolaou, Professor,
Chemical and Biomolecular Engineering.

Committee Members:

Dr. Robello Samuel, Adjunct Professor,
Petroleum Engineering.

Dr. Gangbing Song, Professor,
Mechanical Engineering.

Dr. Suresh K. Khator,
Associate Dean,
Cullen College of Engineering.

Dr. Ramanan Krishnamoorti,
Professor and Chair,
Chemical and Biomolecular Engineering.

ACKNOWLEDGEMENTS

I would like to sincerely thank my advisor Dr. Robello Samuel, for providing strong support and motivation throughout the project that kept me always excited and enthusiastic towards this study. His practical approach to current industry problems and continuous guidance helped me immensely as I worked my way through the topics under investigation and has led to my all around development as a research student as well as a technical writer and speaker.

I would like to thank my thesis committee comprising of Dr. Michael Nikolaou and Dr. Gangbing Song for their suggestions on this study. I also really appreciate the continuous help and guidance provided by Dr. Tom Holley and Ms. Anne Sturm throughout my program at the University of Houston. Finally, I would like to express my deepest gratitude towards my family and friends for their continuous encouragement and support in all my endeavors.

MODELING OF PIPE FRICTION AND SMEAR EFFECT IN DRILLING OPERATIONS

An Abstract

of a

Thesis

Presented to

the Faculty of the Department of Chemical Engineering

University of Houston

In Partial Fulfillment

of the Requirements for the Degree

Master of Science

in Petroleum Engineering

by

Aniket

August 2012

ABSTRACT

The increased complexity of drilling programs has led to the development of new drilling techniques and has resulted in problems that were not encountered before. This study focuses on two such issues: 1) to model the influence of wellbore friction on downhole temperatures of the drilling fluid, 2) to understand the smear effect mechanism observed in a casing while drilling operation through mathematical studies.

An analytical model has been proposed to estimate the increase in downhole wellbore temperatures during a drilling activity and subsequently validated for a deviated and a horizontal well using real-time data measured in the field. The contribution of wellbore temperatures and plugging of micro-fractures towards improving the fracture gradient of the formation has then been analyzed using quantitative studies aiming to provide a physical insight into the smear effect mechanism. Various parametric analyses have also been presented to help optimize future drilling programs.

TABLE OF CONTENTS

LIST OF FIGURES

NOMENCLATURE

N = Normal force on the drill string in a curved section of the wellbore

μ = Coefficient of friction

r_o = Outer radius of drill string

r_p = Average radius of drill string

r_i = Inner radius of drill string

r_w = Radius of the wellbore

θ_1 = Inclination angle over which the drill string comes in contact with the wall

θ_2 = Inclination angles over which the drill string loses contact with the wall

θ_{avg} = Average inclination angle over the contact area

w = Unit weight of drill string

R = Radius of the drop-off section

θ = Inclination angle for the differential element

F_a = Axial force acting at the bottom of drill string

F_μ = Resisting frictional force

P_{wf} = Power loss owing to wellbore friction

rps = Rotations per second of the drill string

q = Mud flow rate

ρ = Mud density

C_p = Heat capacity of the drilling mud

$\tau(\theta)$ = Torque acting in the drill string as a function of the angle of inclination

U = Overall heat transfer co-efficient across drill string

T_p = Temperature of drilling fluid inside drill string

T_a = Temperature of drilling fluid in the annulus

T_{pi} = Temperature of the drilling fluid at the inlet of the drill string

Q_p = Heat sources inside drill string

Q_a = Heat sources in the annulus

h_o = Heat transfer co-efficient across the wellbore wall

T_f = Formation temperature

T_s = Surface temperature

G = Geothermal gradient

z = Any given depth of the well

F_s = Side force acting on the casing string

$\tau_c(\phi)$ = Torque acting on the casing string

r_c = Outer radius of the casing string

Ω = Whirl velocity of the casing string on the borehole wall

ϕ = Angle during a rotation that forms the point of contact of the casing with wall

dm = Mass of the differential element

ω = Rotations per minute during the casing while drilling operation

g = Acceleration attributable to gravity

k = Stiffness coefficient of the casing string

P_c = Power loss due to casing contact with the wellbore wall

v_{cp} = Net velocity at the contact point of the casing and the wellbore wall

$\Delta\sigma_T$ = Change in tangential stress due to wellbore temperature

ΔT_m = Change in temperature of the drilling mud at any given depth

β = Thermal expansion coefficient

E = Young's Modulus

ν = Poisson's ratio

α = Biot's constant

Δp_{fp} = Change in fracture pressure due to wellbore temperature

T_{fin} = Final temperature after casing while drilling operation

T_{init} = Initial temperature before casing while drilling operation

σ_{11} = Effective minimum horizontal stress

σ_{22} = Effective maximum horizontal stress

σ_{rr} = Effective radial stress around the wellbore

$\sigma_{\theta\theta}$ = Effective tangential stress around the wellbore

$\sigma_{r\theta}$ = Effective shear stress around the wellbore

$S_{\theta\theta}$ = Absolute tangential stress around the wellbore

S_h = Absolute minimum horizontal stress

p_w = Pressure due to drilling fluid inside the wellbore

p_o = Pore pressure due to the formation fluid

σ_t = Tensile strength of the formation

p_f = Fracture pressure

p_{mud} = Hydrostatic pressure due to the drilling mud

p_{fric} = Frictional pressure losses in the annulus

w_f = Fracture width of micro-fractures

L_f = Fracture length of micro-fractures

p_{fp} = Fracture propagation pressure

K^c = Fracture toughness of the formation

ΔL = Length of the fracture from the point of plugging till the fracture tip

CHAPTER 1

INTRODUCTION

1.1 Overview

The oil and gas industry has made rapid advances towards drilling of highly complex wells to maximize the reservoir productivity. Drilling of very deep deviated, horizontal, and extended-reach wells have helped us exploit parts of the reservoir that were previously inaccessible and have played a pivotal role in the industry over the last decade. However, the increased complexity of the drilling program has led to problems that have not been encountered before. Wellbore stability, lost circulation in depleted zones, wellbore friction and failures due to undesired downhole mud temperatures are some of the problems currently being faced by the industry.

Deviated, horizontal, and extended-reach wells have an intrinsic problem associated with them pertaining to wellbore friction. The drilling of these complex wells experiences large lateral forces on the drill pipe as well as the drill collars against the low side of the wellbore owing to gravity. The continuous rotation of the drill string is responsible for the excess torque, drag, and high frictional forces that it experiences. However, this rotation is very essential for the smooth flow of mud and required hole cleaning operations. Hence, the heat generated downhole as a result of wellbore friction has been considered a potential cause of drill string and tool failures as well as changing the properties of the drilling fluid downhole. These concerns of downhole heating have escalated over the last few years as we have drilled extremely deep wells that have thousands of feet of drill string rotating against the wellbore wall. An analysis of wellbore friction would certainly play of major role in future drilling operations.

Several new drilling techniques have also been developed and are being tested zealously to address the concerns pertaining to wellbore stability and lost circulations. Drilling the well with a casing string is one of the most promising methods currently practiced in the industry and has the potential to improve the stability of the wellbore and eliminate problems related to loss of the drilling fluid. Conventional techniques require drilling the well with a drill pipe until the target depth and, then, running and cementing a casing string to stabilize the wellbore and to prevent any undesired interaction between different formation fluids. The new Casing while Drilling (CwD) operation utilizes the casing string itself to drill the well instead of the drill pipe. This operation was started initially with the sole objective of eliminating the non-productive time (NPT). However, as the number of casing while drilling operations have increased over the last few years, several other benefits have been realized.

It has been observed that drilling the well with a casing leads to an improvement in the wellbore stability by plastering the wellbore wall with drilled cuttings, thereby, increasing the fracture gradient of the formation. The larger size of the casing as compared to the drill pipe is responsible for providing a continuous contact between the casing and the wellbore wall, generating a lot of heat downhole as well as plugging of the natural and induced fractures and the pores paces. This mechanism has been termed as the smear effect (or the plastering effect) and has been utilized in more than a few cases to drill a well more economically as well as reach a target zone that was previously considered unfeasible due to formation properties. The smear effect mechanism is of particular interest to the industry as it has the potential to address various drilling problems while reducing the cost of operations.

1.2 Problem Statement

An accurate estimation of the downhole temperatures of the drilling fluid plays a very significant role in the planning of a successful drilling program. A thorough knowledge of the temperature variation with depth is extremely helpful in revealing information about the downhole conditions, as well as in the precise selection of the most suitable drilling fluid and its properties. Several studies have been conducted to calculate the drilling fluid temperatures; however, all the heat transfer analyses performed earlier have been done assuming a vertical well and have ignored the effects of the heat generated due to wellbore friction.

This study tries to carry these analyses a step further by aiming to quantify the heat generated as a result of wellbore friction in deviated, horizontal, or extended-reach wells, and incorporating the heat source in the wellbore heat-transfer model under steady-state conditions to analyze the variation in downhole temperatures due to friction. It also aims to provide a better understanding of the effect of drilling parameters and fluid properties on temperature to help prevent undesired operating conditions. The proposed model should then be validated with real-time data measured in the field using MWD tools for both deviated and horizontal wells, and potential field applications should be numerated.

The downhole temperatures of the drilling fluid should then be investigated for a casing while drilling operation to understand the influence of wellbore temperatures on the smear effect mechanism as well as on the fracture gradient of the formation. The continuous contact between the casing and the wellbore wall should be modeled to quantify the heat generated downhole and used, subsequently, in the heat transfer model

to estimate temperatures. Field case studies should also be presented to suggest possible improvement in the fracture gradient and the contribution of wellbore temperatures in realizing the benefits of the smear effect.

Casing while drilling operations also experience high equivalent circulating densities (ECDs) due to very narrow annular clearances between the casing string and the wellbore wall. It is considered that these high ECDs are responsible for inducing micro-fractures in the wellbore wall that are plugged by the drilled cuttings and the added lost circulation materials. This plastering mechanism helps increase the wellbore stresses and results in an improvement in the fracture gradient. This study also aims to analyze the initiation of drilling induced fractures due to high ECDs and, then, estimate the increase in the fracture gradient due to plugging of those fractures. Field case studies should also be presented to better understand the contribution of the induced fractures on the smear effect mechanism.

1.3 Objectives

- Study an analytical model to quantify the heat generated due to wellbore friction.
- Propose a model to estimate the downhole temperatures of the drilling fluid incorporating the effect of wellbore friction.
- Validate the proposed model with real-time field data measured using MWD tools for a deviated as well as a horizontal well.
- Study the influence of wellbore temperatures on the smear effect mechanism.
- Analyze the initiation as well as plugging of drilling induced fractures in casing while drilling operations and study their contribution to the smear effect.

CHAPTER 2

LITERATURE REVIEW

2.1 Wellbore Friction

Drilling of deviated, horizontal and extended reach wells have instigated a new found interest to understand the wellbore friction as well as the underlying torque and drag. Several softwares and models have come up in the industry to estimate the frictional forces acting on the drill string. Most of these existing computational methods follow a numerical solution technique to understand and calculate the forces downhole. However, this study strives to work on and propose analytical mathematical models for understanding the wellbore friction and its effect on downhole temperatures of the drilling fluid. Analytical methods help provide a better physical insight to understand the applicable system as well as the effect of its underlying parameters, even though they may be cumbersome to use and may not be as highly accurate as the numerical techniques.

Aadnoy *et al.* (2008) undertook a mathematical study to analyze the published friction models and have presented the derivation of a generalized friction model by identifying a lot of symmetries in the solution by selecting the appropriate signs for the coefficient of friction and the well inclination. They have shown that their model is valid for tubulars, both in tension and in compression, for all the geometries like vertical and tangent sections as well as build-up and drop-off bends. They have also presented a field case with their model and concluded that bends contribute significantly to well friction and that the bend friction depends on the axial force.

Johancsik *et al.* (1984) developed a computer model to predict the drill string torque and drag and have calibrated the model using a rotary torque meter. The underlying principle of their proposed model is that torque and drag forces in directional wellbores are primarily caused by the sliding the friction. They have presented the detailed development of their model as well as field measurement techniques for torque and drag to compute the coefficient of friction from field data. They concluded that the sliding friction coefficient for seawater-based mud typically lies between 0.25 and 0.4.

Samuel (2007) also studied the wellbore tubulars in comprehensive detail and provided a mathematical treatise to understand the static and dynamic forces acting on the drill string during the different drilling operations. He suggested a simple computational technique to calculate the side force acting on the tubulars at any given depth in the well which in turn is used to compute the applicable torque and drag downhole using a friction factor. This method certainly helps to better understand the effect of underlying parameters on the wellbore friction.

2.2 Wellbore Heat Transfer

The principles of wellbore heat transfer have been investigated by several authors and a good volume of literature currently exists on the subject. Most of the proposed methods and studies conducted in this field are again divided into two types of computational methods, the analytical models and the computational techniques.

Holmes *et al.* (1970) developed an analytical mathematical model to predict the mud temperature in the drill pipe and in the annulus during drilling at any depth in the well. They have proposed a steady state heat transfer solution between the fluids in the annulus and the fluids in the drill pipe combined with the transient heat transfer between

the fluids in the annulus and the formation. They have also applied their model to a 15,000 ft Gulf Coast well and have successfully predicted the logged bottomhole temperatures using their model. However, their method is applicable only for vertical wells, as it does not incorporate the effect of wellbore friction on downhole mud temperatures existing in the deviated sections of the wellbore.

Marshall *et al.* (1982) developed a computer model that utilizes a direct solution technique to solve the finite difference equations describing the transient heat transfer in the wellbore. They have considered heat generation in the system due to different energy resources namely, rotational energy due to work required to rotate the drill string, work done by the drill bit as well as the viscous energy due to frictional pressure losses. However, their method does not include the heat source due to the drill string and borehole wall contact in the curved sections of the well. They have also conducted a parametric study to understand the influence of fluid and formation properties on the wellbore temperature distribution and compared the deviation in temperatures from their model and those from a steady state heat transfer solution.

Schoeppel *et al.* (1971) numerically modeled the unsteady temperature distributions in a circulating drilling fluid and the surrounding formation based on a set of fourth order partial differential equations. They have considered heat flow by forced convection in the wellbore and by conduction in the adjacent formation and have presented a numerical error analysis to determine the accuracy of their method. They have compared the temperature distribution calculated by their model to those published by Raymond *et al.* (1969) with fairly good accuracy. However, they do not provide a parametric analysis of the underlying variables for a better understanding of their model.

Kabir *et al.* (1996) have presented an analytical model for the flowing fluid temperature in the drill pipe / tubing and in the annulus as a function of well depth and circulation time based on an energy balance between the formation and the drilling fluid. They have proposed solutions to both the forward and backward circulation scenarios and show that the maximum temperature occurs not at the well bottom, but at some distance higher from the bottom for flow up the annulus. They also present an analytical expression for calculating the depth at which the maximum annular fluid temperature occurs when the flow is down the tubing and up the annulus. However, their analysis again does not address the effects of wellbore friction encountered while drilling deviated, horizontal, and extended-reach wells.

2.3 Casing while Drilling (CwD) Operations

Drilling a well with a casing string has become quite popular over the last decade and has led to the development of casing while drilling technologies by several players in the industry. Various studies have been conducted and are present in the literature that focus on better understanding the operational and economical advantages of using a casing while drilling system over a conventional drilling program.

Karimi *et al.* (2011) have studied the main advantages of casing while drilling in great detail by focusing on lost circulation reduction, wellbore strengthening, improved wellbore stability and drilling induced formation damage mitigation. They suggest that casing while drilling reduces the mud lost to the reservoir section and can be directly correlated to a reduced skin factor and hence improved productivity of the wells. They also suggest that the wellbore plastering creates an impermeable mud cake on the wall as shown in Fig. 1 to Fig. 3, thereby, augmenting the pressure containment of the borehole.

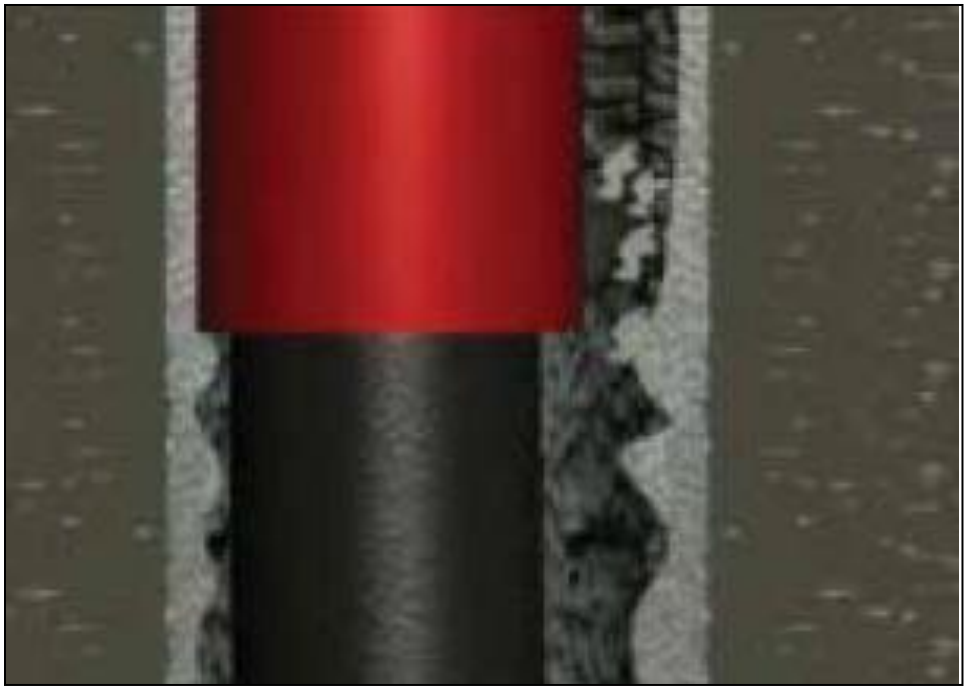

Fig. 1 – Casing string rotates in continuous contact against the wellbore wall due to its large diameter as compared to a drill pipe, Karimi *et al.* (2011).

Fig. 2 – Smearing of the drilling mud into the formation helps build up an impermeable filter cake, Karimi *et al.* (2011).

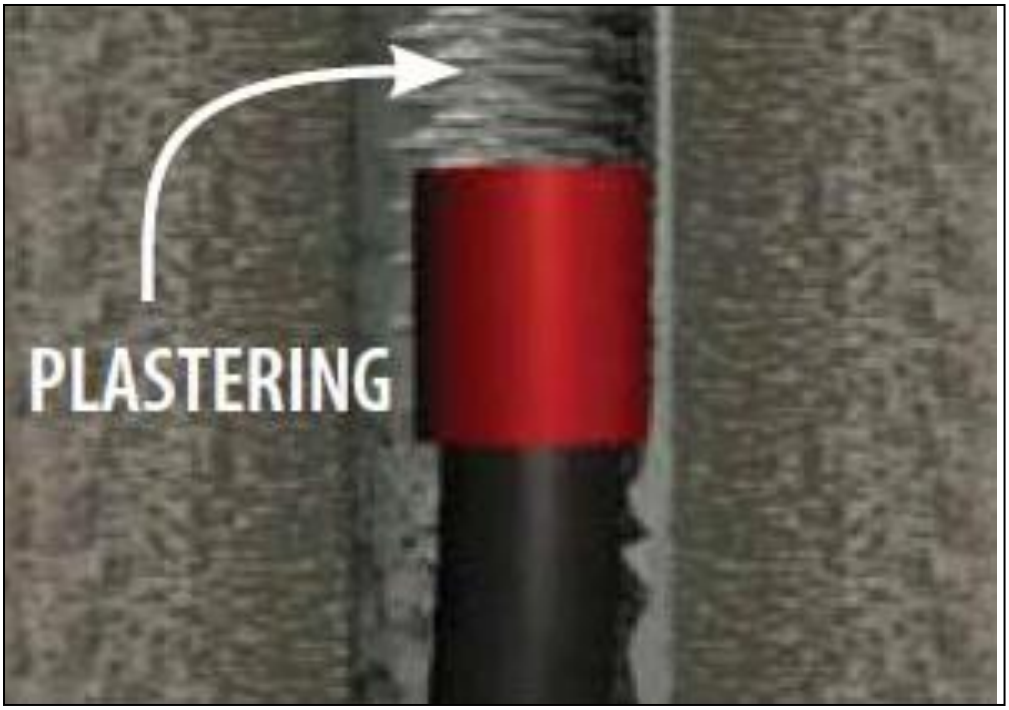

Fig. 3 – The plastering of the wellbore wall by the casing leads to the sealing of natural and induced fractures as well as pore spaces, Karimi *et al.* (2011).

They consider that wells with stability problems are the best candidates for using a casing while drilling system as this process helps increase the fracture gradient of the formation in the near wellbore region resulting in a wider operational window. The other benefits that they have listed are: No Tripping, Gauged Well, Less Drilling Time, Efficient Borehole Cleaning and Superior Hydraulics. They have also presented various successful Casing / Liner Drilling case studies to further stress on the applications of this promising technology.

Diaz *et al.* (2004) presented three modeling approaches to determine the equivalent circulating density (ECD) in a casing while drilling operation, namely, using the hook load measurements, pump pressure measurements, and conventional hydraulic models for a narrow slot flow approximation. They have compared the model results with experimental and field data and have shown that the difference between the calculated and measured bottomhole pressures was within a range of ±8%. They concluded that the

hook load measurements correlated well with the flowing bottom hole pressures and that the pipe rotational speed played a very important role in determining the equivalent circulating density in the annulus of a wellbore.

Radwan *et al.* (2011) introduced casing while drilling as a potential method for drilling HPHT wells by investigating its benefits and limitations in correlation with the current HPHT challenges. They suggest that casing while drilling can significantly reduce the cost of drilling through harsh environments as the drilling hazards of HPHT wells are minimized by eliminating problems such as stuck pipe, well control incidents, surge and swab effects, wellbore instability and lost circulation. Reduction of rig time, number of casing strings, tubulars as well as cement and mud volumes further help lower the overall drilling costs involved with a casing while drilling system. They also suggest that the operational mud weight window could be widened through the smear effect mechanism which can prove to be very crucial for HPHT environment. The authors finally recommended a pilot project to study their proposed methodology and its applicability in deepwater HPHT wells.

Moellendick *et al.* (2011) also conducted a qualitative analysis of the advantages of a casing while drilling operation pertaining to improving the wellbore stability. They consider that the smear effect or the plastering effect strengthens the wellbore by smearing the generated cuttings and available particle size distribution into the formation and sealing fractures and pore spaces to widen the operational mud weight window. They also suggest that casing while drilling leads to drilling of a gauged borehole due to the large diameter of the casing and more efficient hole cleaning due to a mono-bore annulus that can be achieved as shown in Fig. 4 to Fig. 6.

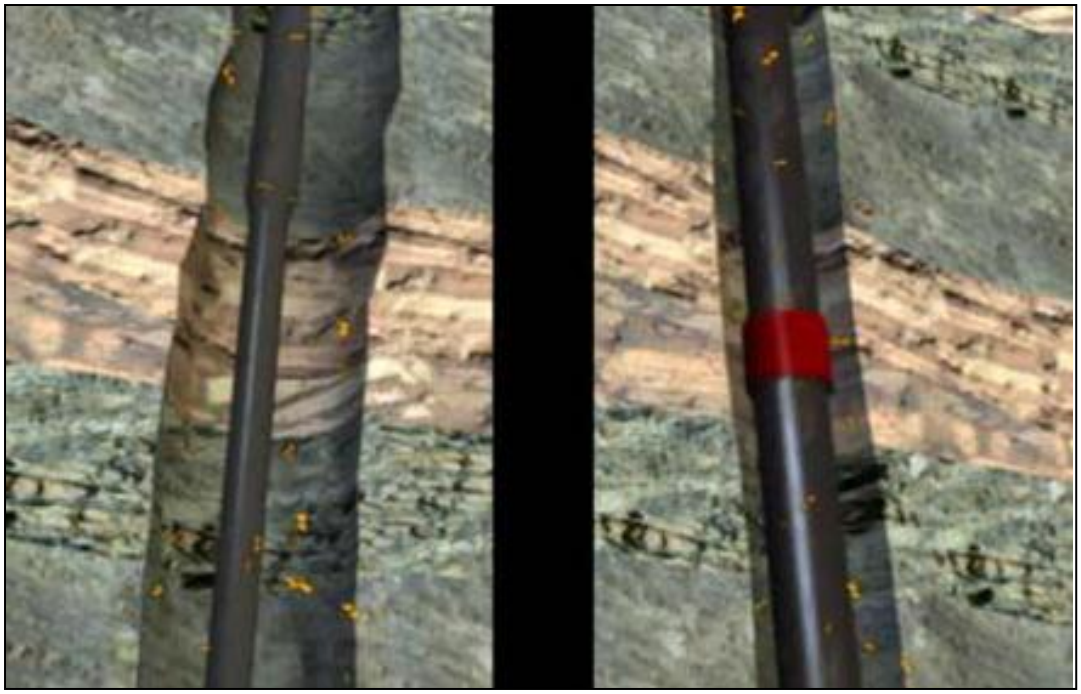

Fig. 4 – Larger diameter of the casing string leads to drilling of a more gauged wellbore, Moellendick *et al.* (2011).

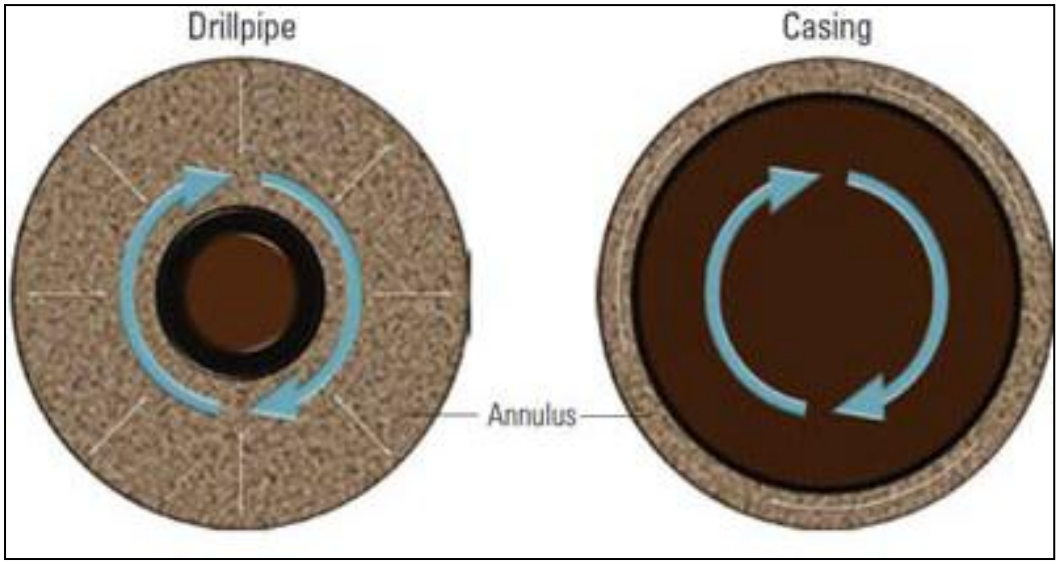

Fig. 5 – Comparison of casing while drilling with conventional drilling shows a smaller annular clearance that leads to higher annular velocity facilitating cuttings transport, Moellendick *et al.* (2011).

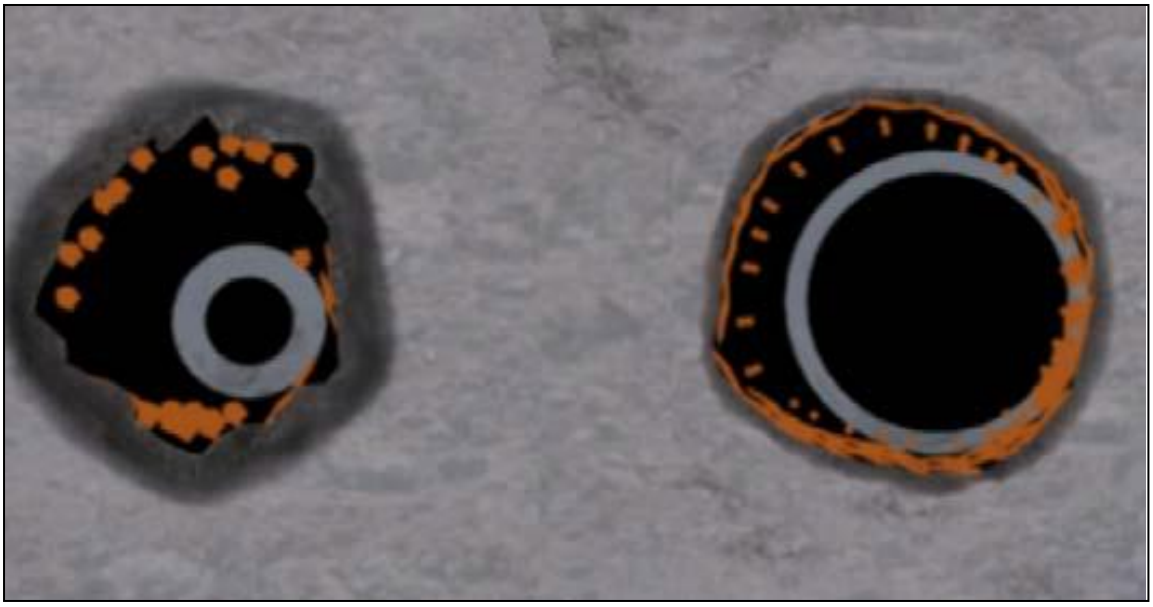

Fig. 6 – Plastering of cuttings on the wellbore wall due to the larger diameter of the casing string, Moellendick *et al.* (2011).

2.3.1. The Smear Effect

The smear effect or the plastering effect mechanism has been addressed and studied extensively in the literature using qualitative analyses by various authors. It has been broken down into four small steps by Moellendick *et al.* (2011) as follows:

- Grinding and pulverization of the cuttings as they travel up the annulus by the smooth rotation of the casing which are then smeared into the formation face.
- Eccentric motion of the drill string in casing while drilling provides smooth contact with the wellbore wall.
- Initiation of small fractures due to higher equivalent circulating densities experienced while drilling with a casing.
- Plugging of natural and induced fractures as well as existing pore spaces by the cuttings and added lost circulation materials to realize the benefits of the plastering effect.

Watts *et al.* (2010) provided a comprehensive analysis of the application of particle size distribution principles for determining materials to be added to the mud system during casing while drilling. They explain the details of the casing while drilling operations undertaken in the Piceance Basin of Colorado as well as in the Alaskan Tarn field and have presented the improvement in the fracture gradient achieved in each of those drilling programs. In addition, they have also studied the effect of rotational speed of the drill string on the fracture gradient of the formation. They showed that they successfully achieved a 4.6 ppg improvement in the fracture gradient as shown in Fig. 7 to Fig. 9 while drilling the second well in the Alaskan Tarn field due to the smear effect.

Based on the entire drilling program, they concluded that the improvement in the fracture gradient was not great when the ratio of the casing diameter to the hole diameter is below 0.80. However, for ratios higher than 0.80, improvements in wellbore strength occurred in drilling 40 to 45 ft only. They also concluded that strengthening could be achieved even if the wellbore was first drilled with conventional BHAs and drill pipe and that both the natural and induced fractures could be plugged due to casing while drilling.

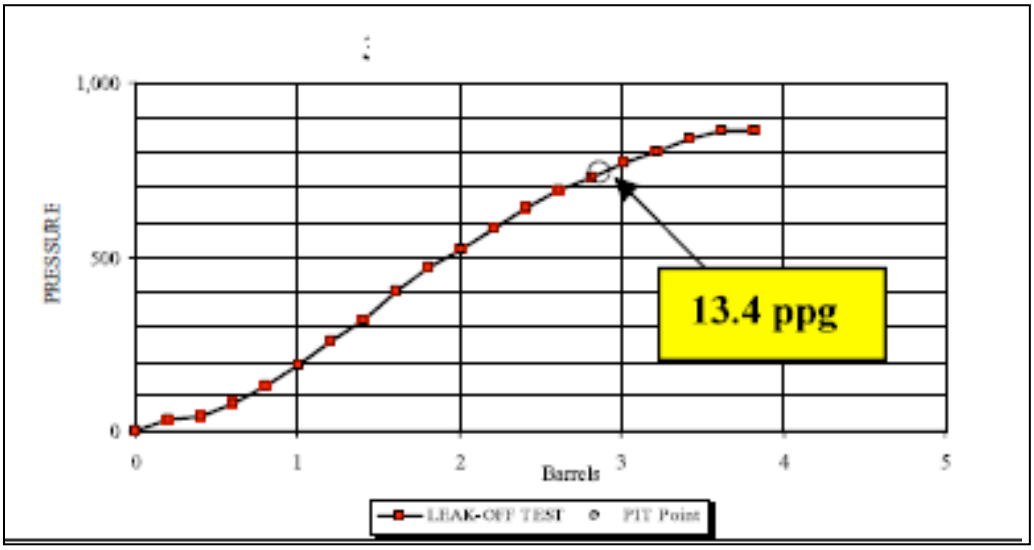

Fig. 7 – Leak off test conducted at 7482 ft for the second well in the Alaskan Tarn field, Watts *et al.* (2010).

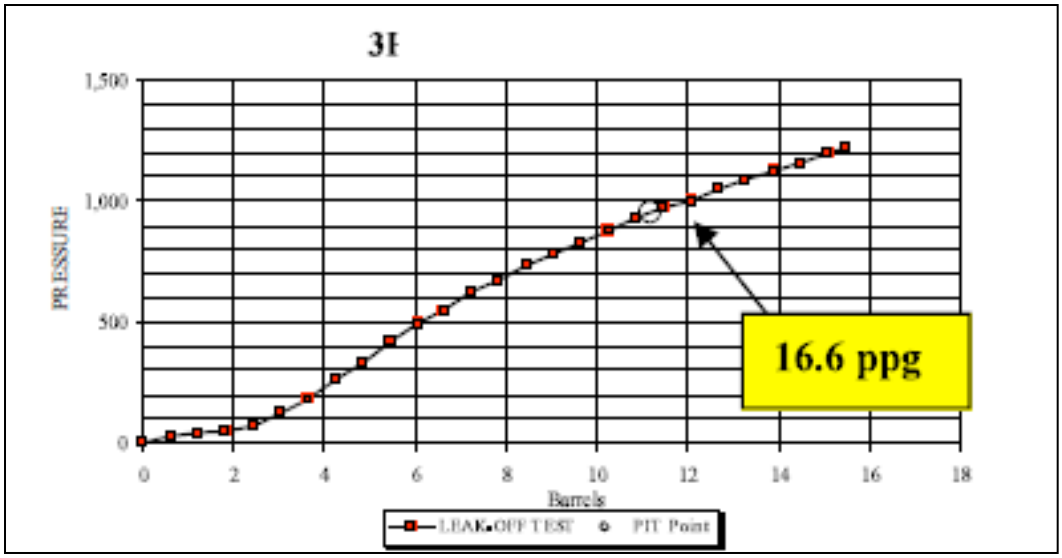

Fig. 8 – Leak off test conducted at 7620 ft after casing while drilling to the top of the first reservoir sand, Watts *et al.* (2010).

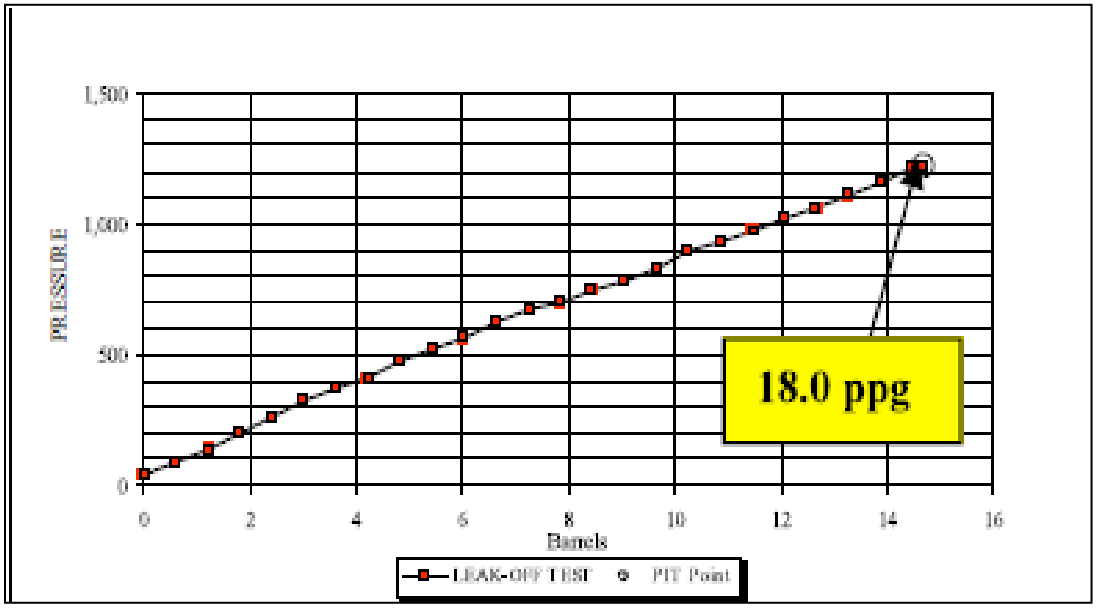

Fig. 9 – Leak off test conducted after the first reservoir sand using a casing while drilling system, Watts *et al.* (2010).

Karimi *et al.* (2011) carried out a qualitative analysis of the contribution of pipe diameter to the smear effect mechanism observed in casing while drilling. They suggest that a significant contributor to creating the plastering effect is the higher casing diameter / hole size ratio in a casing while drilling operation as compared to a conventional drilling

operation using a drill pipe. They analyzed the effect of the pipe contact angle, the pipe contact area and the penetration depth into the filter cake for both casing while drilling and conventional drilling operations aiming to understand the effect of larger casing sizes on the plastering mechanism. They also concluded that in all the successful applications of the smear effect, the casing diameter / hole size ratio has been in the range of 0.75 to 0.90.

Karimi *et al.* (2011) also investigated the influence of cuttings size in casing while drilling to plug pore spaces to control the fluid loss and reduce the formation damage. They suggest that the casing while drilling process grinds the drilled cuttings as they travel up the annulus and creates a larger particle size distribution (PSD) profile than conventional drilling operations. The PSD analysis carried out by them determined that the smaller size and wider range of these cuttings led to adherence to the wellbore helping seal the pore spaces and preventing further invasion. They recommended that the particle size distribution of the mud should be continuously monitored while drilling depleted reservoirs to make the most effective utilization of the plastering effect. They finally suggested that the reservoir sections, drilled with casing, leads to enhanced productivity by as much as twice than the wells that were drilled using conventional techniques because casing while drilling helps mitigate the formation damage occurring during the drilling process.

2.3.2 Wellbore Wall Contact

The contact between the wellbore wall and the casing string for a casing while drilling operation has not been investigated in the context of developing a mathematical model by any of the previous studies. However, a striking similarity exists between the

scenarios presented by the whirling motion of the drill collars and the mechanism of the casing contact with the wellbore wall. This is due to the larger outer diameter of the drill collars compared to the drill pipe that leads to a rotational contact against the borehole wall and resultant forward or backward whirl mechanisms.

Vandiver *et al.* (1990) explained the phenomenon of drill collar whirling in a very simple effective manner. They have presented whirling as "the centrifugally induced bowing of the drill collar resulting from rotation" and have analyzed the two whirling mechanisms, namely, forward synchronous whirl and back ward whirl as shown in Fig. 10. They suggested that serious surface abrasion of the drill collars occur due to rubbing on the wall by forward synchronous whirl in which the same side of the collar is in continuous contact with the side of the hole. In a pure backward whirl, they consider that the drill collar rolls without slipping on the inside of the hole in a direction opposite to the imposed rotation rate. However, this does not lead to significant surface abrasion as very little relative velocity exists between the drill collar and the wall. They have also presented a simple set of equations to calculate the whirl velocity based on the rotational speed of the drill string, and the collar and borehole radii.

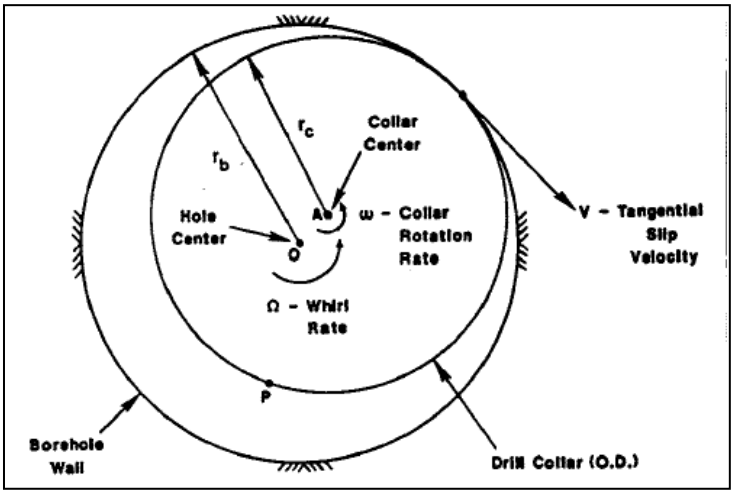

Fig. 10 – Cross-section of the borehole and drill collar in a whirling scenario, Vandiver *et al.* (1990).

Jansen *et al.* (1992) also studied the forward and backward whirl of drill collars using the theory of rotor dynamics and have derived analytical equations for both these models. They suggested that drilling with a slightly, bent drill collar may result in violent, lateral vibrations that are analogous to the whirling motion of an unbalanced centrifuge. They also show that if the frequency and direction of the whirling motion does not coincide with that of the excitation, the asynchronous drill collar whirl takes place that which in an extreme case cause the collars to roll backward without slipping. This is known as the asynchronous backward whirl.

Stroud *et al.* (2011) performed analytical and experimental backward whirl simulations to predict the dynamic behavior of the BHA and drill collars and gain a better understanding of the dominant factors that cause backward whirl. They have validated their analytical model by correlating their results using a full scale test rig capable of initiating and sustaining full rolling contact backward whirl. Their two major findings were that a transition phase or a "partial whirl" phase precedes full backward whirl in most cases as shown in Fig. 11 and that full backward whirl could not occur close to gauged hole unless there was a very high coefficient of friction between the borehole and the drilling assembly.

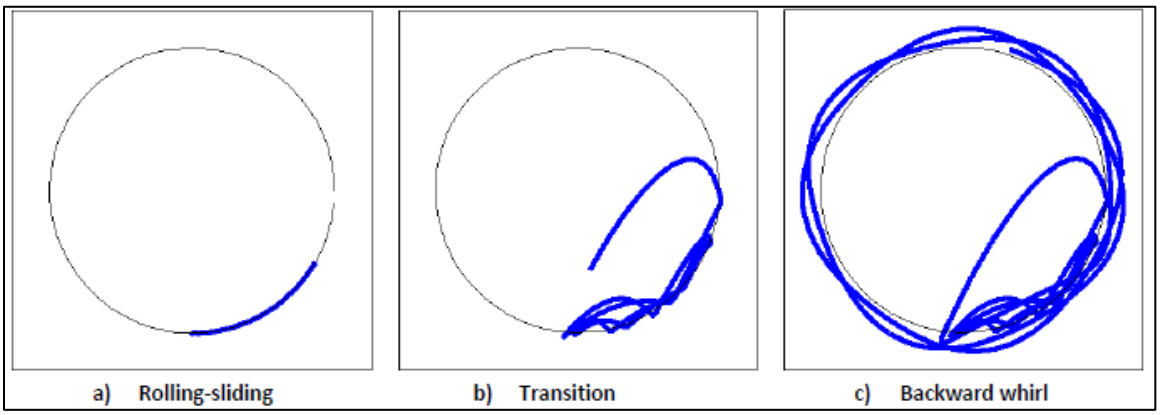

Fig. 11 – The three phases of backward whirl initiation, Stroud *et al.* (2011).

They have also studied the effect of radial hole clearance on whirl initiation and frequency as well as the effect of friction co-efficient at the pivot to borehole interface. They recommended that their analytical model could prove to be a very efficient tool for predictive analysis to better design drilling assemblies in the future.

2.3.3 Effect of Temperature on Fracture Gradient

One of the most important advantages of a casing while drilling operation is an improvement in the fracture gradient achieved due to the smear effect mechanism. Here, we investigate the role played by downhole wellbore temperatures in contributing to the increase in fracture gradient, if any. Various authors have investigated the influence of temperature on stresses and wellbore stability and have correlated a change in downhole mud temperatures to a corresponding change in the fracture gradient through analytical models as well as field case studies.

Gonzalez *et al.* (2004) presented the thermal effects of wellbore stresses on the effective fracture gradient of the formation. Their findings suggest that lower bottom hole temperatures than the static geothermal gradient due to circulation on bottom results in a cooling effect that reduces the effective fracture gradient whereas higher wellbore temperatures lead to an increase in the same. They studied the drilling data from various lost circulation events in detail to correlate changing downhole temperatures to mud losses. Their analysis of three of those has been presented in Fig. 12 to Fig. 14. They then performed a series of temperature dependent leak-off tests and successfully achieved a 1.5 ppg equivalent mud weight increase in the effective fracture gradient corresponding to a temperature increase of 61°F as shown in Fig. 15.

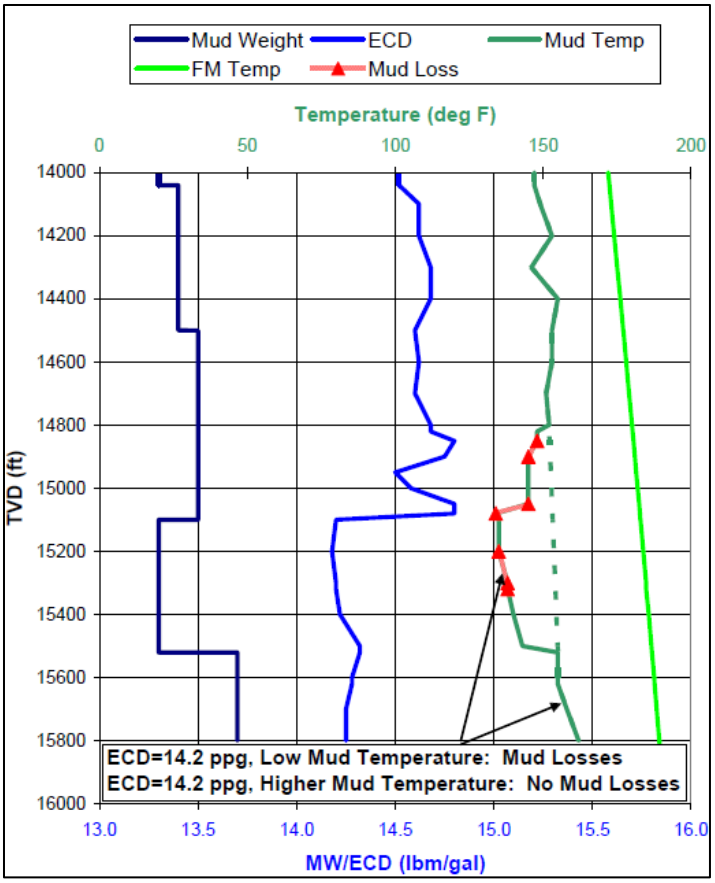

Fig. 12 – Well #1 analysis to correlate mud losses & temperature, Gonzalez *et al.* (2004).

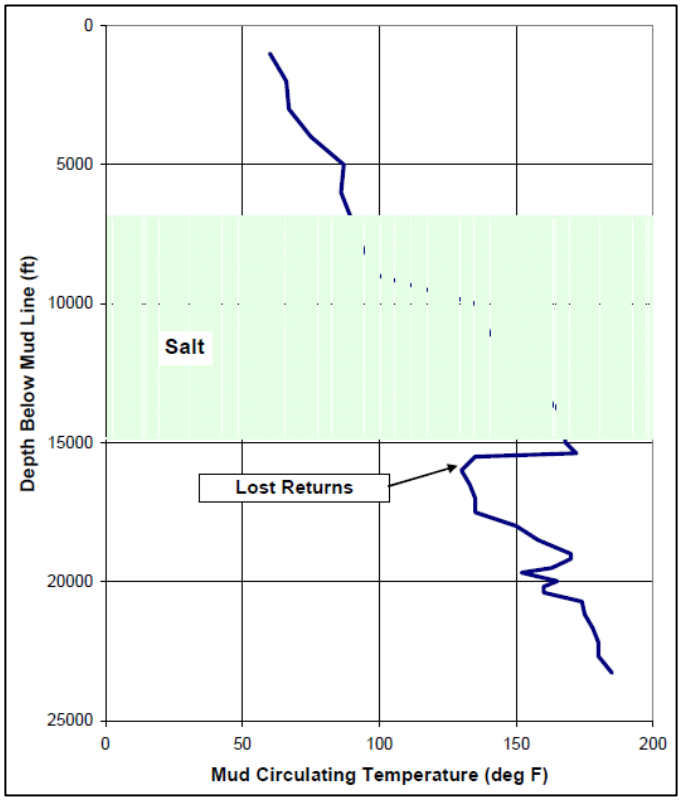

Fig. 13 – Well #2 analysis to correlate mud losses & temperature, Gonzalez *et al.* (2004).

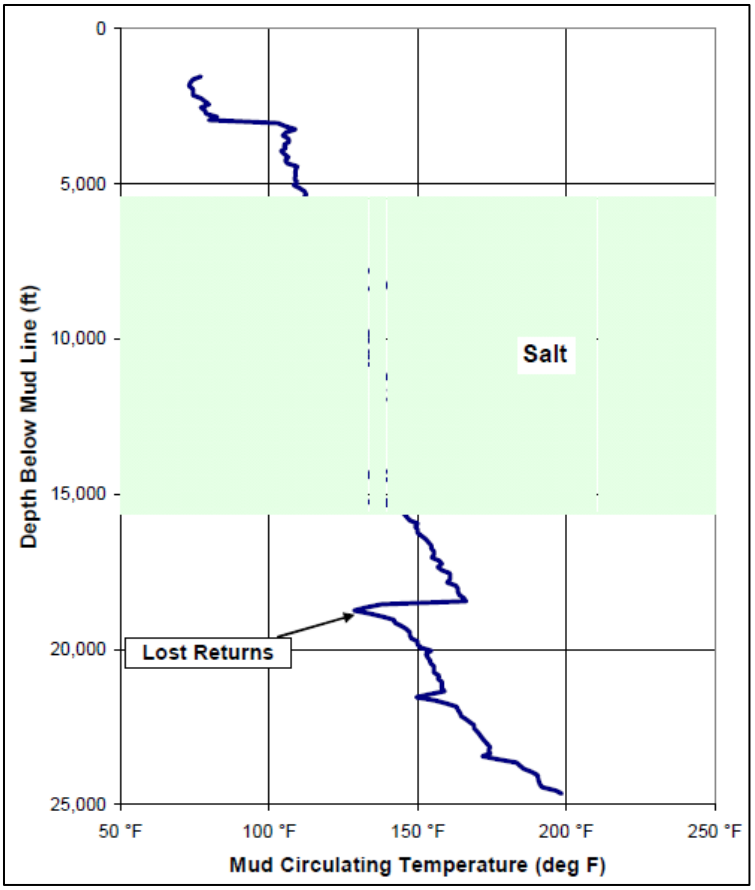

Fig. 14 – Well #3 analysis to correlate mud losses & temperature, Gonzalez *et al.* (2004).

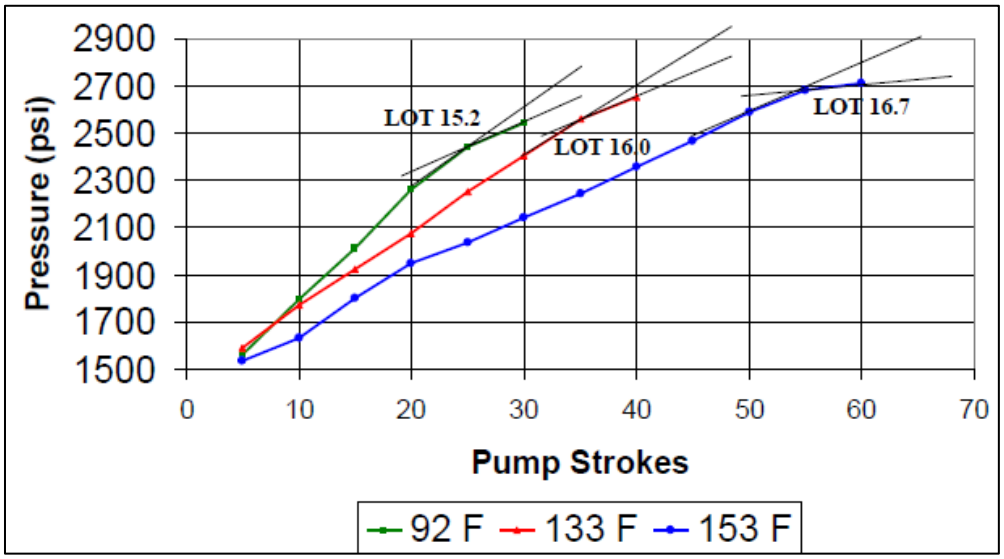

Fig. 15 – Temperature dependent leak-off test results at three different drilling fluid temperatures, Gonzalez *et al.* (2004).

They finally analyze a deepwater well case aiming to explain the significantly lower LOT measurements than fracture gradient prediction methods in such environments.

Gil *et al.* (2006) proposed the use of wellbore cooling in combination with classical wellbore strengthening processes to permanently increase the fracture gradient without the risk of circulation losses. Their method recommends lowering the temperature of the drilling mud, thereby, reducing the hoop stress at the borehole wall and subsequently creating an improved "stress cage" even in low permeability formations. They presented a finite element model based on their method and concluded that the effect of rock cooling was large enough to cause a significant reduction in the magnitude of tangential stress at and near the wellbore wall. This phenomenon further creates the possibility of setting the stress cage at much lower pressures than in a standard approach as some micro-fractures have already been initiated by lower temperatures.

Addis *et al.* (2001) explored lost circulation events associated with the drilling program in the Brent field in the UK North Sea. One of the various factors studied by them was the contribution of the thermal stresses induced at the wellbore on the occurring mud losses. They use a simple analytical method to estimate the change in the tangential stress at the wellbore wall due to a decrease in temperature based on the formation properties of the field under investigation. They suggest that the temperature change might have been one of the possibilities that resulted in a significant change in stresses acting around the wellbore, resulting in initiating a fracture and subsequent mud losses experienced in the Brent field.

Aadnoy *et al.* (2009) presented an analytical study to model the load history leading to the fracturing of the borehole. They suggest that the Kirsch equation for hoop stress has not been very useful for performing an analysis of the load history and developed a new fracturing equation by imposing a volumetric strain balance. They incorporate the effect of Poisson's Ratio due to the borehole being loaded in the radial

direction and causing a tension in the tangential direction. In addition, their solution also includes the effect of temperature history on the fracturing pressure. They suggest that if the borehole is heated or cooled, the fracturing pressure changes due to a corresponding change in hoop stress by expansion or contraction. Their derived solution is similar to the general equation to calculate the change in fracture pressure due to temperature except that they propose a different scaling term. They finally present some numerical examples to suggest that if the Poisson's effect is neglected, the fracture pressure is severely under predicted and calculate the difference in fracturing initiation pressure for hot has and cold water injection.

2.3.4 Wellbore Strengthening

Wellbore strengthening has been a widely studied subject and has been the area of investigation of various authors. Out of the various wellbore strengthening methods that have been proposed, this study focuses particularly on the strengthening methods by plugging of fractures at the wellbore.

Barrett *et al.* (2010) presented the details of the application of a software tool designed to determine the optimum blend of wellbore strengthening materials (WSM) to drill a particular formation. They have studied the existing theories on wellbore strengthening namely: "Stress Cage" for hoop stress enhancement, "Fracture Closure Stress" theory utilizing high fluid loss materials, and "Fracture Propagation Resistance" involving isolation of the fracture tip; they suggested that these three theories are complementary in many respects based on a successful utilization of a blend of WSM for opening and sealing of fractures. They finally applied their WSM design software in the challenging Cashiriari field in Peru and present their success results.

Alberty *et al.* (2004) presented their groundbreaking work on the "Stress Cage" theory and described the mechanism that allowed the fracture resistance to increase through the addition of mud additives. They explain the formation of a "Stress Cage" as near wellbore region of high stress induced by propping open and sealing shallow fractures at the wellbore wall. They use a finite element model to show that high concentric stresses can be developed in the near wellbore region by inducing fractures and plugging and sealing them with particles as shown in Fig. 16 below.

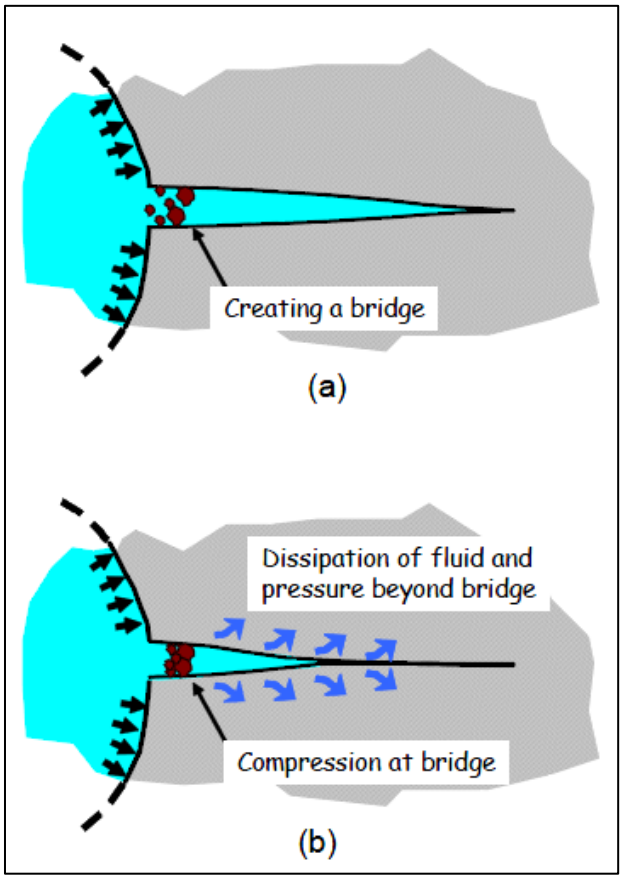

Fig. 16 – Process for formation of a "Stress Cage", Alberty *et al.* (2004).

Salehi *et al.* (2011) studied the existing wellbore strengthening theories in detail and have classified them into two broad categories: strengthening due to increasing wellbore hoop stress by wedges inserted into fractures and strengthening due to fracture tip isolation with suitable materials to enhance fracture propagation pressure. They

presented numerical as well as analytical solutions for different field cases to compare the existing theories and from their results suggested that wellbore hoop stress cannot be higher than its ideal case in the fractured zone by plugging fractures as shown in Fig. 17. However, they concluded that the wellbore could be strengthened and that the fracture gradient could be improved by enhancing the fracture propagation pressure.

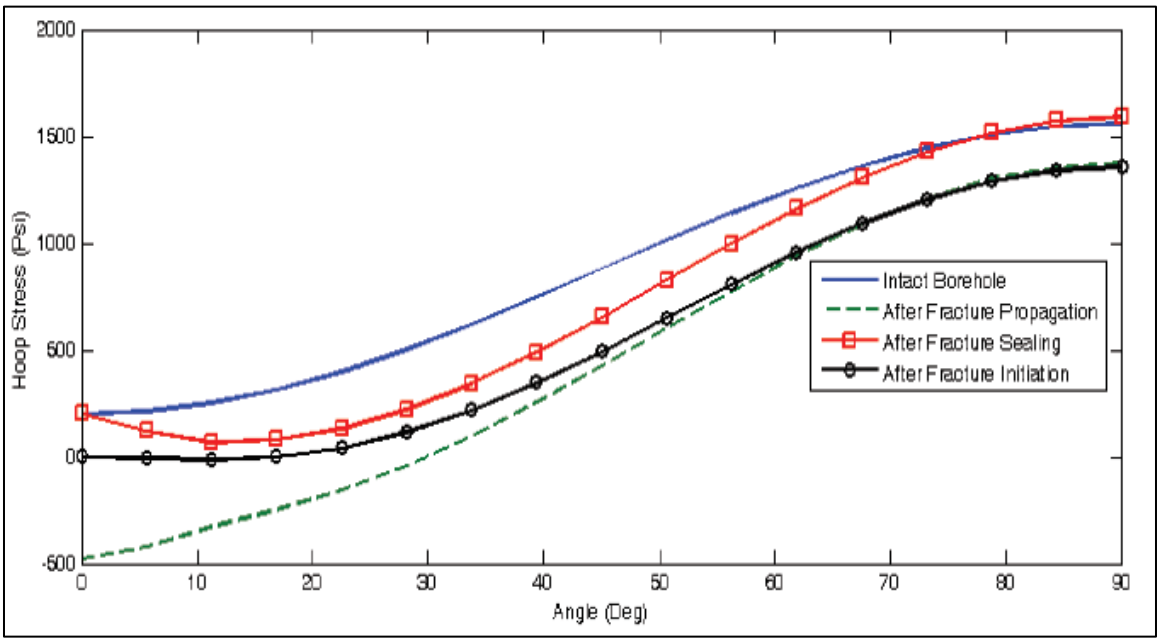

Fig. 17 – Wellbore hoop stress for before and after fracture initiation, propagation and sealing, Salehi *et al.* (2011).

Oort *et al.* (2009) presented their theory on wellbore strengthening by introducing the concept of "Fracture Propagation Pressure" (FPR) enhancement and share experimental results, field data and case histories based on this subject. They have critically analyzed the existing theories on "Stress Cage" and "Fracture Closure Stress" and point out the drawbacks associated with each of them. They present the unique features and operational benefits of an FPR approach and suggest essential elements to make it successful. They conclude that FPR might be the actual mechanism underlying the borehole strengthening effects that had been attributed previously to increasing the wellbore stresses.

Morita *et al.* (2011) presented a set of simplified analytical equations to clarify the wellbore strengthening methods and conducted parametric studies to identify the advantages and disadvantages of each method. They have studied in detail four typical wellbore strengthening methods and analyze the existing preventive lost circulation methods in the industry. They presented mathematical equations for fracture systems considering a micro-fracture propagation that has been plugged at the mouth or at some distance from the mouth, macro-fracture propagation as well as theory of borehole stability incorporating the effect of temperature. Their model for micro-fracture plugged at its mouth has been shown in Fig. 18 for reference.

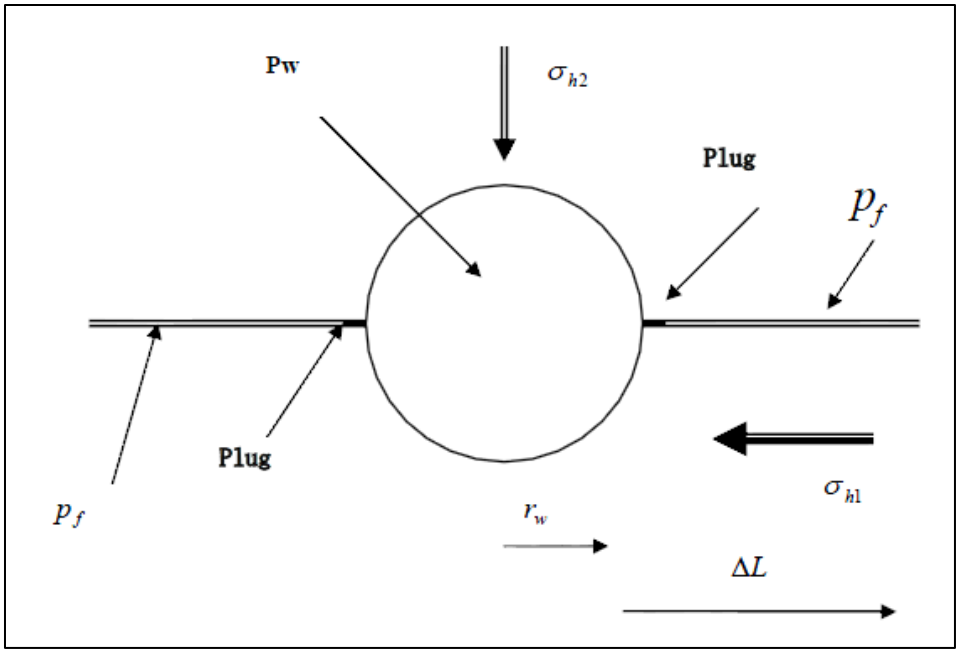

Fig. 18 – Micro-fracture plugged at the mouth, Morita *et al.* (2011).

Loloi *et al.* (2010) extended the concepts used in fractured injector geomechanics to improve the wellbore strengthening procedures. They presented a model in which the fracture length and width are related to mud weight and rock properties and the plugging particle size is optimized based on the fracture geometry and leakage scenarios. They concluded that a combined effect of plugging material isolating the fracture tip and

increase in tangential stresses arises when the fracture is plugged within itself and not at the mouth. Their problem configuration for plugging at the fracture tip as well as for plugging at any point within the fracture has been shown in Fig. 19.

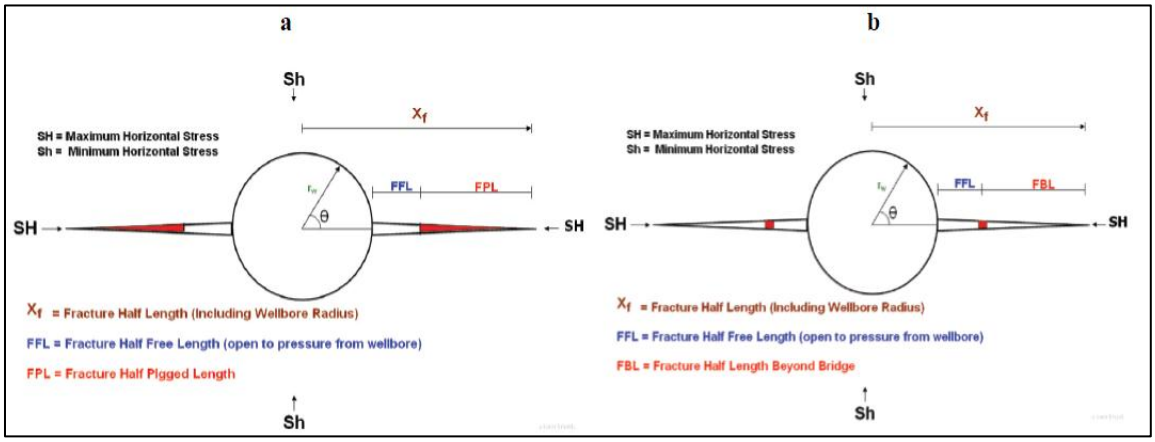

Fig. 19 – Fractures plugged in at the tip as well as at any location along itself to prevent pressure communication, Loloi *et al.* (2010).

Kumar *et al.* (2010) studied the effect of mechanical properties of lost circulation materials (LCMs) on wellbore strengthening in comprehensive detail by using an experimental set up capable of simulating a wide range of fracture closure stresses. They observed significant crushing of common LCMs (like ground marble and ground nut shells) at high confining pressures and suggested improvements in the resiliency of these materials with small additions of resilient graphite carbon (RGC). They finally make recommendations on different combination of LCMs that may be used more effectively to provide improved wellbore strengthening.

Wang *et al.* (2007) also presented analytical and numerical methods to investigate the improvement of wellbore pressure containment by propping fractures with lost circulation materials to strengthen the wellbore. From their results, they concluded that wellbore pressure containment can be improved beyond its ideal value defined by the Kirsch's tangential stress equation.

CHAPTER 3

WELLBORE FRICTION & HEAT TRANSFER

3.1 Introduction

The advent of deviated, horizontal, and extended-reach drilling has led to increased effects of friction on the drill string and the drilling fluid. Wellbore mechanical friction (attributable to pipe rotation or to torque and drag) plays a significant role in drilling operations and is considered to influence the temperatures downhole. An analytical mathematical model will help to provide physical insight to understand the borehole conditions.

This section of the study aims to develop a simple mathematical model to analyze the heat generated from borehole friction and to predict the temperature of the drilling fluid during a drilling operation at any depth in the well. The model presents a steady-state solution for heat transfer between the drill string and the fluids in the drill pipe and annulus, as well as heat transfer between the annular fluid and the formation. Heat generated from friction has been modeled using the torque acting on the drill string as a result of contact forces. A linear temperature gradient for the formation and a constant borehole wall temperature has been assumed to simplify the model. Frictional pressure losses in the drill pipe, in the annulus, and across the bit have been incorporated in the model because they have a significant contribution to the heat generated in the borehole.

This section will also present the derivations of the generalized heat transfer model and the application of the model in a field case. The temperature of the drilling fluid has been calculated both in the annulus as well as inside the drill pipe at various

depths for the considered well profile. The drill string temperature profile has been estimated using the calculated drilling fluid temperatures. Wellbore mechanical friction and downhole temperatures were thoroughly studied by varying the underlying drilling parameters in the model. Some of the parameters that affect the drill string and drilling fluid temperatures are as follows:

- Fluid properties – Viscosity, Density & Heat Capacity
- Flow profile – Laminar or Turbulent
- Wellbore Friction
- Well depth and profile
- Viscous pressure losses
- Geothermal gradient
- Drill string properties

3.2 Analytical Model for Wellbore Friction

Aadnoy *et al.* (2008) derived a simple model to calculate the torque owing to wellbore friction in case of directional and horizontal drilling, having rotational contact between the drill string and the wellbore wall. A normal side force 'N' results from the contact of the drillstring with the low side of the wellbore for a build section and with the high side of the wellbore for a drop-off section. As the drill string is rotating, a frictional force 'F_μ' resists the motion, and the torque resulting from this force is responsible for heat generation downhole.

The resisting friction force 'F_μ' is equal to the co-efficient of friction 'μ' multiplied by the resisting Normal Force 'N' (Coulomb Friction) and is given as

$$F_\mu = \mu . N. \quad (1)$$

The Normal Force 'N' is derived from the model in Fig. 20 assuming that the axial force 'F' is the same at both the ends of the small element and that $\Delta F = 0$. From the model in Fig. 20, the normal force is given by

$$dN = (F_a + w.R.\sin\theta).d\theta, \tag{2}$$

where w is the unit weight of drill string, R is radius of the drop-off section, θ is the inclination angle for the differential element chosen, and F is the axial force acting at the lower end of the drill string. For a small change in inclination angle, $d\theta = \Delta\theta$ and Eq. 2 can be approximated to be

$$\Delta N = F_a.\Delta\theta + w.R.\Delta\theta.\sin\theta_{avg}, \tag{3-a}$$

where θ_{avg} is the average inclination angle over the area of contact. This model as shown in Fig. 20 considers no change in azimuth of the wellbore with the section of the well under investigation lying in a 2D plane to simplify the analysis. Samuel (2007) has presented the comprehensive relation to estimate the side force also incorporating the effect of a change in azimuth as mentioned below

$$\Delta N = \sqrt{(F_a\Delta\alpha\sin\theta_{avg})^2 + (F_a\Delta\theta + w.R.\Delta\theta\sin\theta_{avg})^2}, \tag{3-b}$$

where $\Delta\alpha$ is the change in azimuth over the section length.

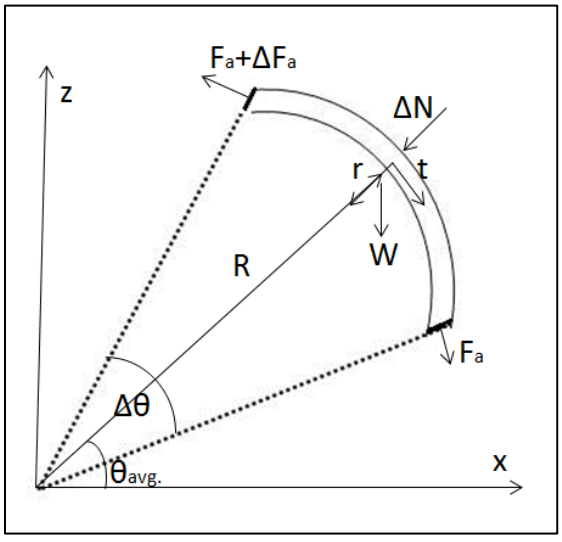

Fig. 20 - Forces acting on a small differential element of the drill pipe in a drop-off bend.

The torque acting on the drill string can now be calculated as

$$\tau(\theta) = r_o.\mu.\int_{N(\theta_1)}^{N(\theta_2)}|dN|, \tag{4}$$

where $\tau(\theta)$ is the torque calculated as a function of the angle of inclination, r_o is the outer radius of the drill string, and θ_2, θ_1 are the inclination angles over which the drill string is in contact with the wellbore wall. Finally, the heat generated downhole due to wellbore friction can be calculated in terms of power loss and is given as

$$P_{wf} = \tau(\theta).2\pi.rps, \tag{5}$$

where P_{wf} is the heat generated per second or power loss downhole and rps is the rotations per second of the drill string.

3.3 Analytical Model Wellbore Heat Transfer

The model in this study is based on the assumption that the heat transfer between the fluid in the drill pipe, the annular fluid, and the formation can be approximated by a steady-state heat transfer condition. The development of the model is depicted in Fig. 21.

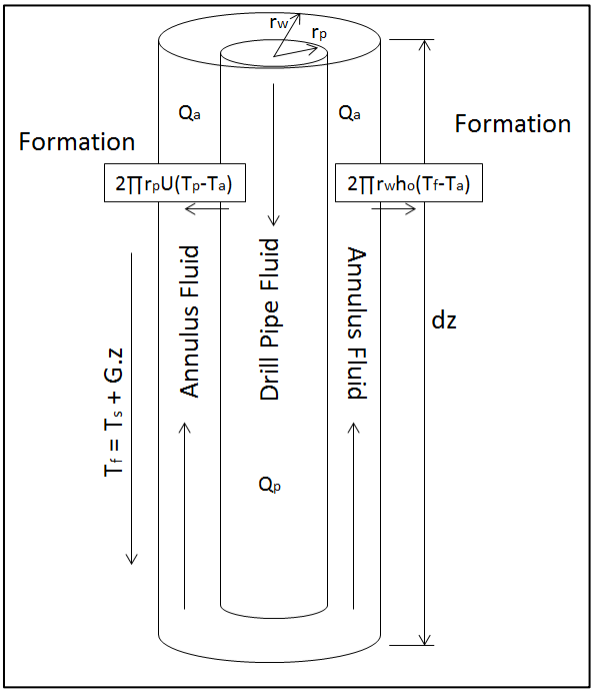

Fig. 21 – Differential element used to derive the heat transfer model.

A slab of thickness, dz, of the wellbore is shown here, assuming heat transfer in the radial direction and no significant longitudinal conduction. The flow of a drilling fluid in the wellbore can be divided into three parts:

- Downward flow through the drill pipe.
- Flow through the drill bit into the annulus.
- Upward flow through the annulus.

Fluid temperatures in each region depend on various thermal processes. The fluid enters the drill pipe at a known temperature and its temperature changes while flowing down the drill pipe based on the rate of thermal convection and rate of convective heat transfer radially between the fluid, the pipe wall, and the annulus. As the fluid flows up the annulus, the temperature is dependent on the rate of convection up the annulus, the rate of radial convection between the annulus fluid, the pipe wall, and the fluid in the drill pipe, and the heat transferred through the formation.

Frictional pressure losses in the drill pipe, across the drill bit, and in the annulus are calculated based on the flow regimes and incorporated in the model as heat generated. The heat generated from wellbore friction has been added to the annular fluid while performing the energy balance in the model. The entire wellbore has been divided into three zones based on the heat generated in different sections of the wellbore. Zone 1 has heat sources only due to the frictional pressure losses in the annulus as well as inside the drill pipe. Zone 2 has heat sources around the drill pipe section due to pressure losses as well as the heat generated from the wellbore friction over the zone of contact. Zone 3 has heat sources due to pressure losses around the drill collars, wellbore friction as well as the frictional pressure loss across the bit.

3.3.1 Assumptions

To arrive at the energy equilibrium equation using the differential element shown in Fig. 21, certain assumptions about the heat transfer mechanisms are required. They have been listed below:

1. Heat transfer within the drilling fluid is by axial convection.
2. The radial temperature gradient within the drilling fluid has been neglected.
3. Heat generation within the fluid by viscous dissipation may be neglected.
4. Fluid properties are independent of temperature.
5. A linear formation temperature gradient and a constant temperature at the borehole wall have been assumed.

3.3.2 Energy Equilibrium

The energy equilibrium within the system can be described by the following set of differential equations. Eq. 6 describes the heat flow inside the drill string as

$$\rho q C_p \frac{\partial T_p}{\partial z} + 2\pi r_p U\left(T_p - T_a\right) + \rho C_p \pi r_i^2 \frac{\partial T_p}{\partial t} = Q_p. \quad (6)$$

The first and second terms on the left represent the vertical convective heat transfer and the radial conductive heat transfer in the system. The third term is the accumulation of energy within the drill string. The right-hand term forms the total of all the energy source terms, respectively. The energy equilibrium in the annulus is expressed by Eq. 7 as

$$\rho q C_p \frac{\partial T_a}{\partial z} + 2\pi r_p U\left(T_p - T_a\right) + 2\pi r_w h_o\left(T_f - T_a\right) + Q_a = \rho C_p \pi (r_w^2 - r_o^2) \frac{\partial T_a}{\partial t}. \quad (7)$$

The terms on the left-hand side represent the vertical convective heat transfer within the fluid, radial conductive heat transfer between the drilling fluid and the drill pipe wall, radial conduction between the drilling fluid and the formation, and sum total of the heat-

source terms in the annulus. The right-hand term represents the heat energy accumulated in the annulus over a period of time. The linear geothermal gradient is given by Eq. 8 as

$$T_f = T_s + G.z. \tag{8}$$

The left-hand term is the formation temperature at any given depth below the surface. The right-hand terms represent the surface temperature and the increment of the temperature downhole with depth.

Assuming steady-state heat transfer conditions, the heat accumulation in the energy-equilibrium equations is assumed to be independent of time. Hence, the two heat transfer equations for energy balance within the drill string and the annulus become

$$\rho q C_p \frac{\partial T_p}{\partial z} + 2\pi r_p U\left(T_p - T_a\right) = Q_p \text{ and} \tag{9}$$

$$\rho q C_p \frac{\partial T_a}{\partial z} + 2\pi r_p U\left(T_p - T_a\right) + 2\pi r_w h_o\left(T_f - T_a\right) + Q_a = 0. \tag{10}$$

Upon solving for T_a from Eq. 9, we get

$$T_a = T_p + \frac{\rho q C_p}{2\pi r_p U}\frac{dT_p}{dz} - \frac{Q_p}{2\pi r_p U}. \tag{11}$$

Substituting Eq. 11 in Eq. 10, we get a second-order differential equation of the form as in Eq. 12 below

$$aT_p'' + bT_p' + cT_p = f(z), \tag{12}$$

where $f(z) = M.z + N$. The values of the coefficients a, b, c of the temperature derivative terms as well as the terms M, N as defined by the formulations are:

$$a = \frac{(\rho q C_p)^2}{2\pi r_p U}, \tag{13}$$

$$b = -\left(\frac{2\pi r_w h_o}{2\pi r_p U}\right).\left(\rho q C_p\right), \tag{14}$$

$$c = -2\pi r_w h_o, \tag{15}$$

$$M = G, \tag{16}$$

$$N = T_s + \frac{(Q_a + Q_p)}{2\pi r_w h_o} + \frac{[Q_p - (\rho q C_p) G]}{2\pi r_p U}. \quad (17)$$

The general solution to this second-order differential equation as defined in Eq. 12 to calculate the temperature inside the drill pipe as a function of the depth below the surface, is of the form as

$$T_p = C_1 e^{r_1 z} + C_2 e^{r_2 z} + Mz + N, \quad (18)$$

where the value of the exponent coefficients r_1, r_2 are give as

$$r_1, r_2 = \frac{(2\pi r_w h_o) \pm \sqrt{(2\pi r_w h_o)^2 + 4(2\pi r_p U)(2\pi r_w h_o)}}{2\rho q C_p}, \quad (19)$$

and the constants C_1, C_2 have to be solved for using the initial and the boundary conditions applicable to the system. The determination of the energy-source terms resulting from the frictional pressure losses within the system involves calculating them from various flow regime relationships developed and the type of the fluid being used. The bit-pressure losses are calculated based on the bit nozzle sizes and the flow rate across the nozzles. The detailed equations for both of these calculation methodologies have been defined in Appendix A-1.

3.3.3 Initial and Boundary Conditions

The initial and boundary conditions to solve the differential equations have been defined below. The temperature of the drilling fluid at the drill pipe inlet has been assumed to be a constant. The temperatures in the drill pipe and in the annulus at the different zone boundaries are equal to each other. The temperature in the drill pipe and in the annulus is also equal at the bottomhole. These six boundary conditions help us solve the six different constants for obtaining a result to the set of differential equations

developed above. The initial and boundary conditions applicable to this system are as follows:

$$T_p = T_{pi} \; at \; z = 0, \tag{20-a}$$

$$T_{p(zone1)} = T_{p(zone2)} \; at \; z = z_1, \tag{20-b}$$

$$T_{a(zone1)} = T_{a(zone2)} \; at \; z = z_1, \tag{20-c}$$

$$T_{p(zone2)} = T_{p(zone3)} \; at \; z = z_2, \tag{20-d}$$

$$T_{a(zone2)} = T_{a(zone3)} \; at \; z = z_2, \tag{20-e}$$

$$T_p = T_a \; at \; z = z_3. \tag{20-f}$$

3.4 Case Study for the Model

The proposed model has been applied to a well profile having 17,000 ft of measured depth (MD) with the drilling parameters and the operating conditions as defined in Appendix B-1. The well profile has also been shown alongside as Fig. 67 in Appendix B-1. The well was assumed to have no drill bit size change and no casing set. The temperature profiles of the drilling fluid in the drill pipe and in the annulus were generated under these conditions. A Bingham-Plastic drilling mud was used to drill the well, and the loss of mud during the drilling operation was neglected. The flow regime in the drill pipe was found to be turbulent while the flow in the annulus of drill pipe and drill collars was laminar. The frictional pressure losses were converted to heat generated downhole and added to the respective heat source terms in the mathematical model developed in the previous section. The well profile consists of a single-build section and then a tangent section.

The drill pipe was assumed to be in contact with the low side of the wellbore throughout the curved section between the inclination angle of 5° and 80°. The drill pipe

was also in contact with the wellbore in the tangent section of the well profile, thus generating a lot of heat from frictional forces. The temperature of the drilling fluid at the drill pipe inlet was taken to be 80°F. The temperature profiles of the mud in the annulus and in the drill pipe as estimated by the mathematical model have been shown in Fig. 22.

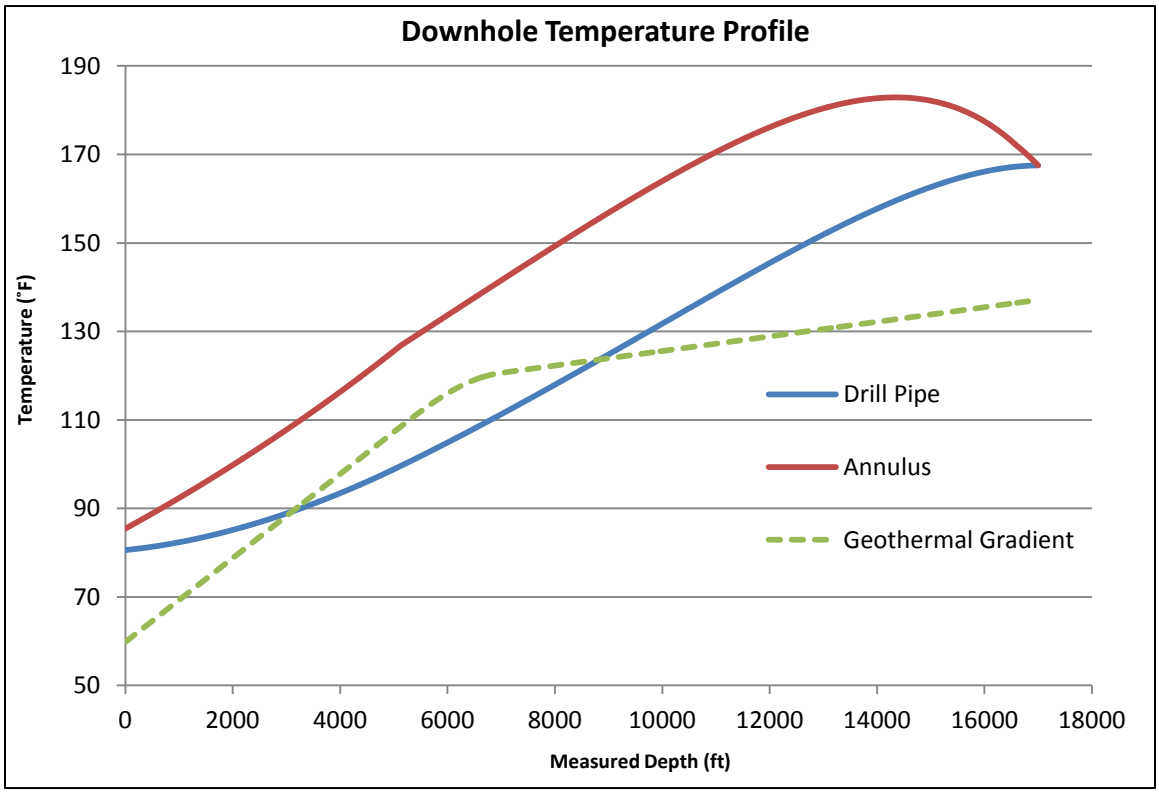

Fig. 22 – Temperature profile of the drilling fluid within the drill pipe and in the annulus during circulation as estimated by the proposed mathematical model.

The model suggests that the maximum temperature of the drilling fluid generally occurs in the annulus of the drill string at some depth above the bottomhole. This phenomenon has also been reported by Holmes *et al.* (1970) as well as Kabir *et al.* (1996), and agrees with profiles obtained from measured mud temperatures during mud circulation. Kabir *et al.* (1996) presented a physical explanation for this phenomenon and also derived a simple analytical expression for the depth at which the maximum fluid temperature occurs. The drilling fluid coming out of the annulus is at slightly higher temperatures than the fluid entering the drill pipe and is within reasonable expectations.

The bottomhole temperature is higher than the formation temperature at that depth owing to the deviated section of the wellbore that results in a very slight increase in temperature along the borehole wall and conducts a lot of heat generated along the entire length of the wellbore.

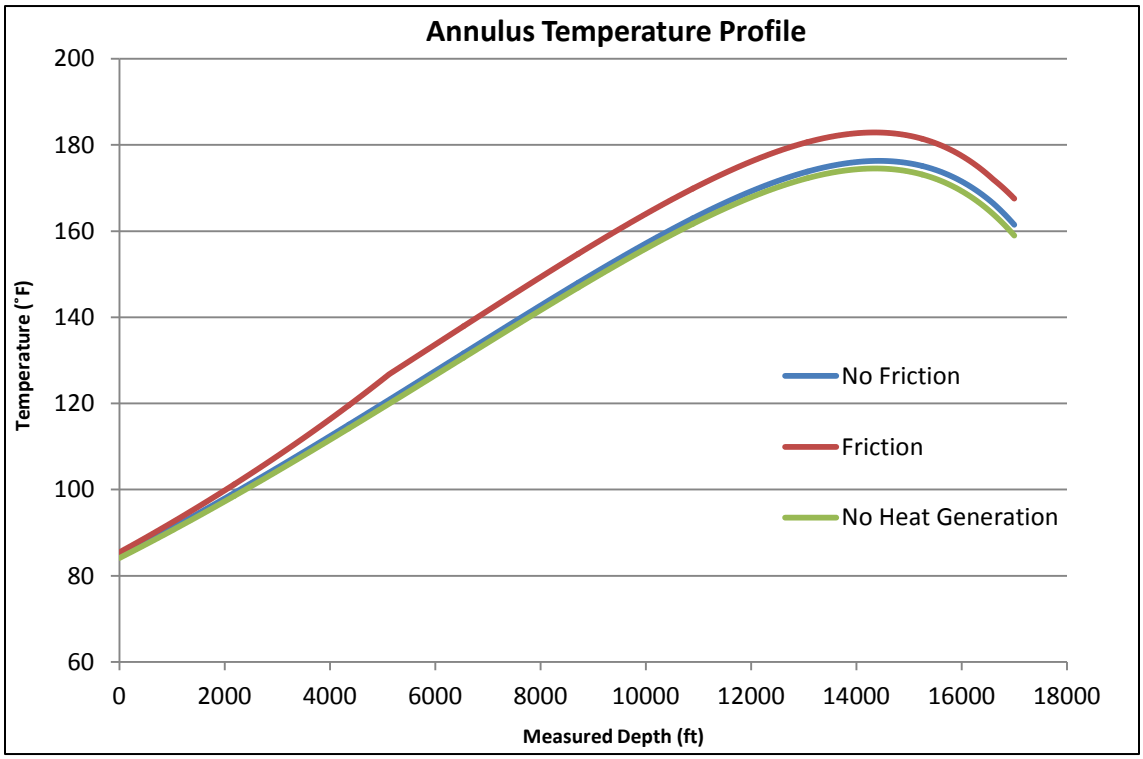

Fig. 23 – Effect of friction and heat generation on annulus temperatures of the fluid.

Fig. 23 shows a comparison of the annulus temperature under varying conditions of heat generation. Heat generated from well friction and pressure losses, heat generated only from frictional pressure losses, and no heat generation conditions are analyzed separately to study the impact of wellbore friction and downhole heat generation. The wellbore friction increases the temperature of the drilling fluid in the annulus by approximately 10˚F for the well profile considered. The maximum temperatures experienced downhole certainly increase as a result of the heat generated by the borehole wall friction as expected. The changes in the annulus temperatures for the no-heat-

generation condition and no-well-friction conditions are also in agreement with the results obtained by Marshall *et al.* (1982). The no-heat-generation condition suggests that frictional pressure losses are not amongst the most significant parameters that affect the downhole temperatures of the drilling fluid.

Fig. 24 below estimates the average increase in temperature of the drill string owing to friction in the contact zone. This increase in temperature is within reasonable expectations and this method of approximation can be effectively used to better understand the temperatures encountered by the drill string downhole.

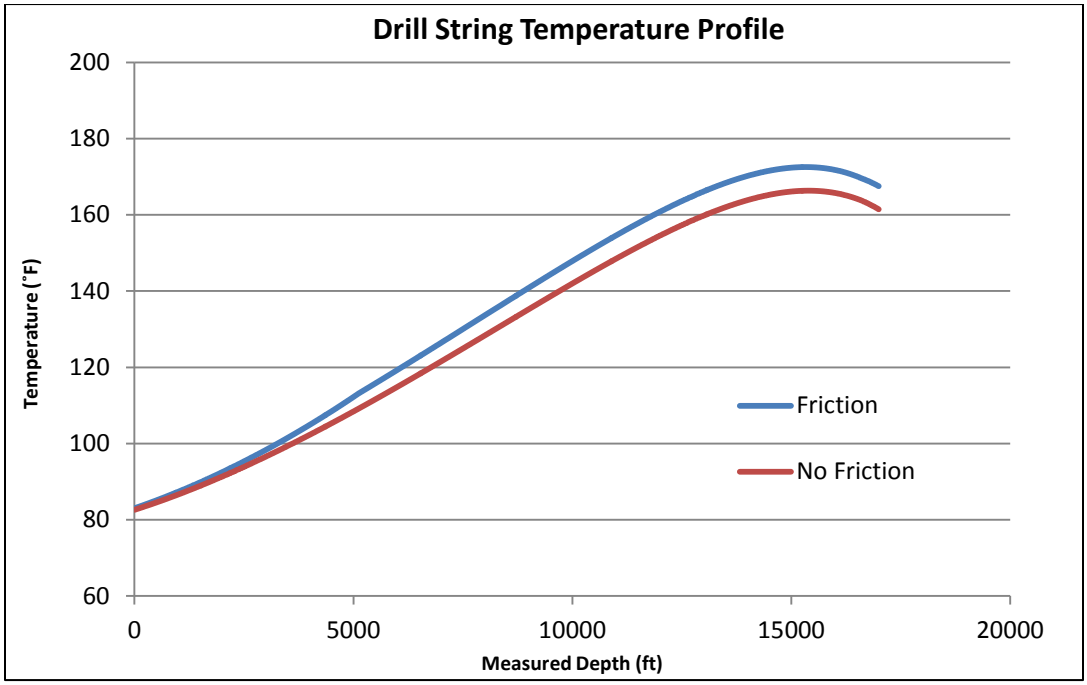

Fig. 24 – Effect of wellbore friction on the drill string temperature profile.

3.5 Variation of Drilling Parameters

The effect of varying mud properties and drilling parameters on the downhole temperature of the drilling fluid in the annulus of the drill string has been shown below in Fig. 25 through Fig. 28. The results obtained are in agreement with the numerical simulation analysis performed by Marshall *et al.* (1982). In addition, Fig. 29 shows the

effect of the rotational speed of the drill string on the annular temperatures in the contact zone and compares it against the case when the heat generated from friction is neglected.

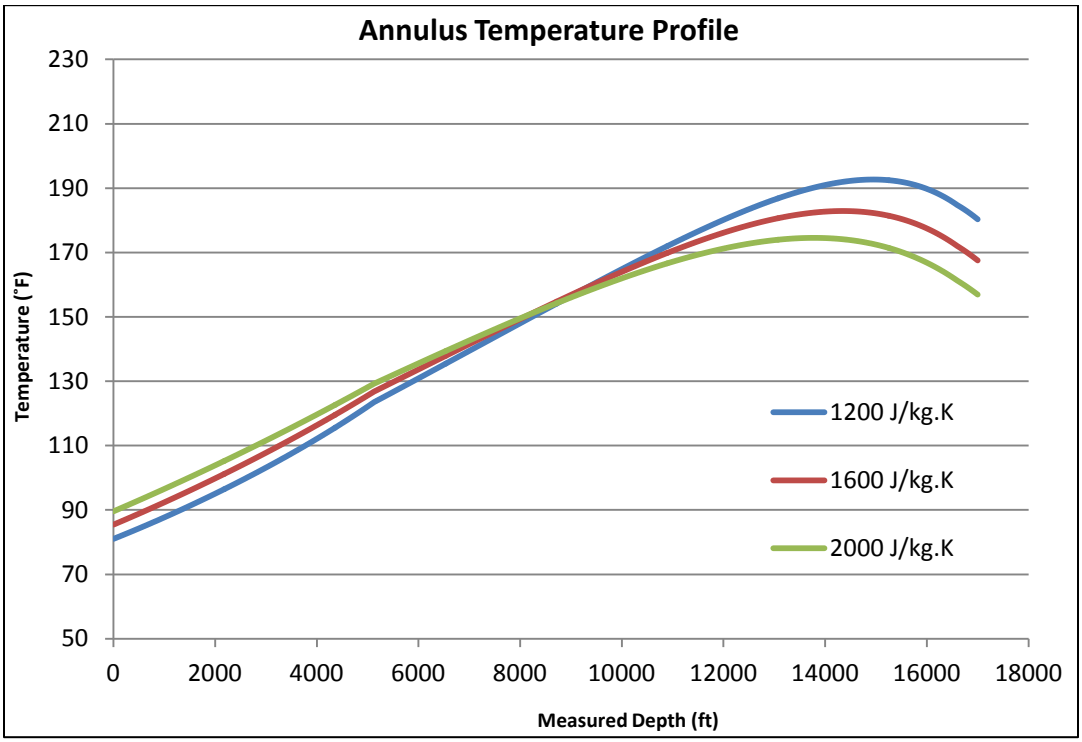

Fig. 25 – Effect of heat capacity of the drilling fluid.

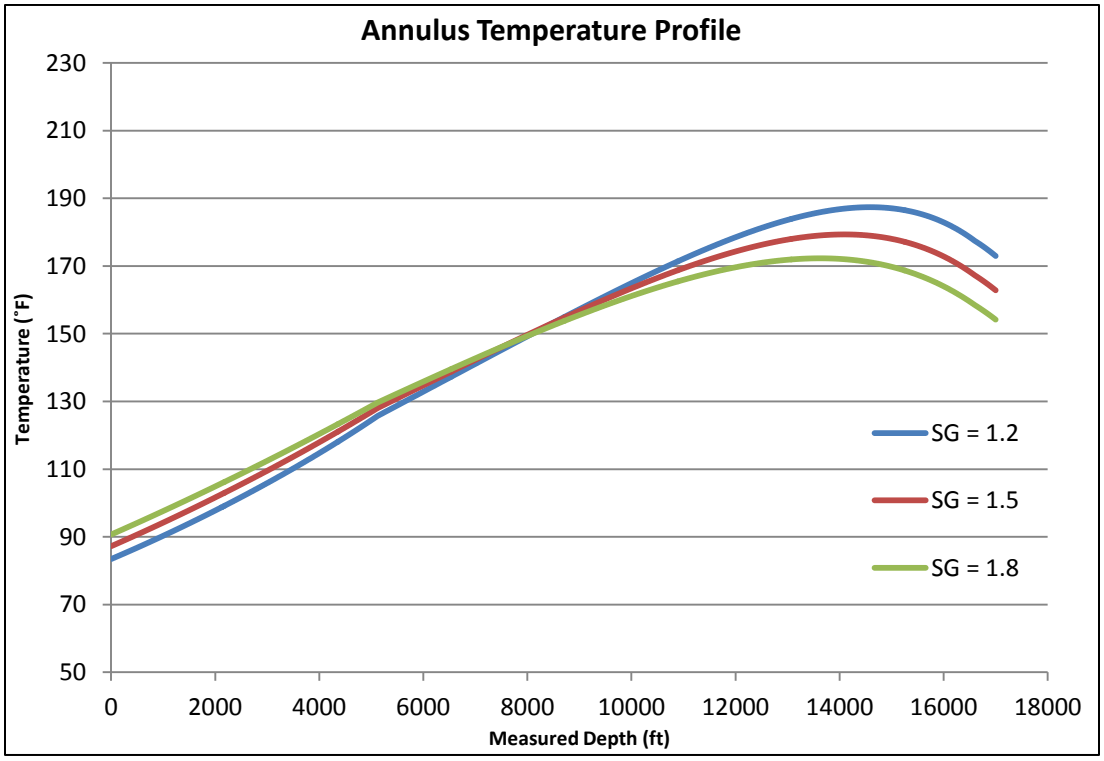

Fig. 26 – Effect of specific gravity of the drilling fluid.

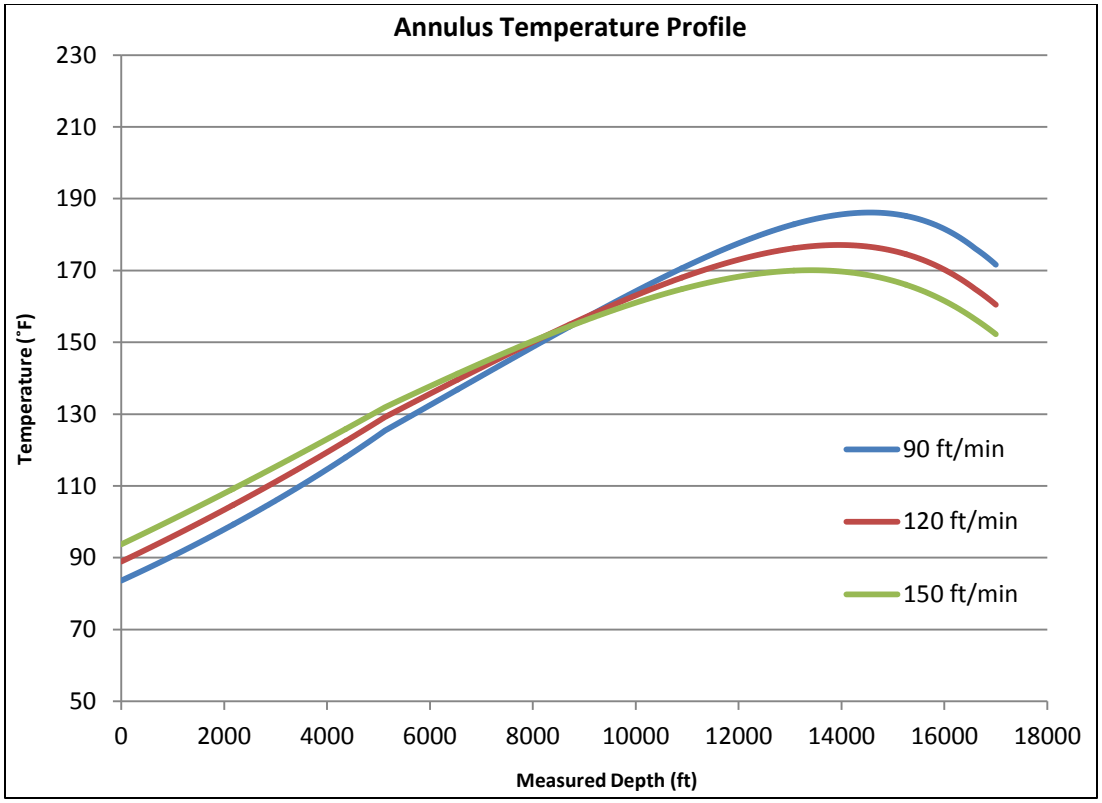

Fig. 27 – Effect of minimum annular flow velocity.

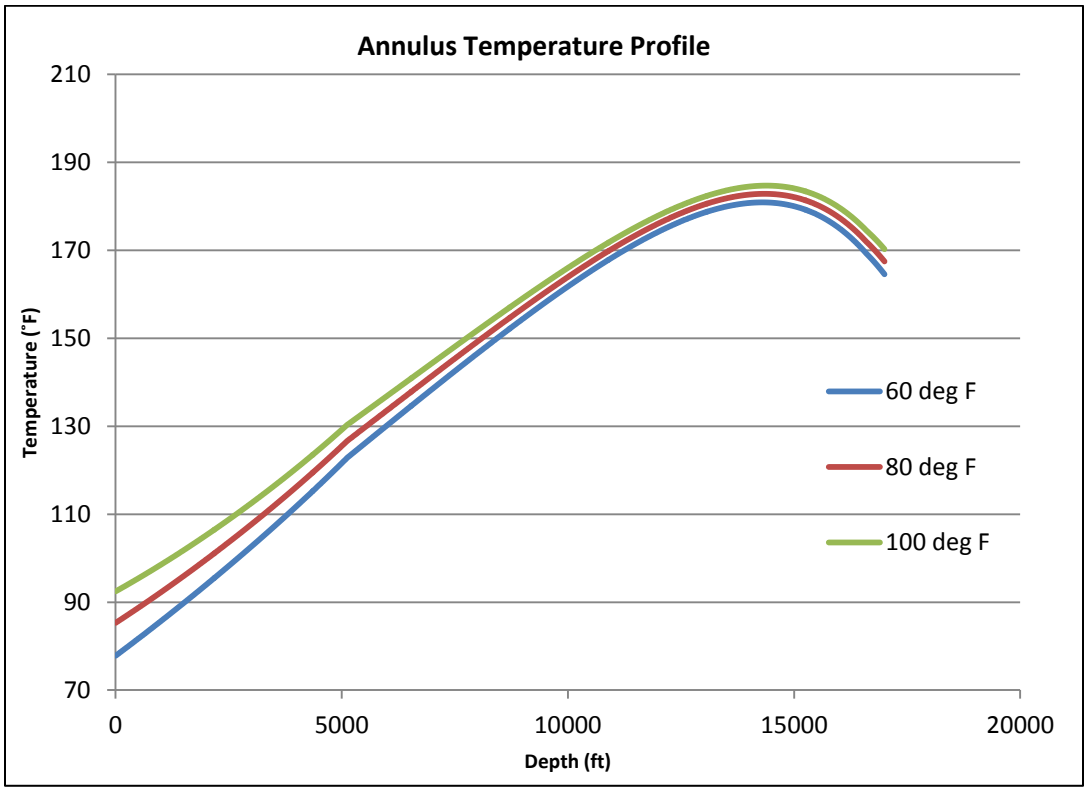

Fig. 28 – Effect of inlet temperature of the drilling fluid at the drill pipe.

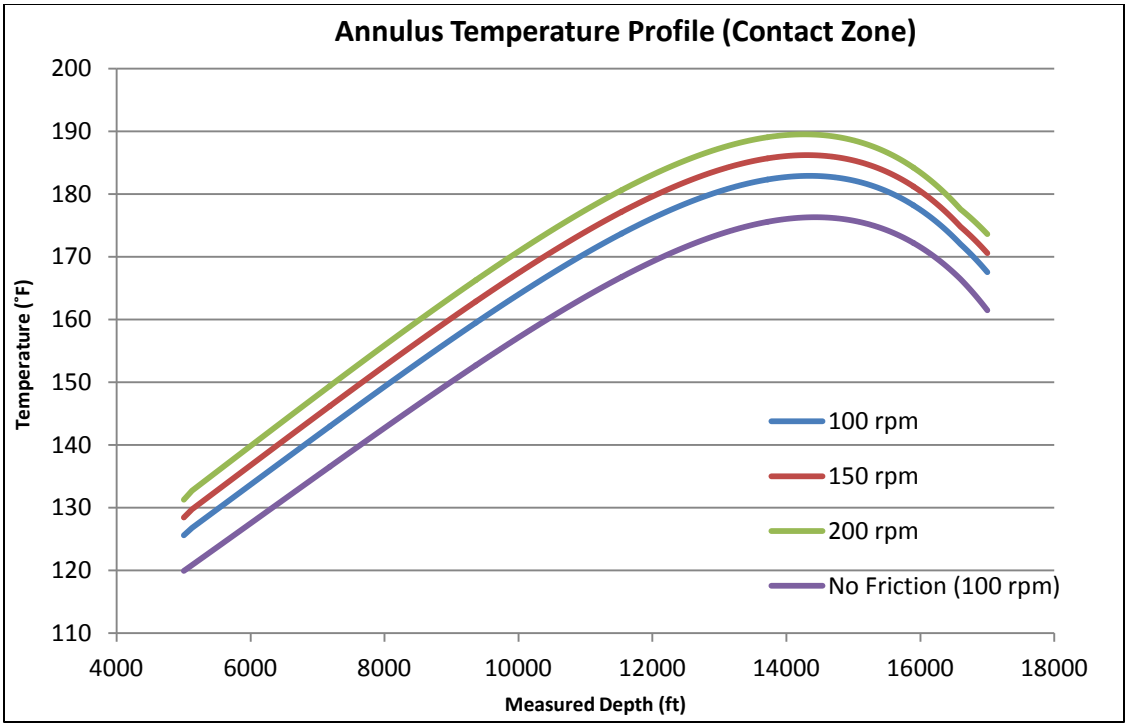

Fig. 29 – Effect of rotational speed of the drill string.

The variations of heat capacity, specific gravity and the minimum annular flow velocity have a similar trend as shown by their respective plots. For all the three cases, the annular temperature profile is steeper for lower values of these parameters suggesting that a higher increase in temperature is experienced along the well path. However, as the value of these parameters increases, the temperature profile becomes less steep showing lower values of maximum temperature encountered downhole. There also seems to be a particular depth where the cross over takes place between the respective curves and the change in underlying parameters has no effect on temperature at that depth. This analysis can be effectively used to control undesired downhole temperatures by varying any of these underlying parameters. The variation of inlet temperatures of the drilling fluid as well as rotational speed of the drill string are pretty straightforward suggesting that higher temperatures will be encountered downhole for higher inlet temperatures as well as high values of rotational speed.

CHAPTER 4

FIELD APPLICATION & VALIDATION

4.1 Introduction

The proposed analytical model for estimating the downhole temperatures of the drilling fluid has been validated in this section of the study using two practical field cases. Two different field cases, one for a deviated well and the other one for a horizontal well, have been presented. The estimated temperature profile using the model is compared against the actual temperature measured downhole using MWD tools. The zones having the maximum increase in temperatures have been identified based on the temperature profile generated during the drilling operation. The increase in temperature for a particular depth in the well for the entire bit run has also been presented as another successful application of this model. The impact of drilling parameters on temperatures has also been analyzed and can be used effectively to maintain a better check on undesired temperatures.

This simple analytical model can be suitably applied to field cases based on the well profile and can be effectively used to predict the maximum temperatures to be encountered downhole while drilling ahead as planned. An accurate estimation of maximum temperatures will help us prevent severe downhole friction heating in the future.

4.2 Deviated Well

The first field case presented here for a deviated well provides the real-time measured values of downhole temperature using two different MWD tools. The field data

reported here comprises the drilling of 26 stands having a total length of 2,431 ft between the measured depths of 11,834 ft and 14,265 ft. This field case is for a deviated well that has a long tangent section, and this considered drilling activity represents further drilling of this tangent section.

4.2.1 Drilling Activity

The progress of the drilling activity with the measured depth that has been reported for real time temperature data while drilling has been shown in Fig. 30. This plot reports the drilling operation as it continues over a period of about two days.

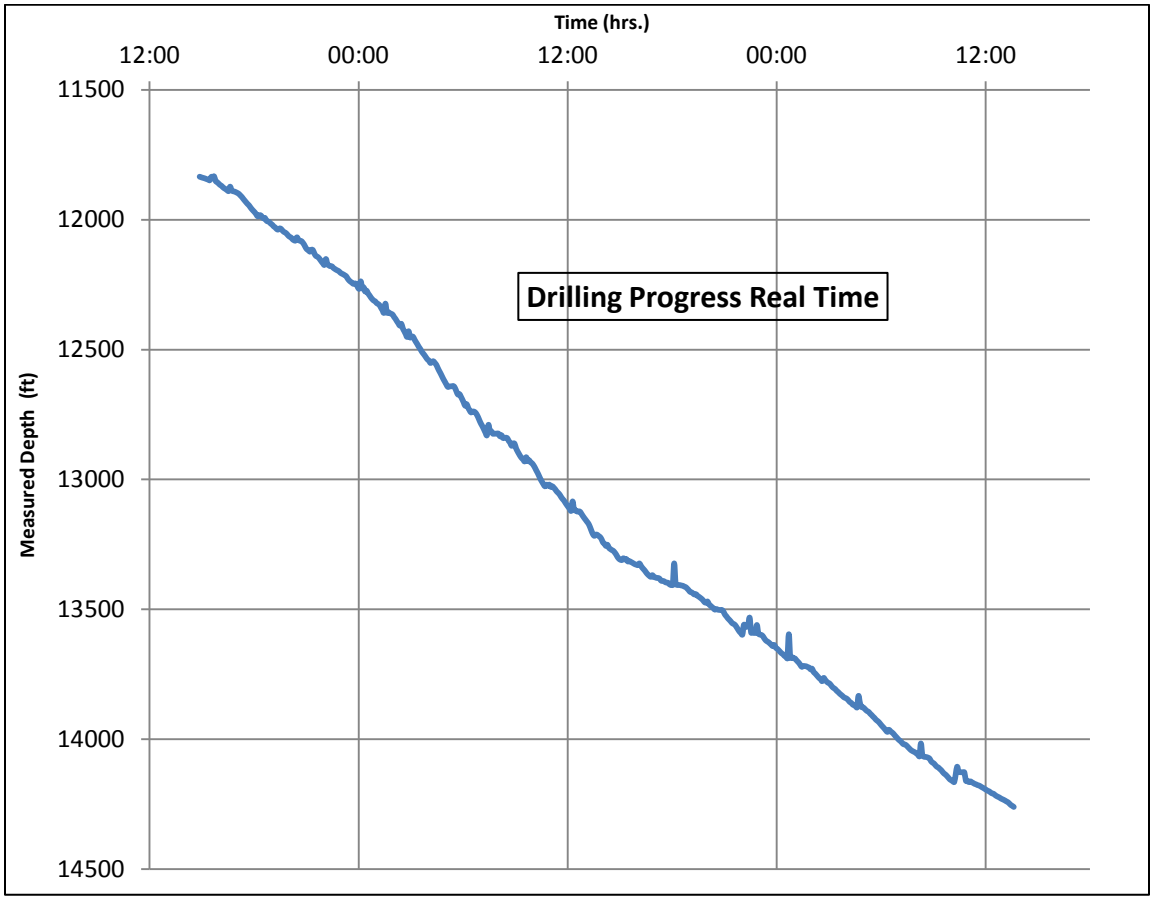

Fig. 30 – Drilling progress in real-time for the case of deviated well.

The drilling parameters for this field case, as reported in Appendix B-2, have been used in the proposed analytical model to calculate the temperature profile of the drilling

fluid within the drill pipe as well as in the annulus. The temperature profile generated using the model after drilling 26 stands has been shown in Fig. 31. This temperature profile is clearly within reasonable expectations and in accordance with the other downhole temperature profiles, as mentioned in literature. The maximum temperatures occurring downhole are not at the bottom of the well, but a depth slightly higher than the bottom as explained in the previous section of this study. The variation of the geothermal gradient, along with the measured depth for the entire well profile, has also been shown.

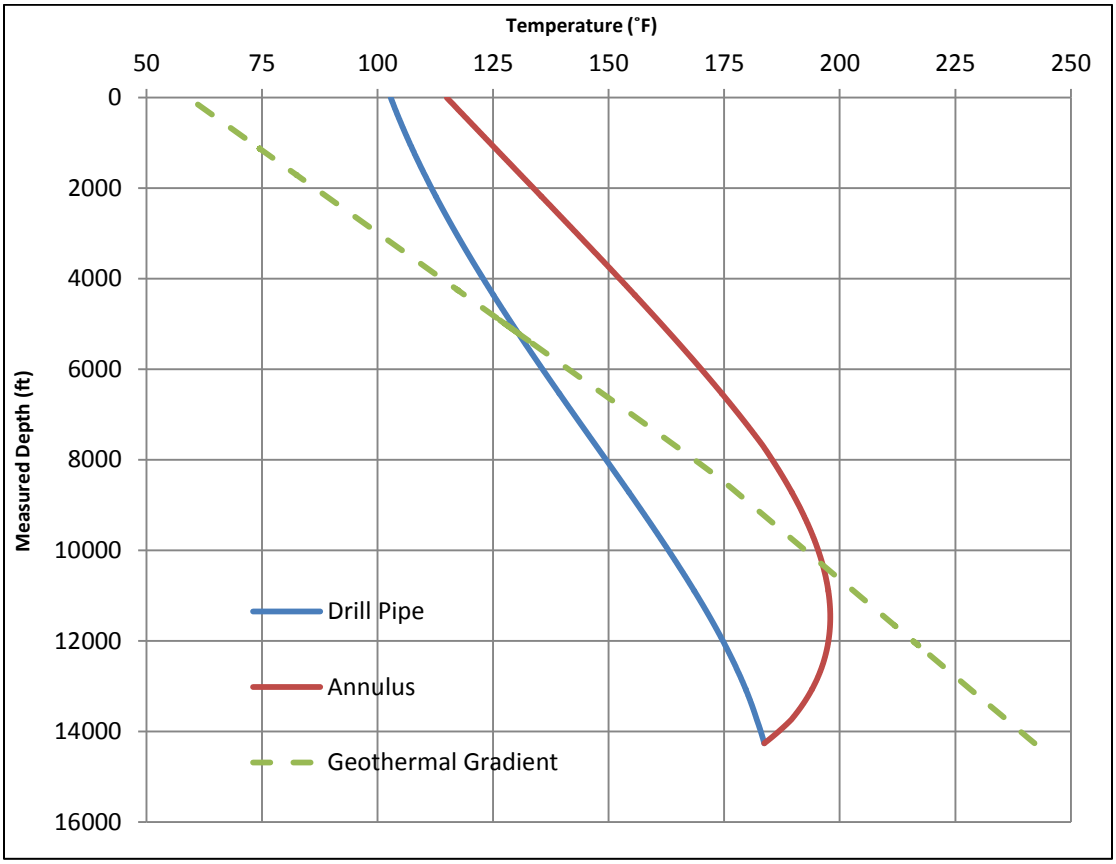

Fig. 31 – Temperature profile of the drilling fluid within the drill pipe and in the annulus after drilling the 26th stand.

4.2.2 Model Validation

The temperature profile for the drilling fluid in the annulus, calculated using the model, has been compared against the temperature data measured in real time by using

two different MWD tools as the well is drilled from the measured depth of 11,834 ft to a depth of 14,265 ft. The temperature profile from the model has been calculated under a steady-state condition for each stand as it is drilled. This annulus temperature at the depth of the measuring MWD tool for each stand drilled has been plotted to compare it against the real-time measured data. The depths of the two different MWD tools from the bottomhole were 95 ft for 'MWD Tool 1' and 37 ft for 'MWD Tool 2'. The comparison between the calculated and the measured values have been shown in Fig. 32 and Fig. 33.

The increase in annulus temperatures as a result of drilling have also been calculated from the model and then analyzed to obtain an estimate of the increase in temperature since drilling the first stand until completing the drilling operation after the 26th stand. The annulus temperature profiles of the drilling fluid for Stand 1 and Stand 26 have been compared in Fig. 34.

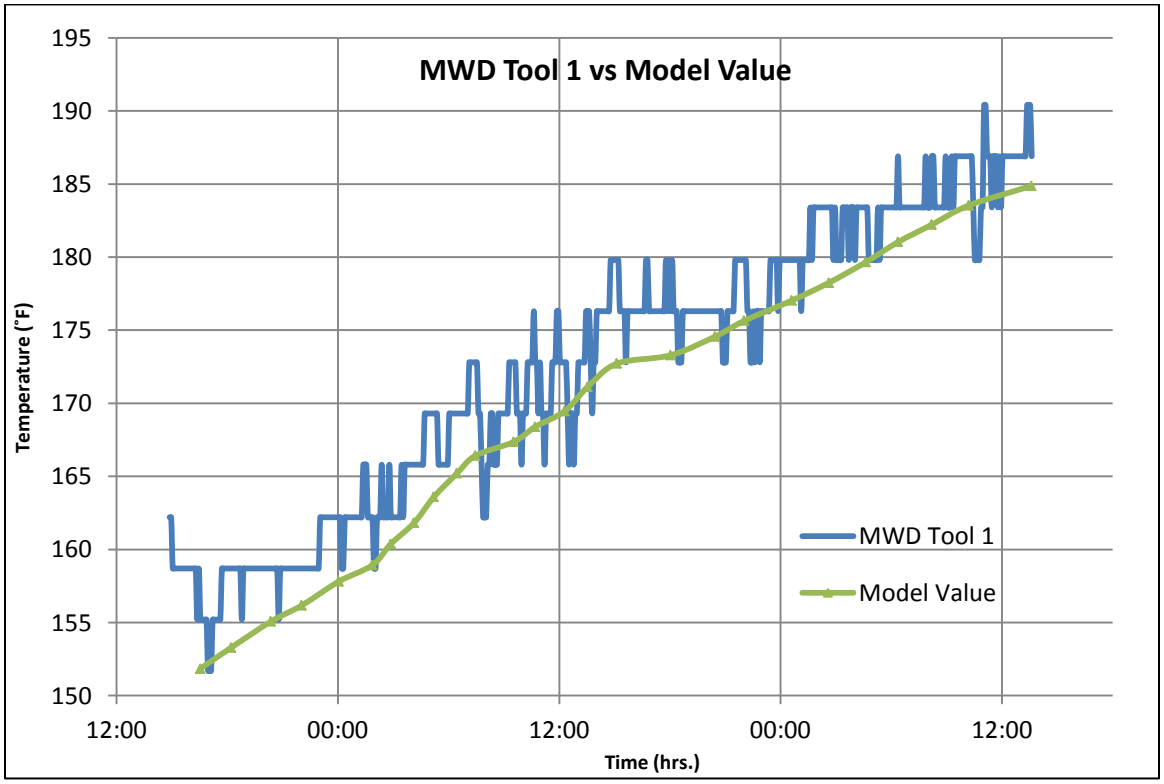

Fig. 32 – Model validation for 'MWD Tool 1' vs. model value.

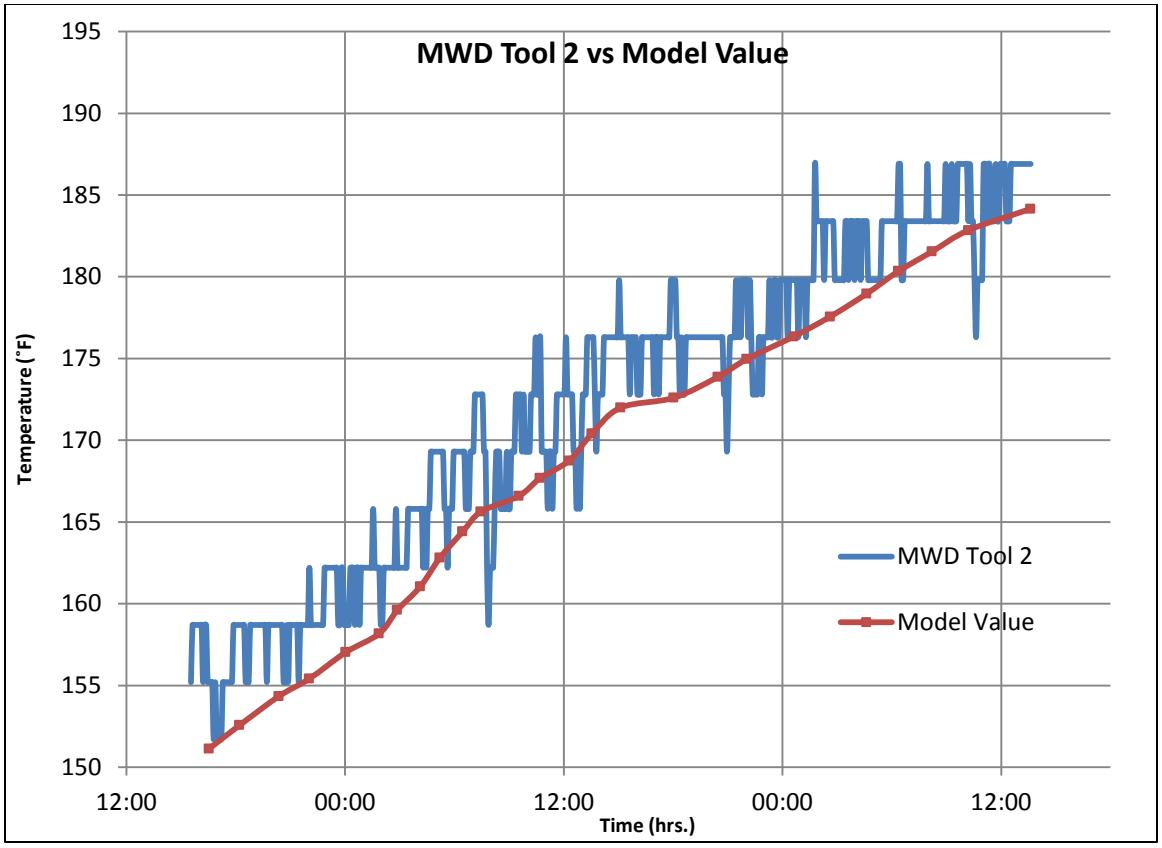

Fig. 33 – Model validation for 'MWD Tool 2' vs. model value.

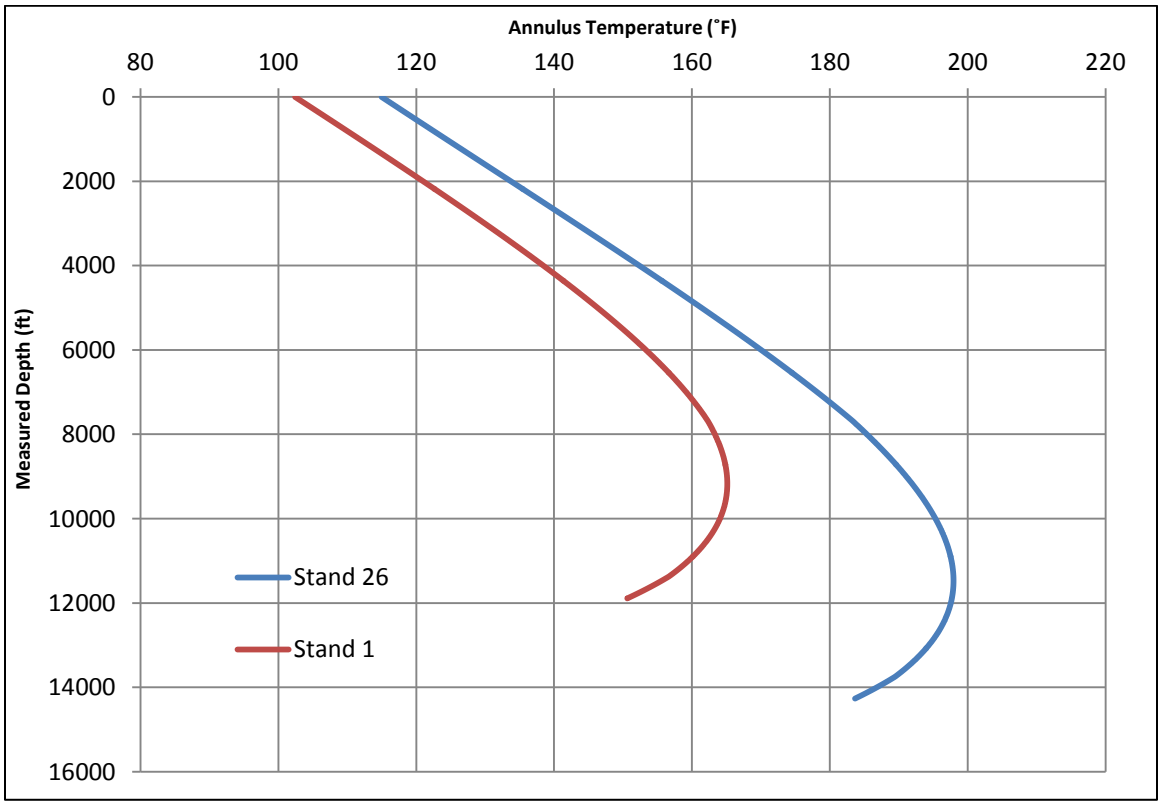

Fig. 34 – Annulus temperature profiles of the drilling fluid after drilling stands 1 and 26.

Fig. 32 and Fig. 33 show that the downhole temperatures estimated by the analytical model closely follow the real time temperatures measured downhole using MWD tools. The values predicted by the model are slightly lower than the actual values due to the lack of availability of all the required field data that led to neglecting some downhole heat sources like mechanical work done by the bit. Fig. 34 shows that the temperature in the annulus of the drilling fluid increased by almost 50°F near the measured depth of 11,900 ft as we drilled from Stand 1 until Stand 26. The increase in annulus temperatures for three different depths at 11,845 ft, 12,845 ft, and 13,845 ft have been plotted in Fig. 35 as the drilling activity progresses. This helps us to better understand and more correctly estimate the increase in temperature at any particular depth with continued drilling activity.

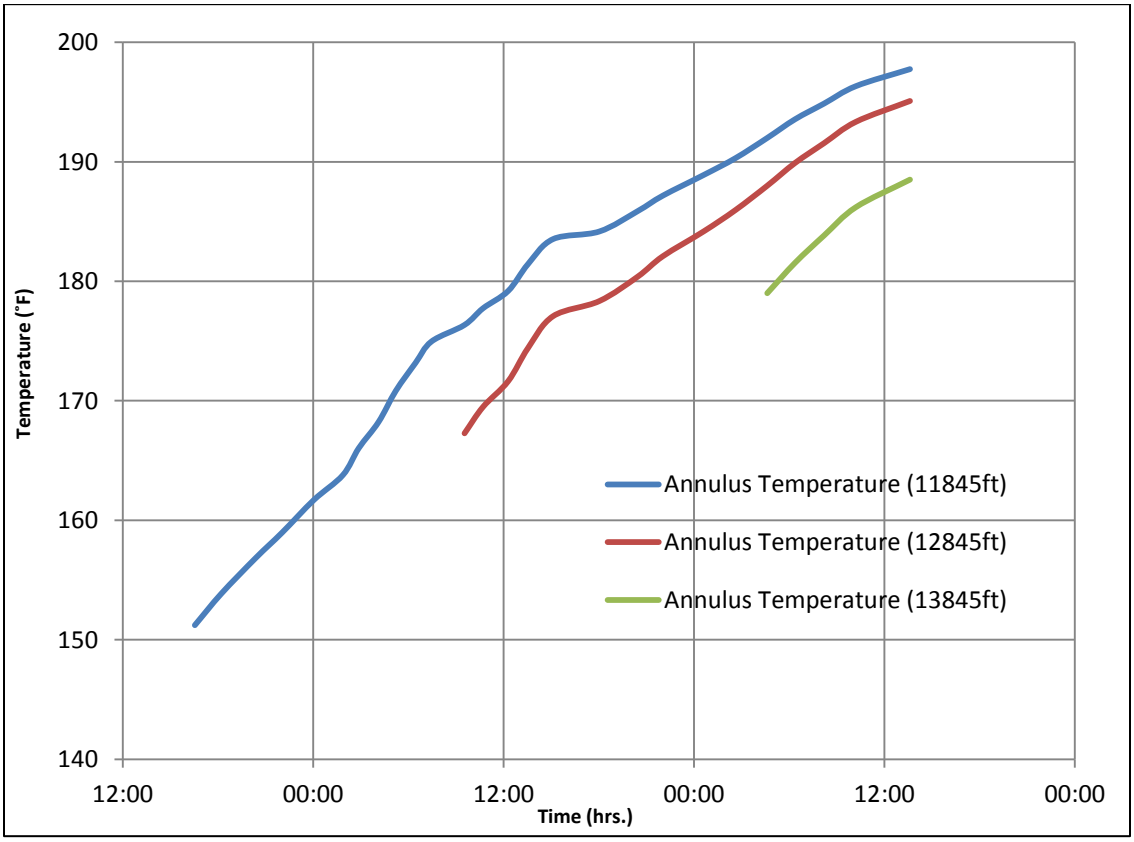

Fig. 35 – Increase in annulus temperatures at three different depths with continued drilling activity after drilling stand 1 until drilling stand 26.

4.3 Horizontal Well

The second field case presented here is for a well that has long tangent section followed by a long horizontal section. The drilling activity reported consists of drilling 62 stands having a total length of 5,929 ft from a measured depth of 17,554 ft until a depth of 23,483 ft. The downhole temperatures have been measured using a MWD Tool and the measured field data is compared with the estimated temperature profile using the model.

4.3.1 Drilling Activity & Validation

The drilling activity reported over the period of about three and a half days to drill this section of the well has been reported for real time operation progress in Fig. 36. The drilling parameters for this field case have been reported in Appendix B-3. The comparison between the measured field data and the estimated downhole annulus temperature using the model has been shown in Fig. 37.

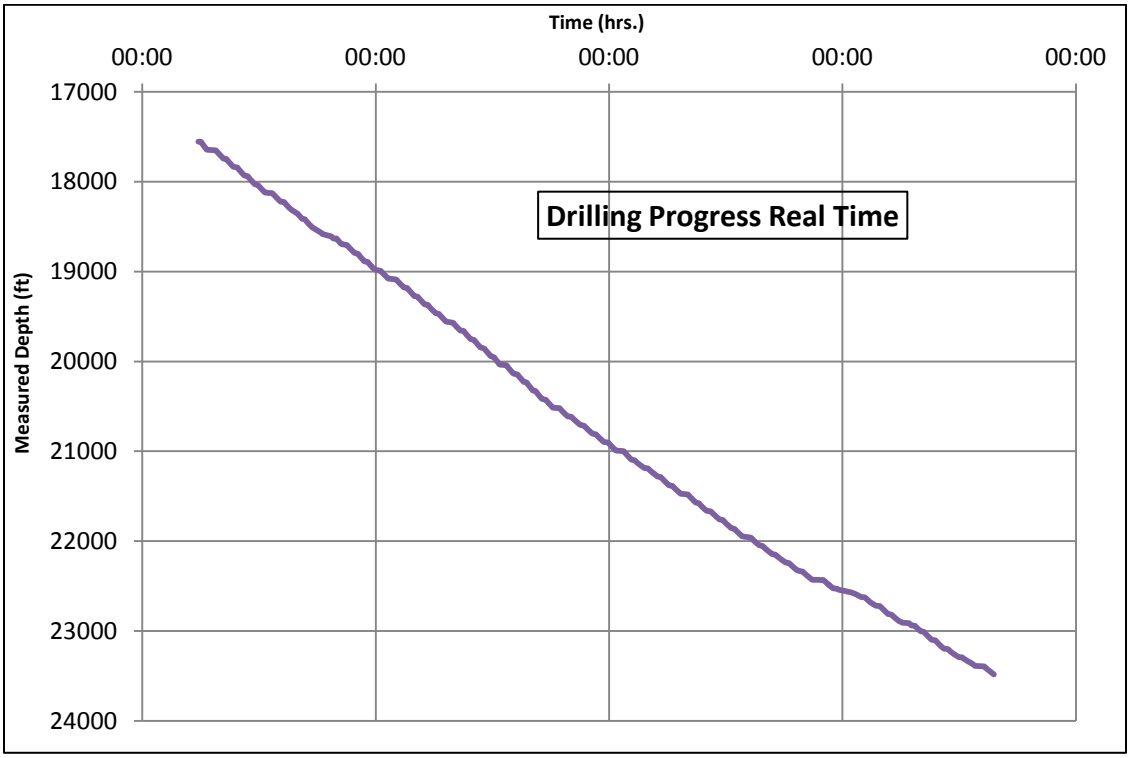

Fig. 36 – Drilling progress in real-time for the case of horizontal well.

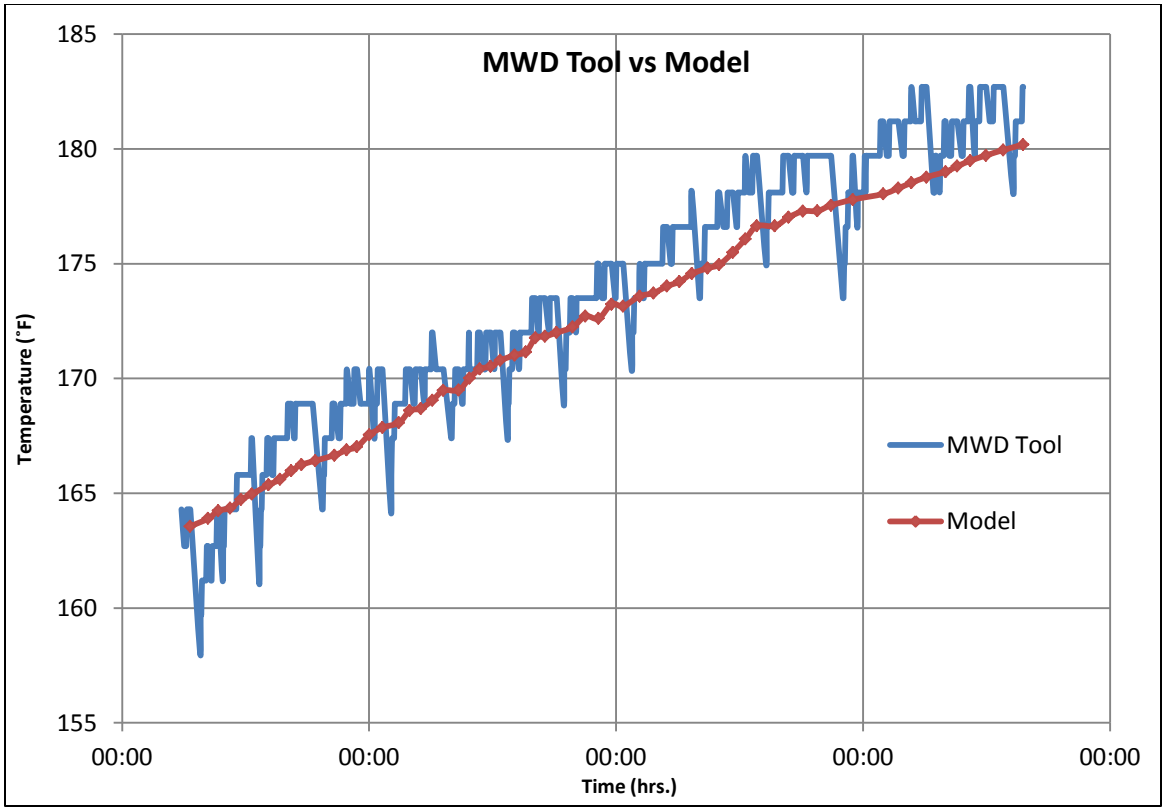

Fig. 37 - Model validation for the real time data measured using MWD Tool and data estimated using the model.

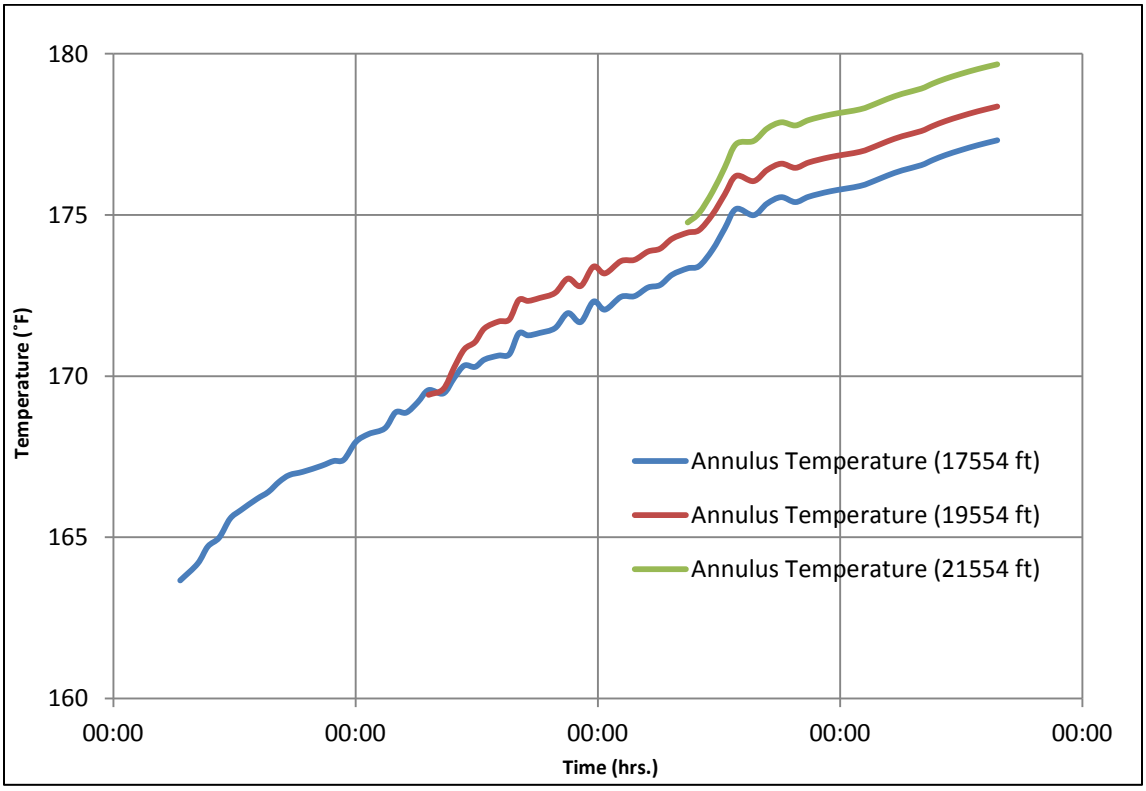

Fig. 38 – Increase in annulus temperatures at three different depths after drilling stand 1 until drilling stand 62.

The downhole temperatures estimated by the model for the case of drilling a horizontal well also closely match the real time data measured in the field as shown in Fig. 37. The predicted values are, again, slightly less than the actual values, due to the lack of availability of all the required real time data to account for all the downhole heat sources.

The increase in annulus temperatures due to the drilling activity has been shown in Fig. 38 and the change in temperature with time has been estimated at three different depths as drilling progressed to the desired target depth. An increase of about 17˚F is predicted for the depth from where this drilling activity started. Higher temperatures are observed as we go into the deeper sections of the wellbore in this analysis unlike the previous case in Fig. 35 as the depth having the maximum fluid temperature in the annulus is below the three well depths that have been analyzed in Fig. 38.

4.3.2 Effect of Friction & Drilling Parameters

The increase in downhole temperatures due to the effect of wellbore friction for this case at a depth of about 17,550 ft has been shown in Fig. 39. This change in temperature during the drilling activity has been attributed to the constant rotation of the drill string against the borehole wall that is responsible for downhole heating. An increase in temperature of about 10˚F has been estimated due to wellbore friction using the model.

The effect of the flow rate as well as the rotational speed of the drill string on downhole temperatures of the drilling fluid at a depth of about 17,550 ft has also been shown in Fig. 40 and Fig. 41. Higher flow rates and rotational speed tend to lead towards higher temperatures for this case of drilling the horizontal well. These drilling parameters can be effectively manipulated to keep a check on undesired temperatures downhole.

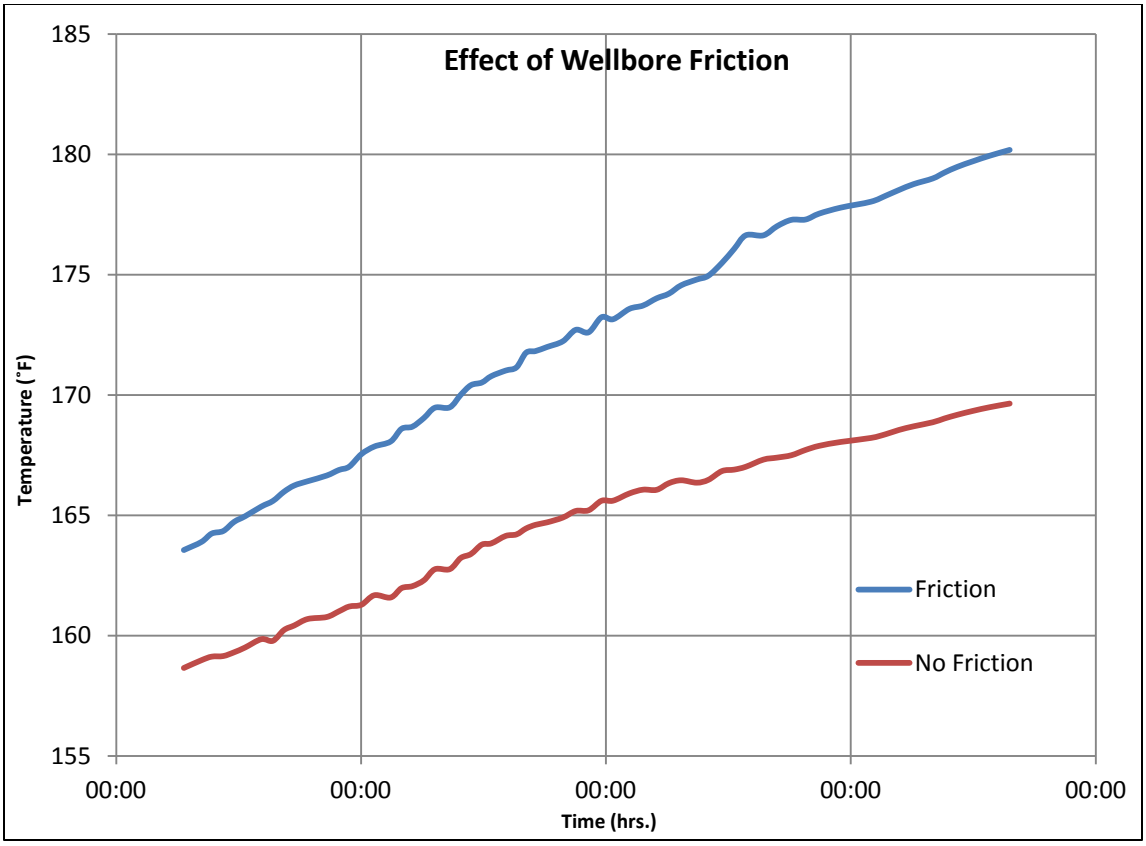

Fig. 39 – Effect of wellbore friction on downhole temperatures for the horizontal well.

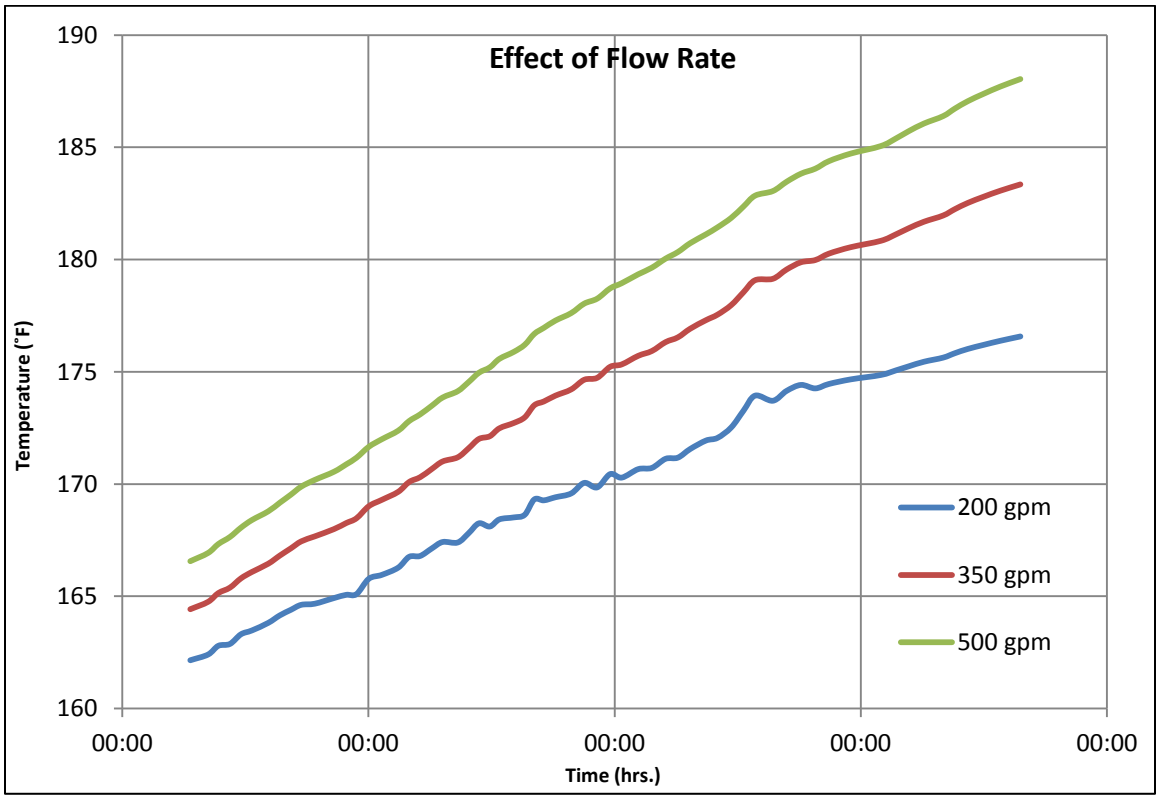

Fig. 40 – Effect of flow rate on downhole temperatures estimated using the model.

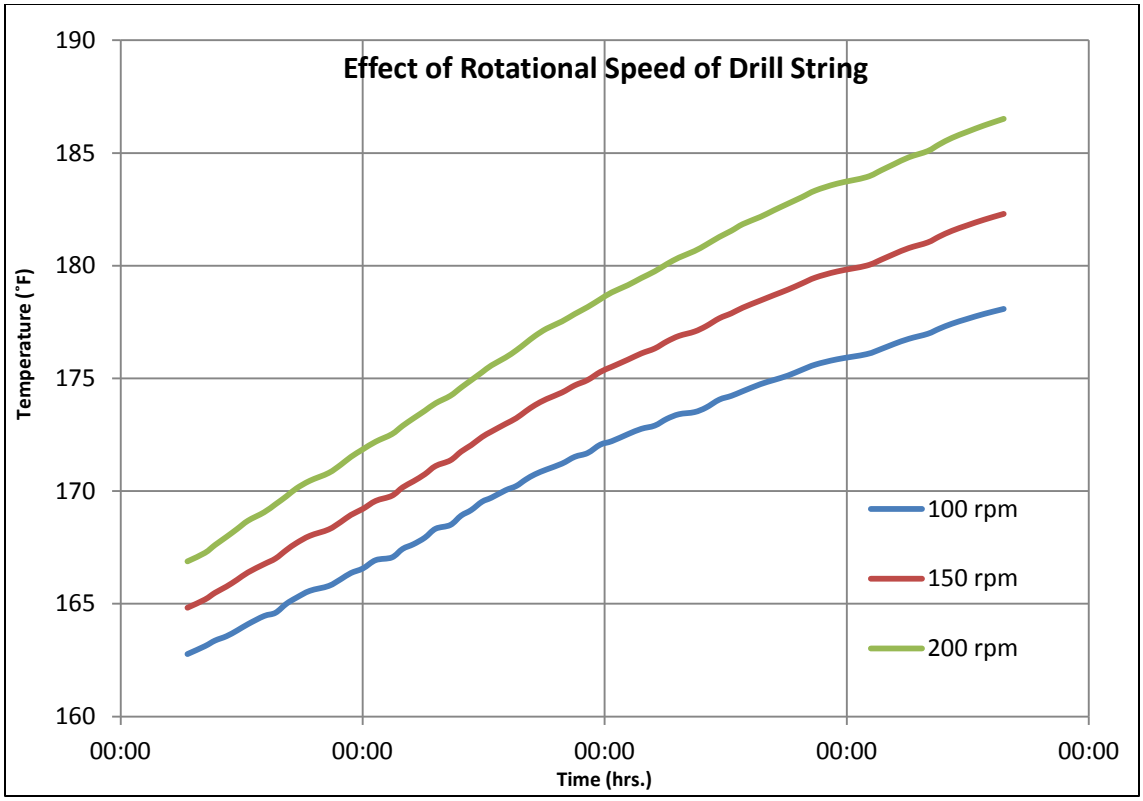

Fig. 41 – Effect of rotational speed on downhole temperatures estimated using the model.

CHAPTER 5

CASING WHILE DRILLING (CwD) OPERATIONS

5.1 Introduction

The benefits of casing while drilling have become apparent to the industry as complex wells are drilled through depleted reservoirs. Casing while drilling operations help to reduce lost circulation, improve wellbore stability, increase the fracture gradient, mitigate formation damage, and eliminate non-productive time (NPT). These benefits, if effectively realized, would be helpful in drilling through depleted zones, providing wellbore strengthening, and completing the well with fewer casing or liner strings.

The plastering effect mechanism responsible for increasing the fracture gradient of the formation is under extensive research and has been studied qualitatively and through field observations. It has been described by Karimi *et al.* (2011) as the smearing or plastering of the generated cuttings and the added lost circulation material into the wellbore wall as a result of the continuous contact between the wellbore and the casing. However, the complex nature of the plastering effect arising from the involvement of multi-disciplinary problems has made it difficult to quantify the realized benefits in terms of a comprehensive model.

This study aims to contribute to the on-going quantitative studies by addressing another important drilling parameter, the downhole temperature of the drilling fluid during casing while drilling, which may play an important role in realizing the benefits of the plastering effect. The casing is believed to be in continuous contact with the wellbore wall as a result of the small annular clearances, thereby generating a great deal of heat

downhole attributable to frictional forces. An analytical model has been proposed by this study to quantify this heat loss and subsequently incorporated in the wellbore heat transfer model as developed in the earlier section to calculate the operating temperatures. An accurate estimate of the downhole temperatures of the drilling fluid while drilling with a casing will help to clarify one of the underlying variables of the plastering effect.

The paper presents four practical casing while drilling field cases to suggest potential applications for the proposed model. Downhole temperatures of the drilling fluid have been calculated along the well profile, and the increase in mud temperature along the target zones has also been estimated. The effect of the increase in downhole mud temperatures while drilling with a casing is then analyzed in the context of improving the fracture gradient attributable to the plastering effect. In addition, the effect of drilling parameters on the increase in fracture gradient has also been presented. This simple analytical model can be applied to casing while drilling operations to enhance our understanding of the plastering effect and to use it to our advantage.

5.2 Analytical Model for Casing Contact

The underlying physical phenomenon of the plastering effect is the continuous rotation of the casing against the wellbore wall, which results in the plastering of the cuttings and the additional lost circulation material. This smooth contact exists as a result of small annular clearances as an implication of the large casing diameter. Karimi *et al.* (2011) have also reported a more circular gauged hole as observed during casing while drilling as a consequence of this smooth rotation.

The rotation of the casing against the wellbore wall has been quantified using an analytical model based on similar studies for backward whirl simulations for rotary

steerable BHAs, as proposed by Stroud *et al.* (2011). The fundamental assumption of the model is that the casing is in continuous contact with the borehole wall, generating traction at contact points that leads to a rolling motion of the casing on the wall. Studies of the whirling motion of drill collars, as presented by Vandiver *et al.* (1990), help to describe the phenomenon of forward and backward whirl and can be suitably applied to the casing contact zone.

Fig. 42 illustrates a differential element showing the contact of the casing with the wellbore wall during a casing while drilling operation. This figure can be used to develop a free body diagram of the considered casing section to calculate the side forces acting on the casing as a result of contact. The free body diagram in Fig. 43 shows the forces acting in the radial direction only. Balancing the forces with the radial acceleration, Eq. 21 has been developed for the side force acting on the casing as a result of the rolling motion.

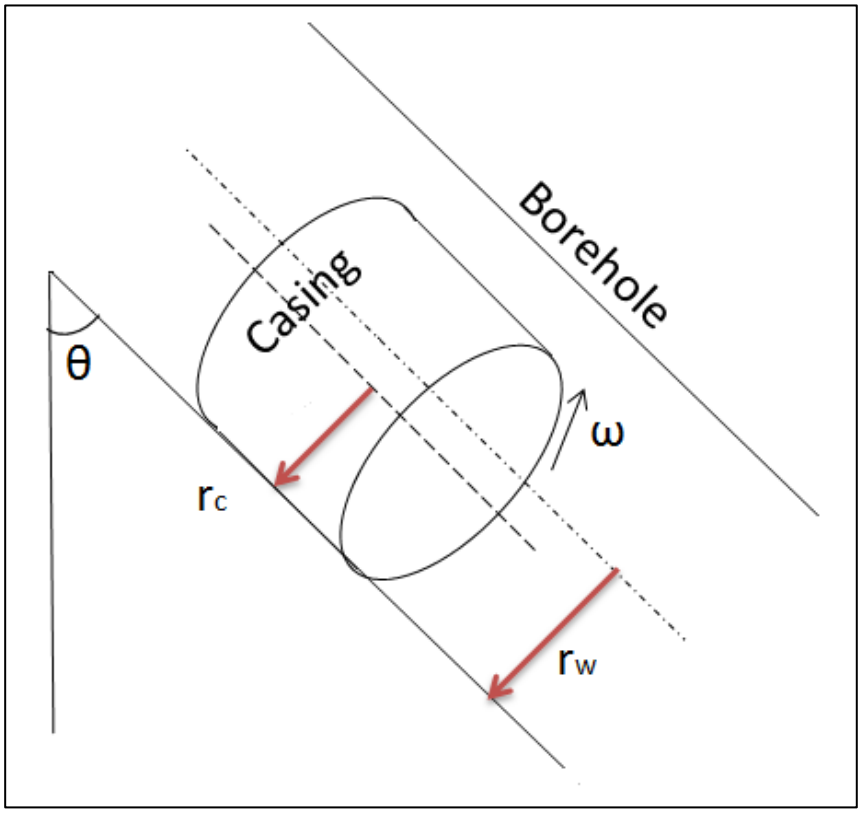

Fig. 42 – Differential element of the casing string having a mass dm.

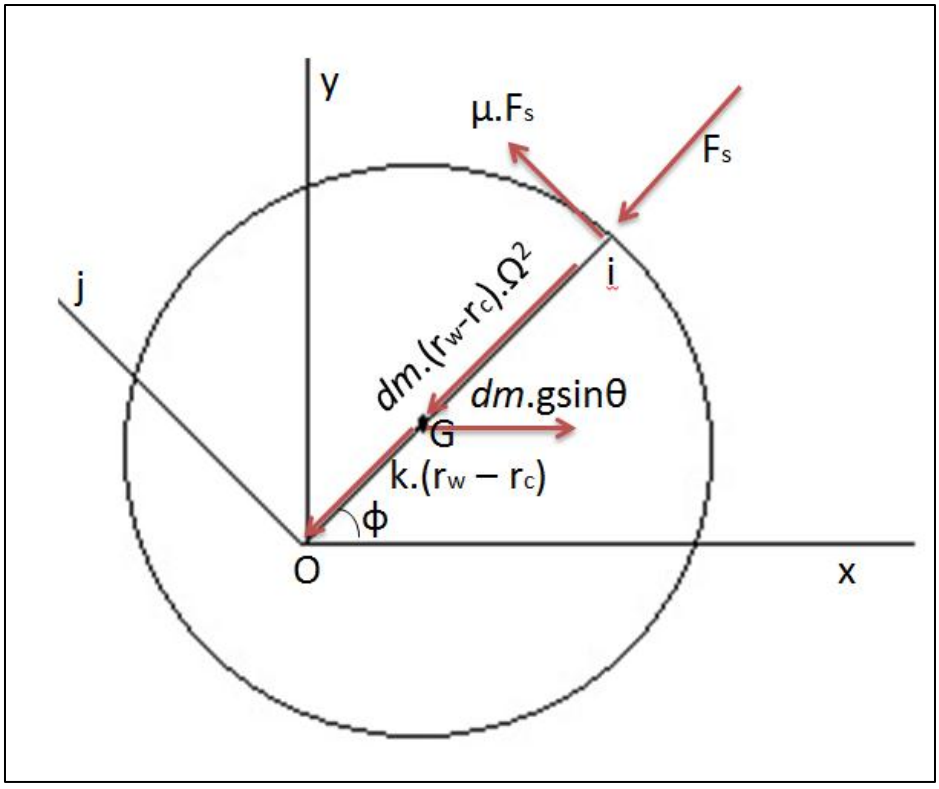

Fig. 43 – Free body diagram with forces acting on the casing string due to contact.

For a mass dm of the differential element and a well having an inclination θ, we calculate the values of the resultant side force F_s, resultant torque τ_c on the casing string and the power loss P_c downhole due to casing contact based on the following equations:

$$F_s = (r_w - r_c)\Omega^2.dm - k.(r_w - r_c) + gsin\theta cos\phi.dm, \quad (21)$$

$$\tau_c(\phi) = r_c.\mu.\int_0^{2\pi} F_s d\phi, \quad (22)$$

$$P_c = \tau_c(\phi).2\pi.rps. \quad (23)$$

The net velocity of the point of contact at the casing outer surface and the inner side of the borehole wall is given as

$$v_{cp} = (r_w - r_c)\Omega + r_c\omega. \quad (24)$$

Vandiver *et al.* (1990) have described this velocity as a measure of the amount of abrasion of the casing arising from the wellbore contact. For a rolling without slipping motion, the net velocity is equal to zero and is analogous to the conditions of perfect

backward whirl. The whirl velocity for this condition is in a direction opposite to the direction of rotation of the drill string and is given by

$$\Omega = -\omega \frac{r_c}{r_w - r_c}. \tag{25}$$

The maximum net velocity, and consequently the maximum abrasion, would be observed in a scenario in which the whirl velocity is equal in magnitude and direction to the rotational speed of the casing and is given as

$$\Omega = \omega. \tag{26}$$

This situation would be analogous to a condition of forward synchronous whirl and would lead to subsequent abrasion of the casing along one particular line of contact. Such a situation would occur for a very high rate of rotation of the casing when the traction would not be sufficient to initiate a rolling without slipping motion. This scenario is undesirable because it may lead to casing failures. Most of the casing while drilling operations are performed at relatively low speeds and would subsequently bring about an establishment of rolling without slipping motion. This type of contact will lead to a more gauged borehole and to a smooth plastering of the cuttings and the lost circulation material on the wellbore wall.

This wellbore heat transfer model developed in the previous section has now been applied to a casing while drilling operation to estimate the temperature profiles in the annulus of the casing and to study its contribution to the plastering effect. The heat generated as a result of the contact between the casing and the wellbore wall has been included as an additional heat source term in the model. The comprehensive model has subsequently been analyzed for four different casing while drilling field cases based on the drilling parameters to suggest potential applications of the model.

5.3 Model Application for CwD Operation

The four casing while drilling field cases consist of the drilling of vertical and deviated wellbores with casing strings accompanied with a BHA, as well casing strings without a BHA. The increase in downhole temperatures of the drilling fluid was estimated as the drilling activity progresses to better understand its effect on the plastering effect. The drilling parameters used for all the field case studies have been reported in Appendix B-4 to Appendix B-7.

5.3.1 Field Case 1 – Vertical Well with BHA

The first case study focuses on the drilling of a vertical wellbore with casing that includes an attached BHA. Fig. 44 shows the temperature of the drilling fluid within the drill string and in the annulus after drilling the 10 stands as planned.

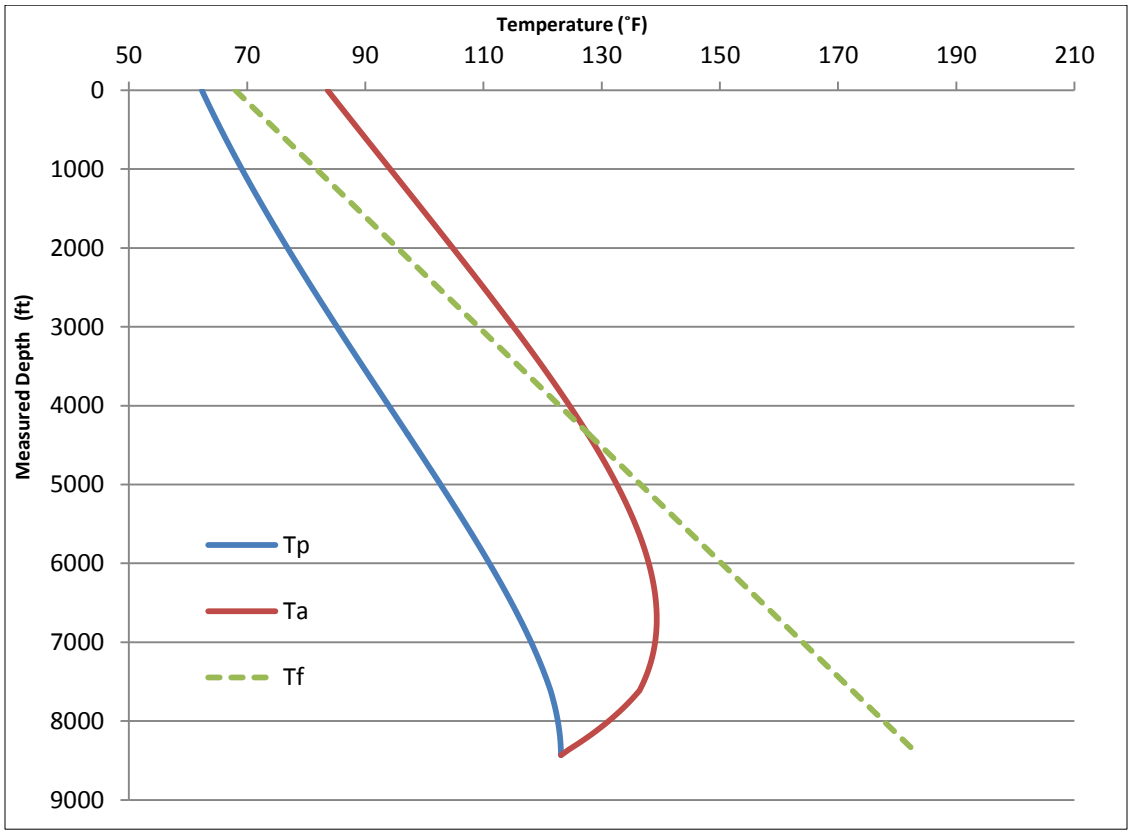

Fig. 44 – Temperature profile after drilling 10 stands (Field Case 1).

The well is drilled 10 stands from a depth of 7,480 ft to a depth of 8,430 ft with 750 ft of 7 in, 26 ppf casing in the drill string. The temperature profile along the borehole wall has also been shown alongside in Fig. 44 and estimates that lower bottom hole temperatures than the nearby formation.

Fig. 45 compares the annulus temperatures after drilling the first stand and after drilling the tenth stand to demonstrate the change in temperature profile with continued drilling activity. Fig. 46 provides estimates of the temperature increases along the top of the casing string and at the starting depth of the casing while drilling operation to demonstrate the temperature changes while drilling with a casing. An increase in temperature of about 20°F has been estimated at a depth of about 7,500 ft for this case.

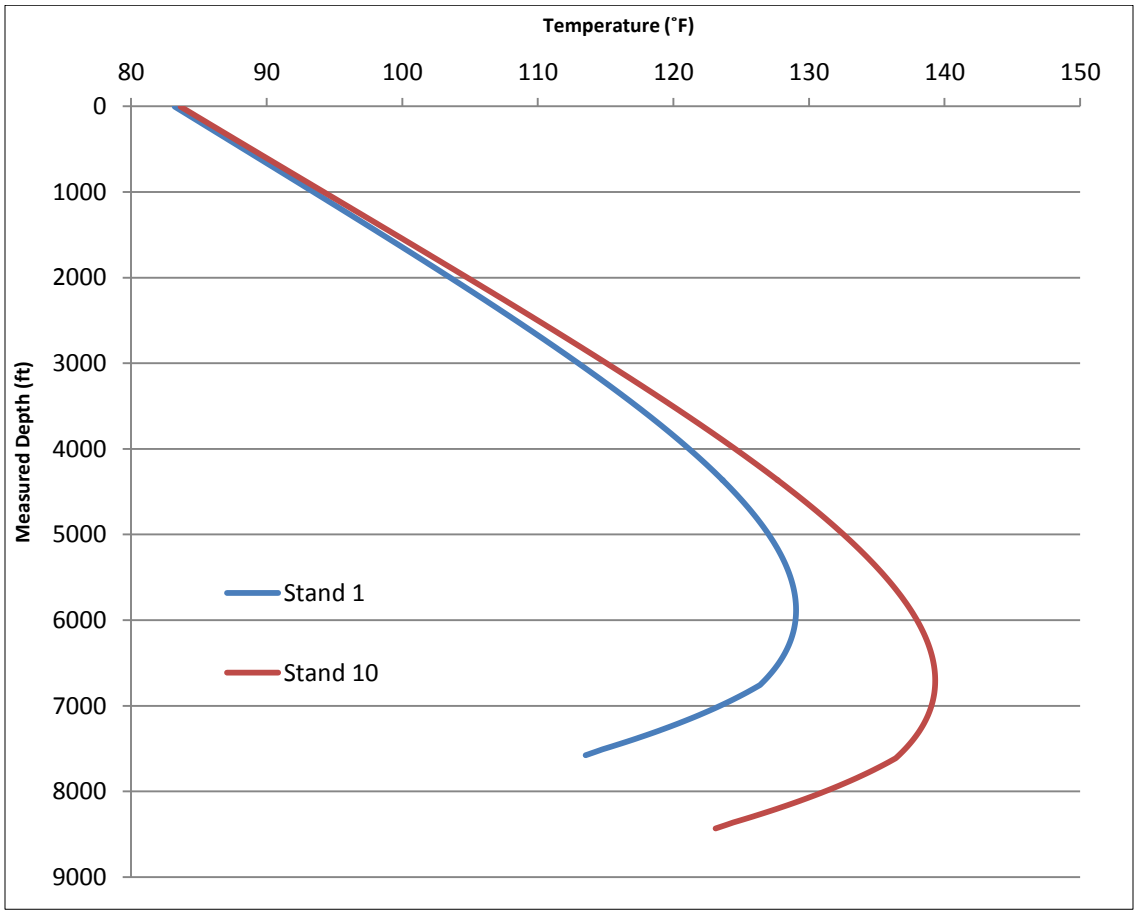

Fig. 45 – Annulus temperature profiles after drilling stand 1 and after drilling stand 10 (Field Case 1).

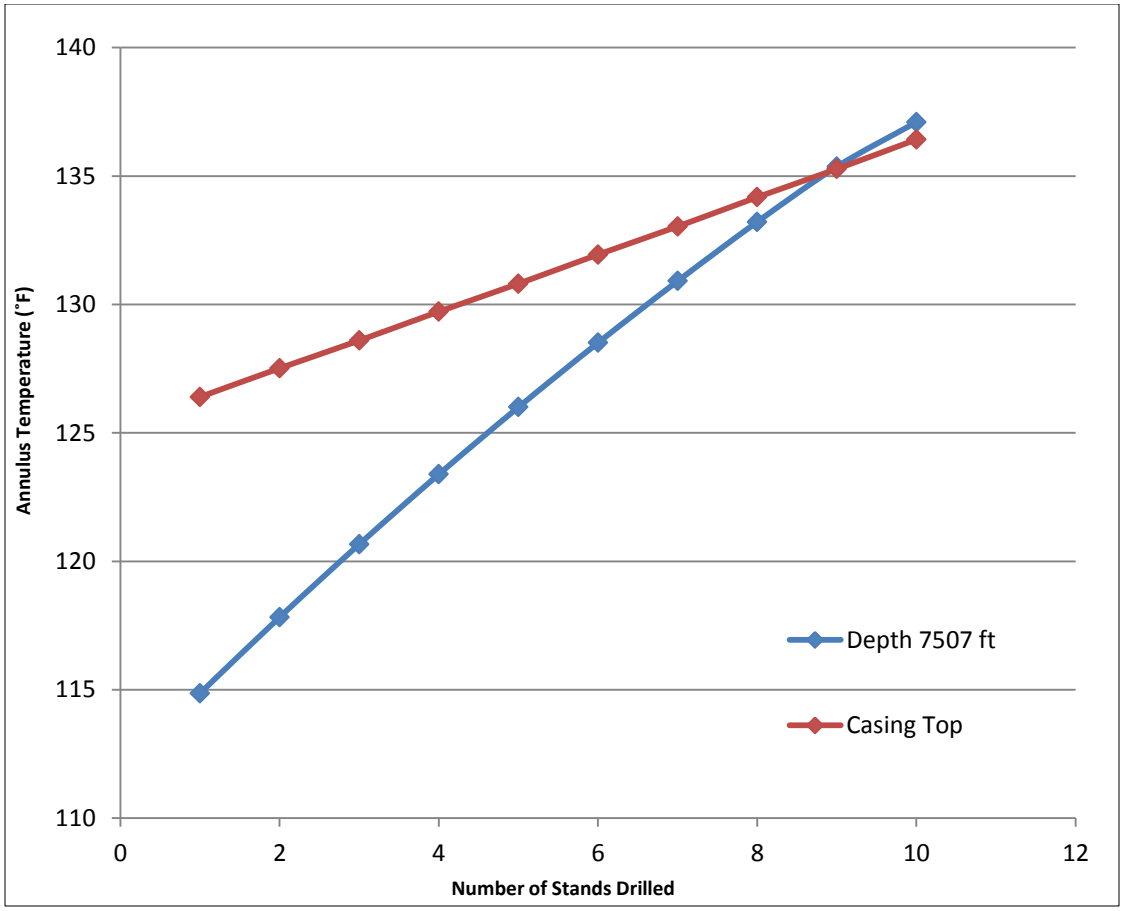

Fig. 46 – Increase in temperature at the top of the casing string and at the start depth of casing while drilling operations (Field Case 1).

5.3.2 Field Case 2 – Vertical Well without a BHA

The second case study presents a vertical wellbore drilled with a casing. However, in this case, the bit was directly attached to the bottom of the casing without an additional BHA. The casing while drilling operation consisted of drilling of 10 stands again from a depth of 9,185 ft to 10,135 ft with a 7.625 in, 47.1 ppf casing string having a length of 840 ft. Fig. 47 shows the temperature increase with drilling activity at the starting depth of casing while drilling operations and at the top of the casing string. An increase in temperature of more than 30°F has been estimated at a depth of 9,185 ft while completing the drilling of just 10 stands for this field case.

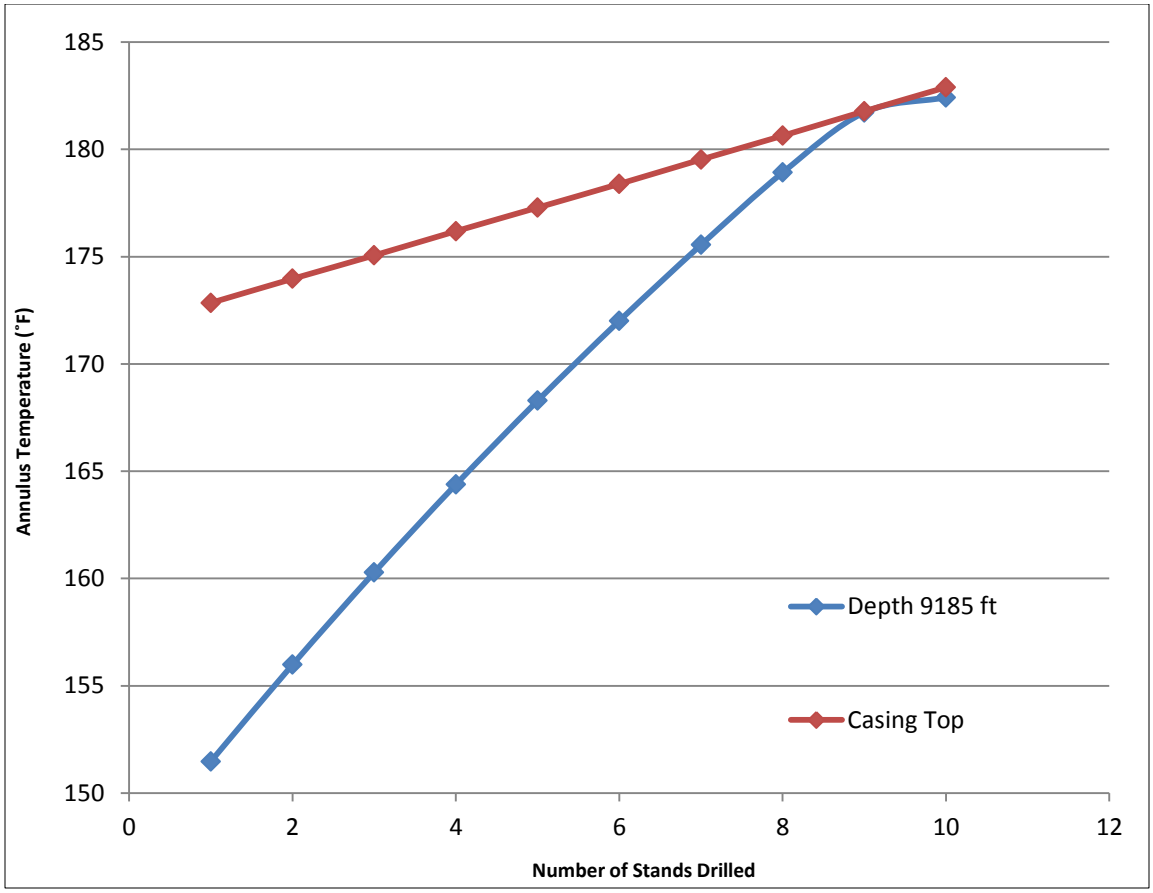

Fig. 47 – Increase in temperature at the top of the casing string and at the start depth of casing while drilling operations (Field Case 2).

5.3.3 Field Case 3 – Deviated Well with BHA

This case study presents the drilling activity of a deviated well with a casing string that also includes a BHA. The well was drilled conventionally with the borehole angle built to the planned tangent angle of 67° with measured depth of 3,675 ft. The casing while drilling operation required holding this angle and drilling of 10 stands to a desired depth of 4,625 ft, using 610 ft of 7 in, 29 ppf casing string. Fig. 48 shows the increase in downhole annulus temperatures for this case. The increase in temperature has been estimated to be only about 10°F at a depth of 3,700 ft while drilling 10 stands and also suggests a low operating temperature range due to the shallow nature of the well.

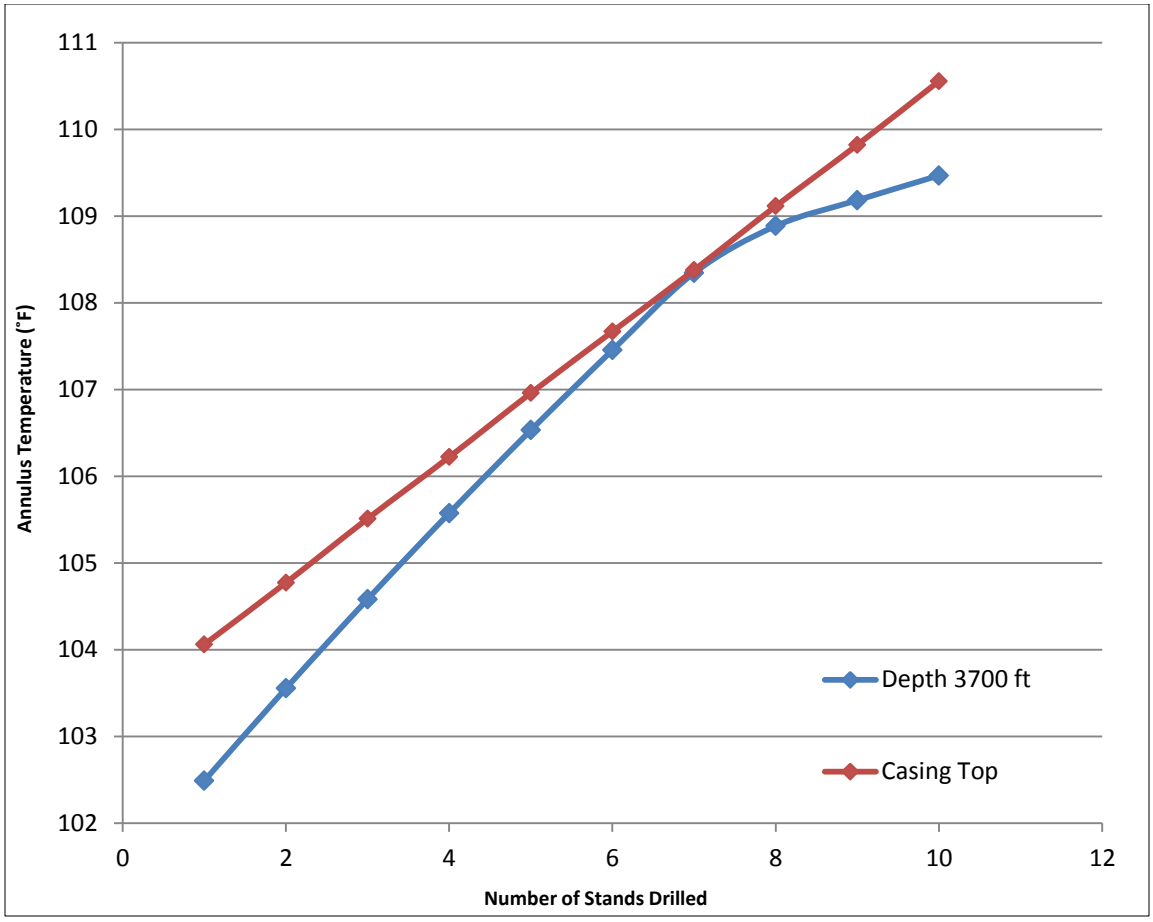

Fig. 48 – Increase in temperature at the top of the casing string and at the start depth of casing while drilling operations (Field Case 3).

5.3.4 Field Case 4 – Vertical Well without a BHA

The fourth case study represents a casing while drilling operation for a deviated well without a BHA. In this case, the wellbore was built conventionally to the planned angle of 45° to a measured depth of 10,250 ft when the casing while drilling operations began. The drilling activity represents the drilling of 10 stands with 690 ft of 7.625 in, 39 ppf casing along the tangent section while maintaining the angle of 45°. Fig. 49 shows the increase in downhole temperatures for this case. An increase of only about 10°F has been estimated based on the drilling and operating parameters as compared to those estimated in Field Case 1 and 2. However, a higher operating temperature range is encountered as the drilled interval in this case penetrates deeper into the formation.

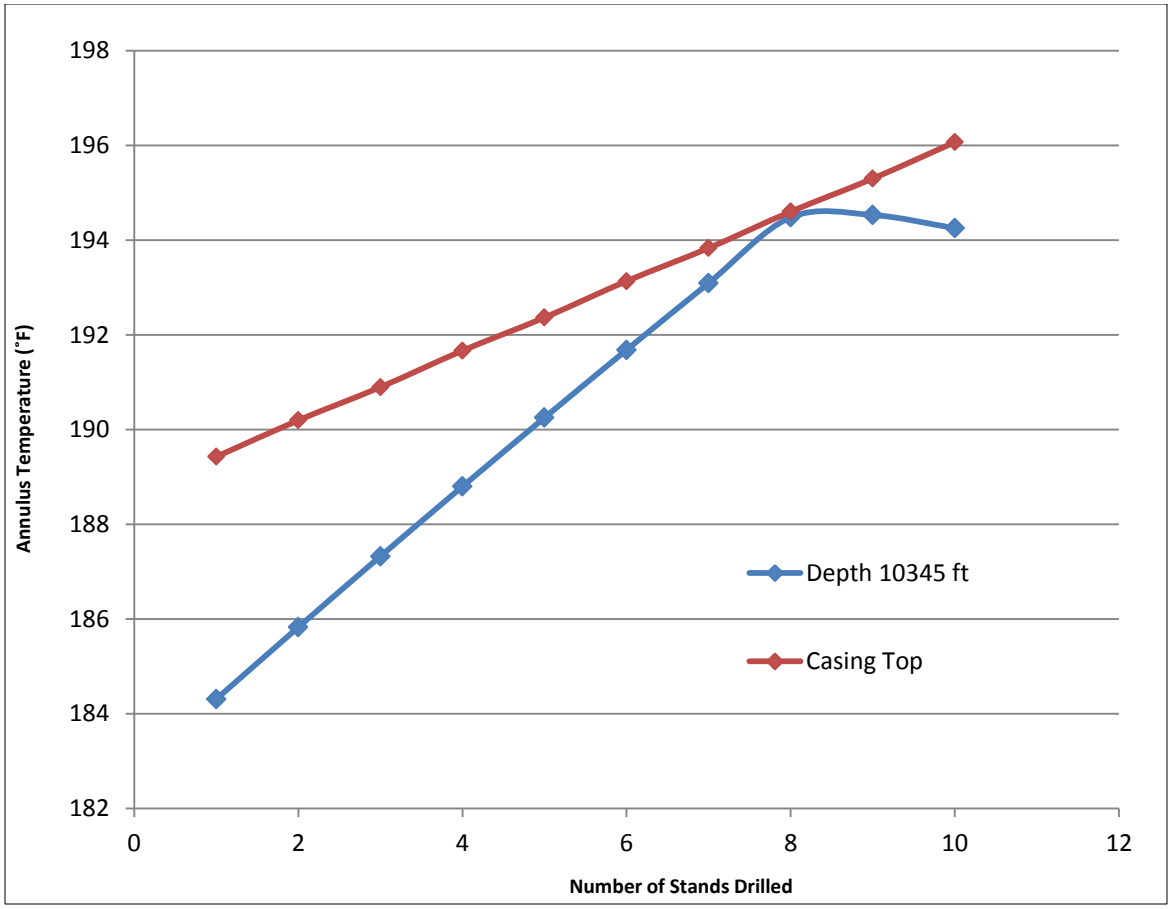

Fig. 49 – Increase in temperature at the top of the casing string and at the start depth of casing while drilling operations (Field Case 4).

5.4 Wellbore Temperatures – CwD vs. Conventional Drilling

The case studies presented above show the increase in temperatures of the drilling fluid observed during casing while drilling operations. Field Case 2 shows an increase of more than 30˚F while drilling 10 stands with a casing string. Fig. 50 below compares the increase in temperature for this field case with a conventional drilling operation if carried out under exactly the same drilling and operating circumstances to show the impact of casing contact. This contact between the casing and the wellbore wall leads to an increase of more than 20°F during the drilling of just 10 stands when compared to the conventional drilling operation that experiences no such wall contact. These higher temperatures for casing while drilling may have an impact on the fracture gradient.

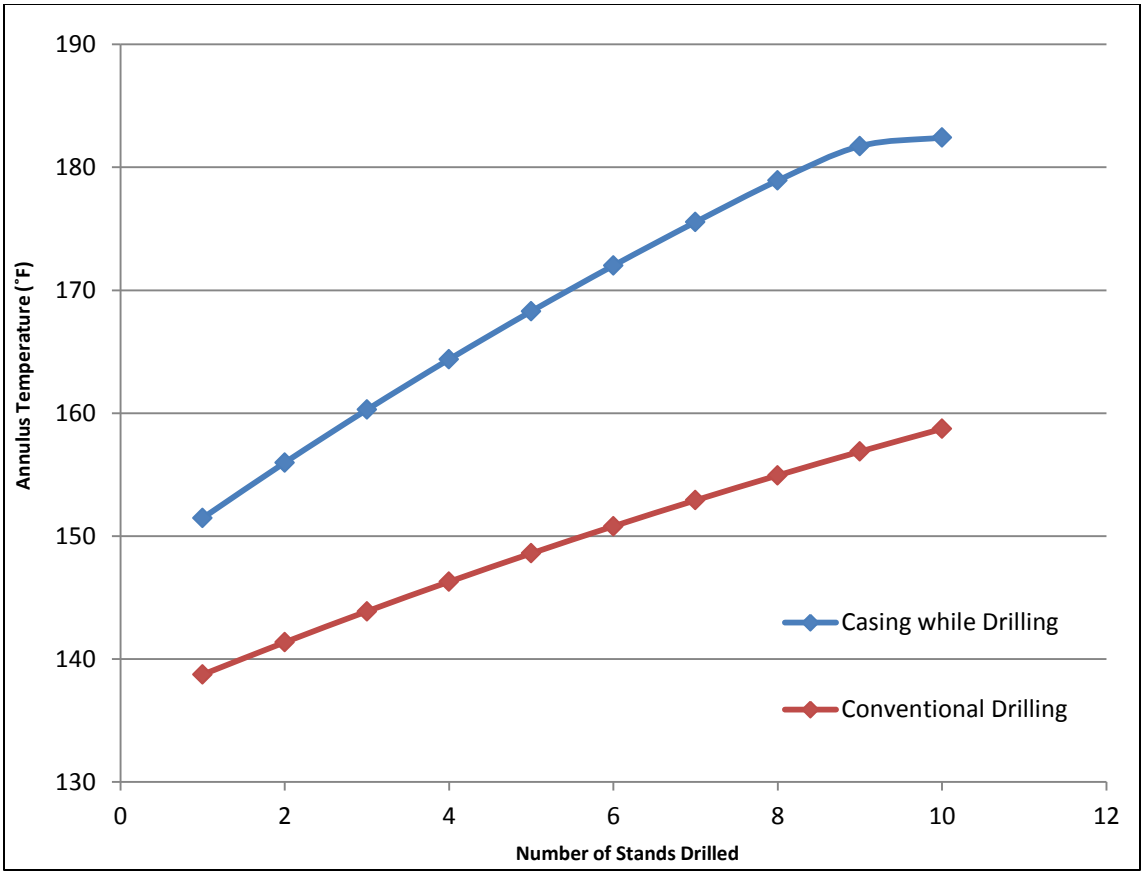

Fig. 50 – Increase in temperature at a depth of 9,185 ft for casing while drilling operation and conventional drilling operation (Field Case 2).

5.5 Influence of Temperature on Smear Effect

The effects of wellbore temperature on the effective fracture gradient of the formation have been comprehensively studied in the literature by various authors. The difference in temperature of the mud and the formation during any drilling operation causes high thermally induced stresses that alter the formation breakdown pressure near the wellbore. The continuous circulation of the drilling fluid leads to bottomhole temperatures lower than the formation resulting in compressive wellbore stresses and lower fracture gradients. An increase of wellbore temperatures will help develop tensile stresses leading to an improvement in this fracture breakdown pressure. The changes in wellbore stresses observed during a casing while drilling operation play a significant role in realizing the benefits of the plastering effect.

The influence of temperature on the plastering effect can be better understood as a two-step phenomenon. Drilling the well conventionally with a drill pipe till the depth where the casing while drilling operation commences will cause wellbore temperatures to be lower than the nearby formation. The lower temperatures will lead to compressive wellbore stresses, thereby inducing miniature fractures around the wellbore at mud pressures used for drilling the well. This phenomenon of creating open fractures due to the cooling effect has also been proposed by Gil *et al.* (2006). The commencement of drilling with a casing will cause a continuous contact between the casing string and the wellbore wall as described in the analytical model proposed above, and will help plug these created fractures with drilled cuttings and the added lost circulation materials.

The contact between the casing and the borehole wall will also lead to heat generation due to friction, thereby increasing the mud temperatures as the drilling activity progresses and induces tensile stresses around the wellbore. This phenomenon will help close the opened fractures and lead to an improvement in the fracture gradient.

Field observations and the qualitative studies on the plastering effect suggest the plastering or smearing of the drilled cuttings and lost circulation material into the wellbore wall by the casing, as the primary mechanism responsible for wellbore strengthening. The role of wellbore temperatures in creating miniature fractures and then closing them with the progress of the casing while drilling operation helps increase the stresses around the wellbore and improve the fracture gradient.

5.6 Models for Variation of Fracture Gradient

Changes in stresses around the wellbore with changing temperatures have been addressed by several studies such as Hettema *et al.* (2004), Tang *et al.* (1998) and Gil *et*

al. (2006). The general equation for change in tangential stress with change in temperature is given as

$$\Delta\sigma_T = \frac{\Delta T_m \beta E}{1-\nu}. \tag{27}$$

Aadnoy *et al.* (2009) have studied the effect of temperature on the fracturing pressure in comprehensive detail and have proposed a new fracturing model using a scaling factor K that includes the Poisson's Effects. They have also shown improvements with the new model and suggest that it might explain some of the discrepancy between models and field data. The equation that they propose for change in fracture pressure with change in temperature is given as

$$\Delta \mathrm{p}_{fp} = \frac{(1+\nu)^2}{3\nu(1-2\nu)+(1+\nu)^2} E\beta(T_{fin} - T_{init}), \tag{28}$$

where K is defined as

$$K = \frac{(1+\nu)^2}{3\nu(1-2\nu)+(1+\nu)^2}. \tag{29}$$

5.7 Wellbore Strengthening due to Temperature

The wellbore strengthening achieved during the casing while drilling operation has been estimated using the above models by calculating the change in fracturing pressure with change in wellbore temperatures over the length of the wellbore. The increase in downhole temperatures due to the continuous contact of the casing string and the wellbore wall will lead to an improvement in the fracture gradient as the drilling activity progresses. The impact of the duration of casing while drilling operation on the fracture gradient has also been presented to help us optimize the planned drilling program.

Fig. 51 gives us the increase in the fracture gradient for the total duration of the drilling operation at the depth of 6,200 ft where the casing while drilling operation commenced. Fig. 52 shows the wellbore strengthening achieved for 1,000 ft of the wellbore with continued drilling activity. This analysis consists of the drilling operation starting at a depth of 6,200 ft and lasting 30 hrs, with 7.625 in, 47.1 ppf casing string having a length of 2,400 ft. The other operational parameters used for calculations have been reported in Appendix B-8.

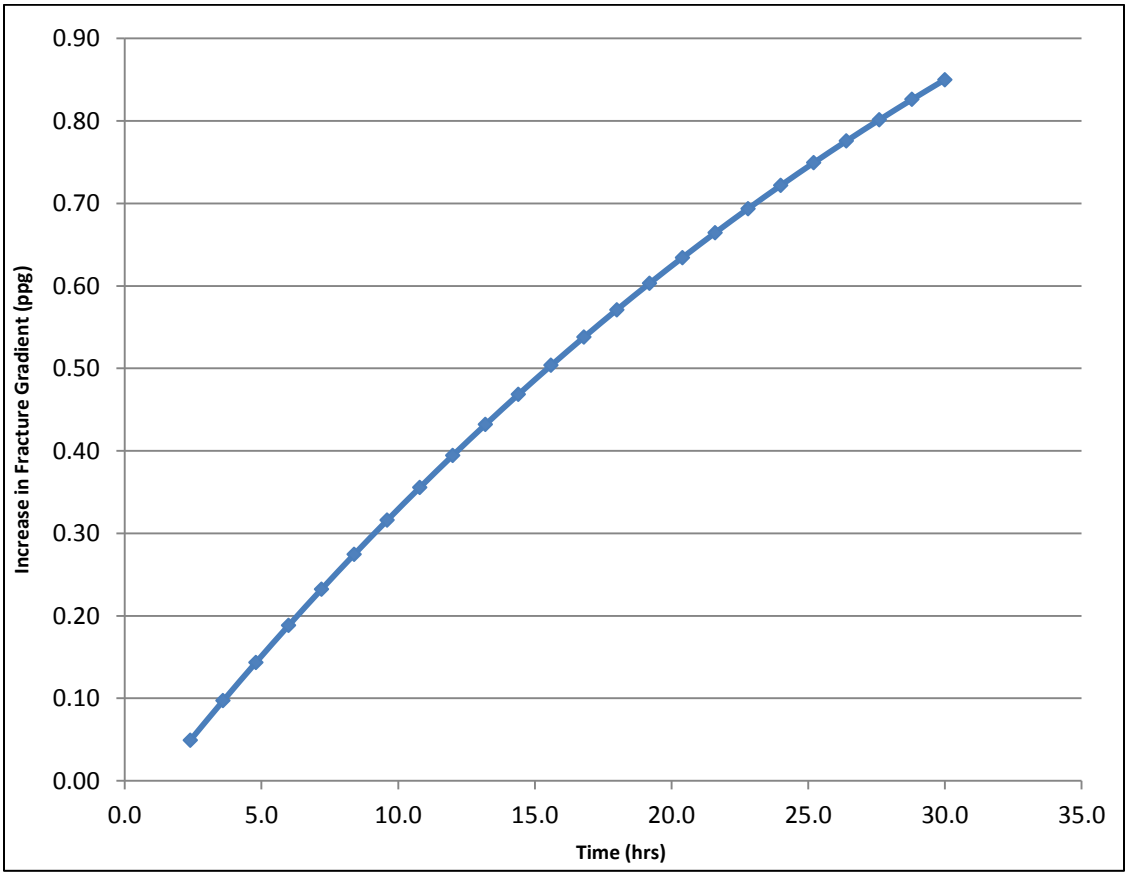

Fig. 51 – Increase in fracture gradient with the total duration of the drilling activity at a depth of 6,200 ft for casing while drilling operation.

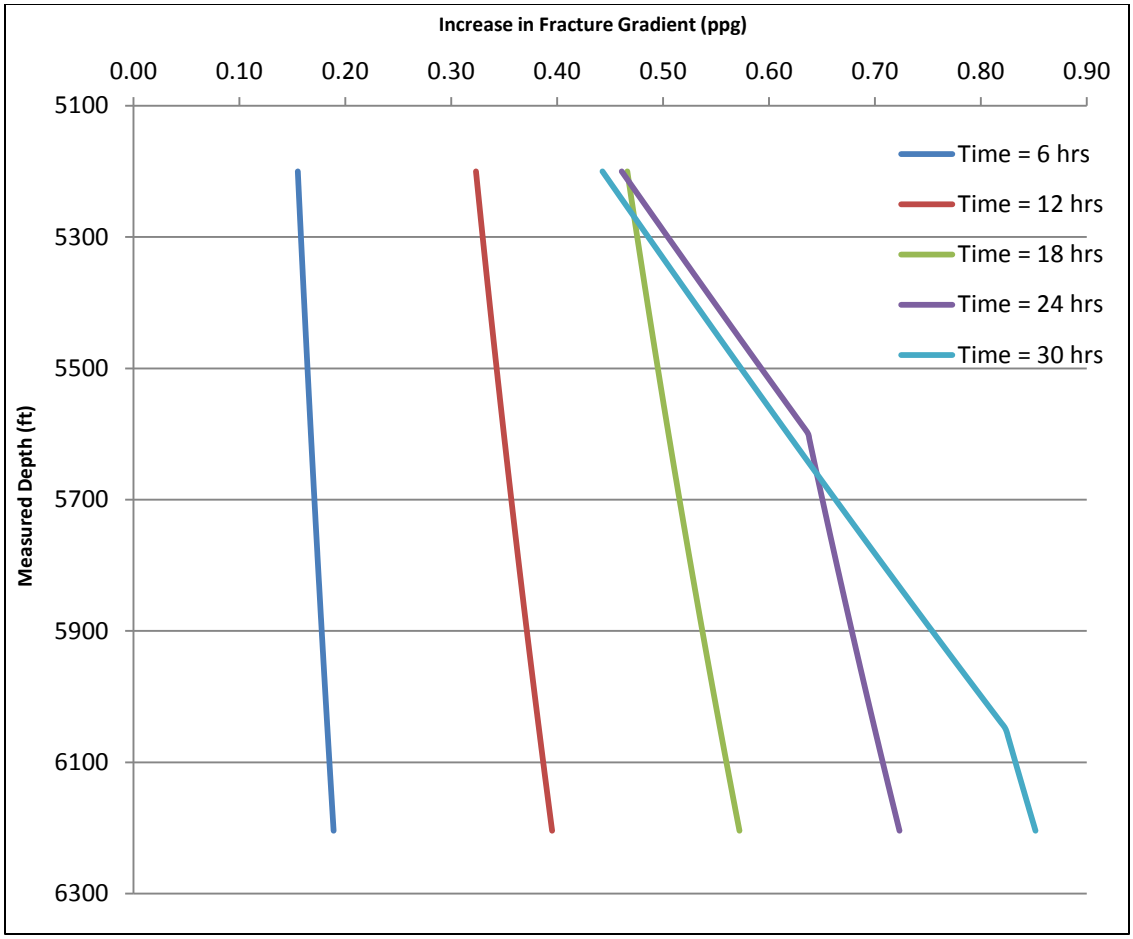

Fig. 52 – Increase in fracture gradient for 1,000 ft of wellbore from a depth of 5,200 ft to 6,200 ft with continued drilling activity.

Fig. 51 suggests a continuous improvement in the fracture gradient for the entire drilling operation as the casing remains in persistent contact with the wellbore wall and leads to higher temperatures. Fig. 52 shows that the fracture gradient increases only partially with depth at any particular drilling time. However, as the casing string moves deeper with the progress of the drilling activity, we may see a decrease in fracture gradient for shallow sections where the casing is no more in contact with the wellbore as it leads to a decrease in drilling mud temperatures. A decrease in fracture gradient can be observed above the depth of about 5,600 ft after drilling for 24 hrs as the top of the casing string crosses over and there is no additional heat generation. A similar decrease in fracture gradient can also be observed above the depth of 6,050 ft for 30 hrs of drilling

operation. This analysis certainly helps us understand the phenomenon of wellbore strengthening achieved for a section of the well profile while simultaneously considering the impact of duration of drilling activity.

5.8 Effect of Drilling Parameters

The change in fracture gradient at a particular depth with drilling parameters like rotational speed of the drill string and the mud flow rate has also been analyzed for Field Case 2 and reported in Fig. 53. The additional parameters used for the calculations have been reported in the Appendix B-9.

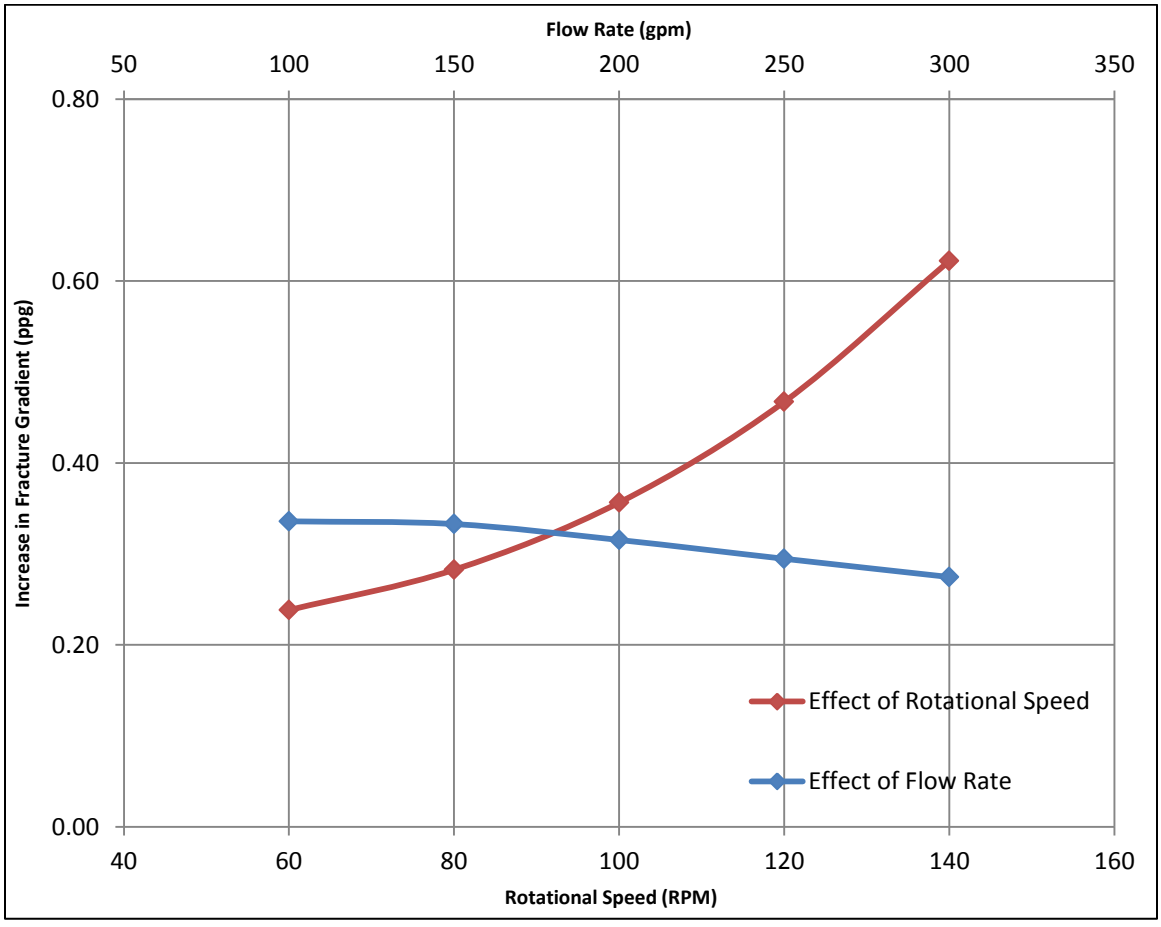

Fig. 53 – Increase in fracture gradient with rotational speed and flow rate at a depth of 9,185 ft for casing while drilling operation (Field Case 2).

This analysis helps us better understand the benefits of the plastering effect mechanism in terms of the drilling parameters so that we may effectively use it to our advantage. However, it may not be possible to maximize the improvement in fracture gradient based on this analysis alone due to existing logistical and operational constraints like casing staring failures that may be encountered at high rotational speeds.

The plot in Fig. 53 shows a significant increase in fracture gradient with increase in rotational speed of the drill string. However, the improvement in fracture gradient achieved due to changes in the mud flow rate remains fairly constant for this casing while drilling operation. The increase in wellbore temperatures combined with the plugging of miniature fractures due to the continuous casing contact helps in wellbore strengthening and better utilizing the advantages of the plastering effect mechanism.

CHAPTER 6

THE SMEAR EFFECT MECHANISM

6.1 Introduction

A detailed investigation of the smear effect mechanism has been of particular interest to the industry and carries the objective of efficiently exploiting all its benefits to successfully perform drilling operations in complex environments. The most important application of the smear effect or the plastering effect mechanism is towards increasing the fracture gradient of the formation by providing wellbore strengthening during the casing while drilling operation, which otherwise cannot be realized by conventional drilling techniques.

The improvement in the fracture gradient has been analyzed in the literature by various authors through field observations as well as qualitative studies and is considered to be a resultant of the following list of phenomena occurring simultaneously in a casing while drilling operation:

- Initiation of micro-fractures at the wellbore wall due to higher ECDs and their subsequent plugging by the casing and wellbore wall contact.
- Plugging of natural fractures, vugs and pore spaces existing around the wellbore circumference by the casing and wall contact.
- Thin mud cake formation having lower permeability and porosity leading to lower fluid losses and mitigating formation damage.
- Higher wellbore temperatures that are observed in casing while drilling as compared to a conventional drilling operation.

Each of the above factors contributes in their own respective way to realize the observed increase in the fracture gradient and need to be analyzed and studied in detail individually. The effect of high wellbore temperatures in casing while drilling operations has been studied thoroughly in the previous section. In this section, we study the contribution of micro-fractures due to high ECDs towards improving the fracture gradient of the formation.

An analytical model has been applied to simulate the generation of micro-fractures around the wellbore wall and then effect of plugging of those fractures has been estimated using mathematical studies. A case study for a simulated well profile has been presented based on the formation properties as listed in Appendix B-10 suggesting an application of the model and the subsequent increase in the fracture gradient has been estimated. The particle size distribution required for the successful plugging of the micro-fractures using the estimated fracture widths has also been presented. The mathematical model used for the simulation of the horizontal wellbore stresses has been presented in Appendix A-2. Finally, the effect of the other underlying parameters like formation properties, operating parameters, casing length and casing diameter / hole size ratios on realizing an improvement in the fracture gradient has been analyzed.

6.2 Analytical Model for Micro-fractures

The initiation of micro-fractures has been analyzed based on the basic equations used to calculate the stress distribution existing around the wellbore due to the maximum and minimum principal horizontal stresses. For a minimum horizontal stress $\sigma_{11}$and a maximum horizontal stress σ_{22}, the wellbore radial, tangential and shear

stresses, σ_{rr} $\sigma_{\theta\theta}$ and $\sigma_{r\theta}$ can be calculated at any particular point using cylindrical coordinates r and θ by the following equations:

$$\sigma_{rr} = \frac{\sigma_{11}+\sigma_{22}}{2}\left(1-\frac{r_w^2}{r^2}\right) + \frac{\sigma_{11}-\sigma_{22}}{2}\left(1+3\frac{r_w^4}{r^4}-4\frac{r_w^2}{r^2}\right)\cos 2\theta, \tag{30}$$

$$\sigma_{\theta\theta} = \frac{\sigma_{11}+\sigma_{22}}{2}\left(1+\frac{r_w^2}{r^2}\right) - \frac{\sigma_{11}-\sigma_{22}}{2}\left(1+3\frac{r_w^4}{r^4}\right)\cos 2\theta, \tag{31}$$

$$\sigma_{r\theta} = \frac{\sigma_{22}-\sigma_{11}}{2}\left(1-3\frac{r_w^4}{r^4}+2\frac{r_w^2}{r^2}\right)\sin 2\theta, \tag{32}$$

where r_w is the wellbore radius. The initiation of micro-fractures is governed by the wellbore tangential stresses only and requires a pressure in the wellbore that exceeds the minimum fracture pressure at the borehole wall. The tangential stress at the wellbore wall can be estimated as a function of θ by

$$\sigma_{\theta\theta}^{(1)} = (\sigma_{11}+\sigma_{22}) - 2(\sigma_{11}-\sigma_{22})\cos 2\theta, \tag{33}$$

where $r = r_w$ and the minimum value of this tangential stress is given by

$$\sigma_{\theta\theta}^{(1)} = 3\sigma_{11} - \sigma_{22} \text{ when } \theta = \frac{\pi}{2}\,\&\,\frac{3\pi}{2}. \tag{34}$$

The tangential stress created by the borehole fluid pressure p_w at the wellbore wall is

$$S_{\theta\theta}^{(2)} = -(p_w - p_o), \tag{35}$$

and that due to the penetration of fluid into the borehole wall is

$$S_{\theta\theta}^{(3)} = -\alpha(p_w - p_o)\frac{1-2\nu}{1-\nu}. \tag{36}$$

where α is Biot's constant. The total tensile stress on the wellbore wall is given by

$$S_{\theta\theta} = 3\sigma_{11} - \sigma_{22} + p_o - (p_w - p_o) - \alpha(p_w - p_o)\frac{1-2\nu}{1-\nu}, \tag{37}$$

and the effective stress can be calculated by

$$\sigma_{\theta\theta} = S_{\theta\theta} - p_w = 3\sigma_{11} - \sigma_{22} - (p_w - p_o)\left(2 - \alpha\frac{1-2\nu}{1-\nu}\right). \tag{38}$$

Fracture breakdown occurs when $\sigma_{\theta\theta}$is equal to the tensile strength of the formation σ_t and the wellbore pressure p_w in that scenario is equal to the fracture pressure p_f that can be calculated as

$$p_f = \frac{3\sigma_{11}-\sigma_{22}-\sigma_t}{2-\alpha\frac{1-2\nu}{1-\nu}} + p_o. \quad (39)$$

A micro-fracture would initiate if the pressure in the wellbore p_w exceeds this calculated values of the fracture pressure p_f based on the formation properties. During a given drilling operation, the wellbore pressure p_w can be estimated by

$$p_w = p_{mud} + p_{fric}. \quad (40)$$

where p_{mud} is the hydrostatic pressure due to the drilling fluid and p_{fric} is frictional pressures losses occurring in the annulus. p_{fric} can be calculated for an applicable flow regime based on the equations in Appendix A-1.

The width of the fracture initiated at the wellbore can be estimated the line crack approximation at the borehole wall from Alberty *et al.* (2004) by the following equation

$$w_f = \frac{4(1-\nu^2)}{E}(p_w - S_h)(r_w + L_f). \quad (41)$$

An analysis of plugging of micro-fractures initiated at the wellbore wall by miniature particles at the mouth of the fracture has been done in detail by Morita *et al.* (2011). They estimate the wellbore pressure required to propagate an existing fracture that has been plugged before using a set of analytical equations using a criteria for fracture toughness. The fracture propagation pressure for the case of a miniature fracture arising from a vertical wellbore in a direction perpendicular to the minimum horizontal stress and plugged at its mouth has been derived by Morita *et al.* (2011) and is given as

$$p_{fp} = \left[K^c/\sqrt{\pi\Delta L} - \sigma_{11}F_\lambda(s)\right]/\{(1-s)[0.637 + 0.485(1-s)^2 + 0.4s^2(1-s)]\}, \quad (42)$$

where p_{fp} is the effective fracture propagation pressure, K^c is the fracture toughness of the formation, ΔL is the length of the fracture from the plugged position to the fracture tip and $F_\lambda(s)$ and s are parameters defined as follows:

$$s = \Delta L/(r_w + \Delta L), \tag{43-a}$$

$$F_\lambda(s) = (1-\lambda)F_0(s) + \lambda F_1(s), \tag{43-b}$$

$$F_0(s) = 0.5(3-s)[1 + 1.243(1-s)^3], \tag{43-c}$$

$$F_1(s) = 1 + (1-s)[0.5 + 0.743(1-s)^2], \tag{43-d}$$

$$\lambda = \sigma_{22}/\sigma_{11}. \tag{43-e}$$

It has been assumed in this analysis that the particles plugging the fracture are very small that have micron-sizes and that the fracture has been plugged at the fracture mouth only. Hence, this leads us to the following approximation

$$\Delta L = L_f. \tag{44}$$

The set of equations described above have been applied to a case study for a simulated well profile in a formation being drilled with a casing while drilling system. The objective of this application is to estimate the possible extent of improvement in the fracture propagation pressure that may be achieved by the plugging of the micro-fractures arising due to high ECDs in a casing while drilling operation. In addition, it also tries to estimate a possible a range of particle sizes required for plugging fractures based on the distribution of the fracture widths at the wellbore.

6.3 Case Study

The case study presented here consists of a casing while drilling operation being carried out on a vertical well without a BHA when the wellbore has been drilled conventionally and cased to a depth of 6,400ft. The casing while drilling system is run in

after the casing has been set and the well is drilled further for about 600 ft to 7,000 ft using 2,400 ft of a 7 in casing string consisting of 60 joints. The wellbore, formation and operating parameters as used in this analysis have been listed in Appendix B-10.

The pore pressure and the fracture gradient profile as expected during the drilling of this well under analysis has been shown in Fig. 54 to give a perspective on the advantages of improving the fracture gradient to reach the target depth of 7,550 ft.

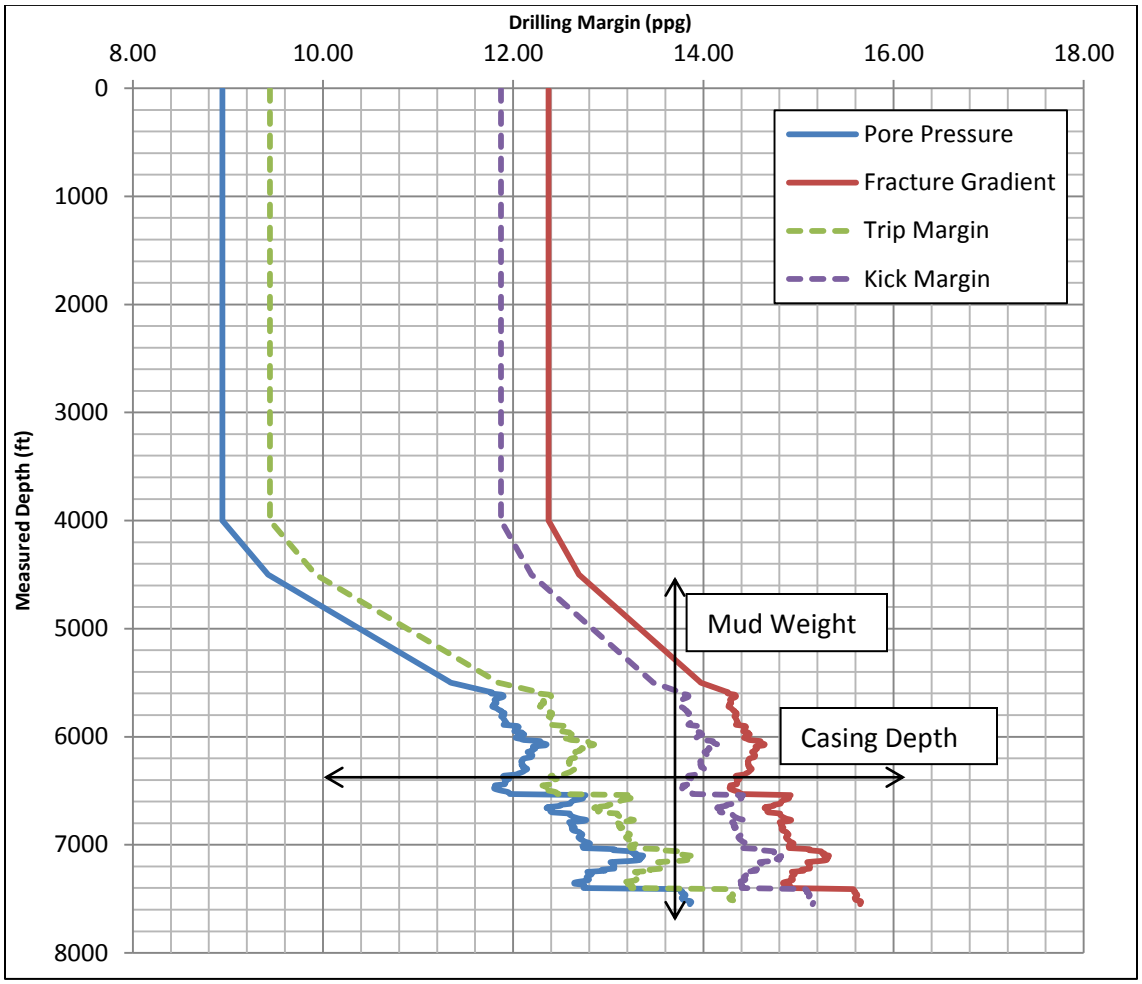

Fig. 54 – Drilling margin for the well undergoing casing while drilling operation.

The casing while drilling operation is aimed at improving the fracture gradient of the formation in the open hole section to be drilled using the casing string from 6,400 ft till 7,000 ft. This section has been drilled using a 13.7 ppg fluid as shown in Fig. 54. An

increase in the fracture gradient will help continue the drilling operation with a higher mud weight beyond the depth of 7,000 ft to safely complete the well till the target depth of 7,550 ft and hence eliminating the need for an additional liner to save costs. The analytical models presented in the previous section have been applied to this casing while drilling operation to analyze the scenarios when the desired improvement in the fracture gradient can be achieved.

Using the parameters as defined in Appendix B-10, the following Fig. 55 has been generated that shows the wellbore pressure, fracture initiation pressure and the possible improvement in the fracture gradient due to plugging of micro-fractures generated by high ECDs. The wellbore pressure is synonymous to the ECDs experienced during the casing while drilling operation performed to drill this wellbore section.

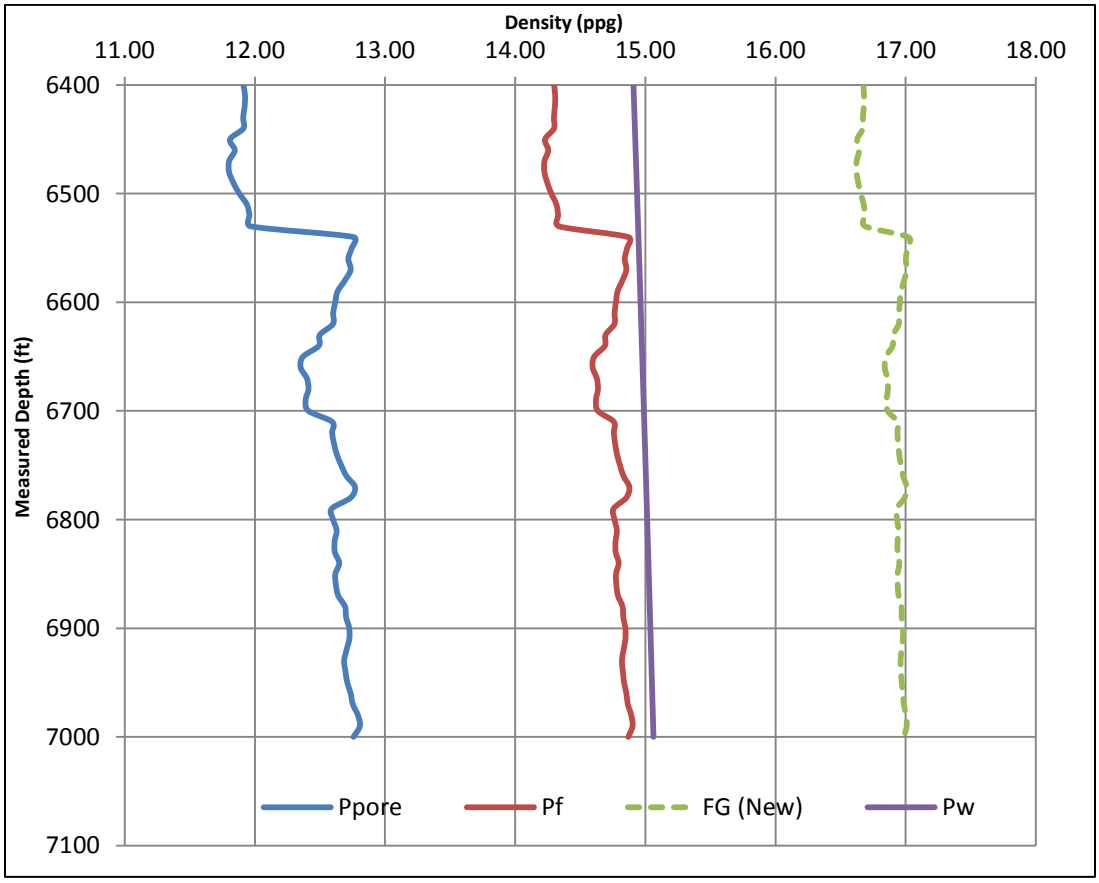

Fig. 55 – Estimated new fracture gradient due to plugging of micro-fractures.

6.4 Results Analysis

Fig. 55 shows that the pressure due to the equivalent circulating densities in the wellbore was sufficient to initiate micro-fractures along the entire length of this 600 ft of the wellbore section. The new fracture gradient plotted alongside suggests the possible improvement in the fracture gradient that may be achieved due to the micro-fractures initiated by ECDs and plugged subsequently due to the continuous contact between the casing and the wellbore wall. This fracture gradient has been derived assuming a fracture length of about 0.5 in from the wellbore wall.

Based on Fig. 54, a leak-off test conducted at the beginning of the casing while drilling operation would have resulted in an equivalent mud weight of about 14.2 ppg at the casing shoe. A leak-off test conducted after drilling till 7,000 ft would suggest the wellbore could now stand an equivalent mud weight of about 16.6 ppg, an improvement of 2.4 ppg in the fracture gradient. However, this analysis is under the assumption that the entire height of the micro-fractures initiated will be plugged in by the ground drilled cuttings and the added lost circulation materials due to the casing rotation against the wellbore wall. If the entire fracture height is not sufficiently plugged in by particles, a leak-off test conducted after the operation would result in only a partial improvement in the fracture gradient which would be equivalent to the original fracture initiation pressure at higher depths of the open hole section between 6,400 ft and 7,000 ft. Such a scenario has readily been described by many authors in literature through field observations when the all the micro-fractures might not have been plugged in and suggests that the partial improvement in the fracture gradient observed might be due to the original fracture initiation pressure at higher depths. If all the micro-fractures have been plugged properly, we should expect a higher increase in the fracture gradient.

This analysis has also been carried out assuming that all the micro-fractures initiated from the wellbore wall have an approximate fracture length of about 0.5 in. Whitfill (2008) has suggested that for a wellbore strengthening operation, the fracture length is limited to only within a few inches from the wellbore circumference to effect good wellbore pressure confinement. Loloi *et al.* (2010) have also described the wellbore strengthening phenomena and consider a maximum of 24 in of fracture length for their analysis. They suggest that "the additive materials will strengthen the borehole and only fractures of a limited extent will develop. It is also considered that if longer fractures develop then there will be little hope of stabilizing the fracture and wellbore strengthening will likely not be possible. Hence, the aim is to retard the fracture growth before the fracture becomes too large."

Fig. 56 below suggests the possible improvement in the fracture gradient that may be expected if the fracture length grows beyond 0.5 in and shows results for a range of fracture lengths from 0.5 in to 4 in from the wellbore. The increase in the fracture gradient depends on the underlying minimum and maximum horizontal stresses as well as the fracture length. A higher increase in the fracture gradient is expected for longer fractures that have been plugged at the borehole wall. The fracture length of the micro-fractures generated due to high ECDs in a casing while drilling operation is expected to be within a few inches from the wellbore, about 0.5 in to 4 in. Hence, the achieved new fracture gradient along the entire open hole wellbore section will be a resultant of the variable fracture lengths that may have been plugged. A leak-off test conducted under this scenario would result in the least possible value of the gradient achieved in the open hole. No improvement in the fracture gradient will be observed if the fracture has not been plugged at the mouth before it starts to extend beyond the near wellbore region.

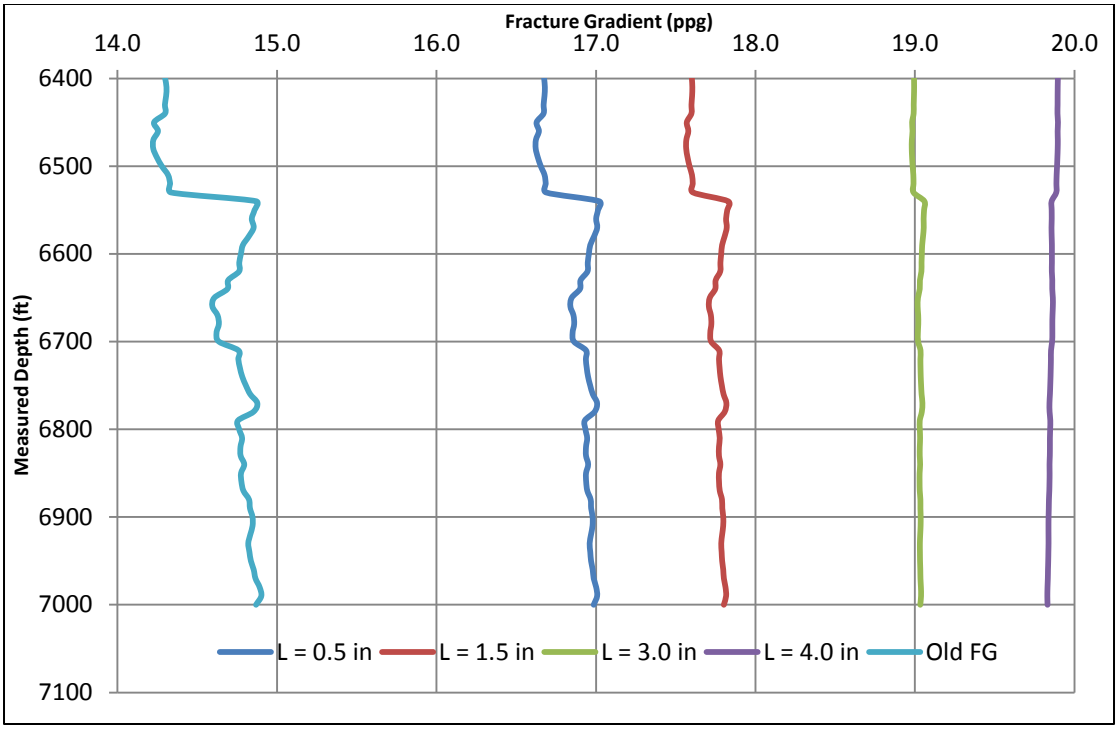

Fig. 56 – Improvement in the fracture gradient due to plugging of micro-fractures having variable lengths.

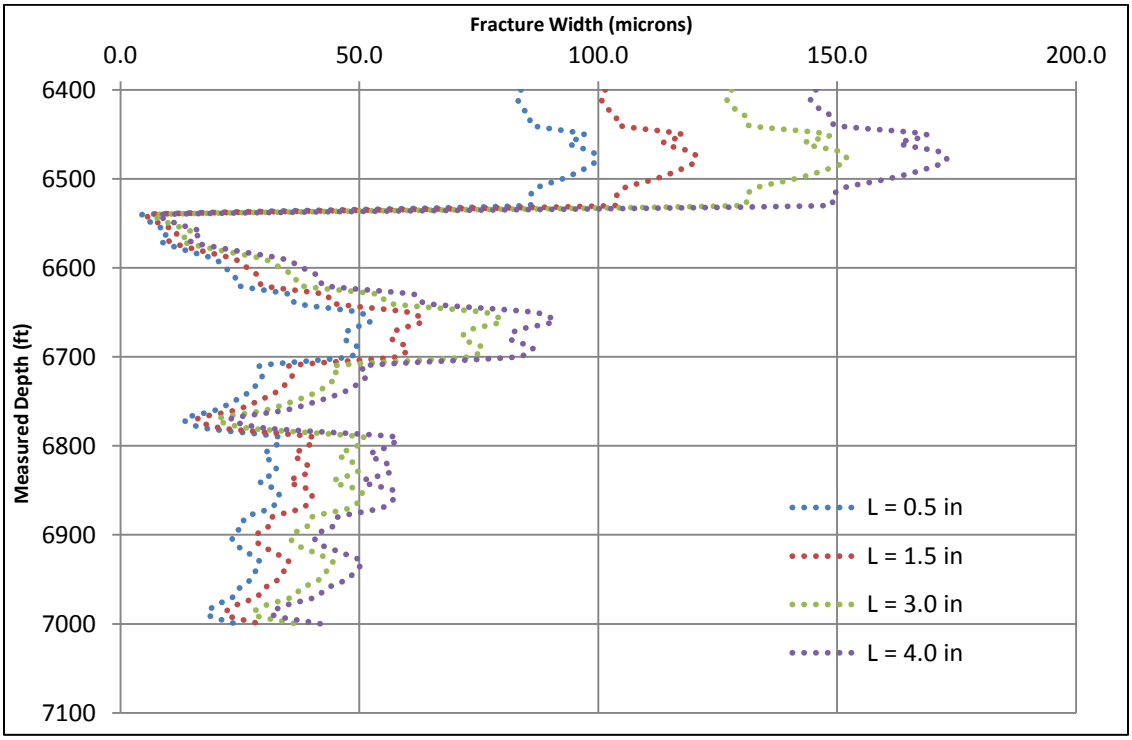

Fig. 57 – Resulting fracture widths for varying fracture lengths.

Fig. 57 shows the possible range of micro-fracture widths that will be generated under the given formation properties and operating conditions for varying fracture

lengths from the wellbore wall. A sharp contrast in fracture width exists around a depth of 6,550 ft due to a drastic change in the underlying pore pressure and formation stresses as shown in Fig. 54 at that depth. This fracture width analysis directly implies the desired particle size distribution to be used in the casing while drilling program to successfully achieve the plugging of micro-fractures at the wellbore wall. An absence of properly sized particles comprising of the drilled cuttings and the additional lost circulation materials will lead to an insufficient plugging at fracture mouths and result in an unsuccessful operation. Kumar *et al.* (2010) have studied the properties of the lost circulation materials in great detail and have summarized the existing models used to select appropriate particles based on size to effectively plug fractures or pore spaces. Their analysis coupled with this study will help in designing the most suitable particle size distribution to be used in a planned casing while drilling operation to effectively realize the benefits of the smear effect mechanism.

This study helps us to understand the contribution of plugging of micro-fractures due to high ECDs in improving the fracture gradient by the smear effect mechanism. A successful casing while drilling program should have a particular set of operating parameters for given formation properties, that ensure initiation of micro-fractures by ECDs while simultaneously having the appropriate particle size distribution of cuttings and additional materials to plug fracture mouths by casing and wellbore wall contact.

6.5 Effect of Casing Size & Length

The effect of casing diameter / hole size ratios has been studied qualitatively in literature by Karimi *et al.* (2011) and suggests that a high value of this ratio is desired to realize the benefits of the plastering effect. Larger casing sizes contribute to the smear

effect mechanism in two possible ways: resulting in higher ECDs due to smaller annular clearances and a smoother rotational contact between the casing string and wellbore wall leading to appropriate plugging of fracture mouths. Here, we study the influence of casing sizes on ECDs to design a casing size that helps successfully initiate micro-fractures considering that casing length is a constant. The variation of ECDs at the casing shoe depth of 6,400 ft for different casing sizes as well as progress of the drilling operation has been shown in Fig. 58.

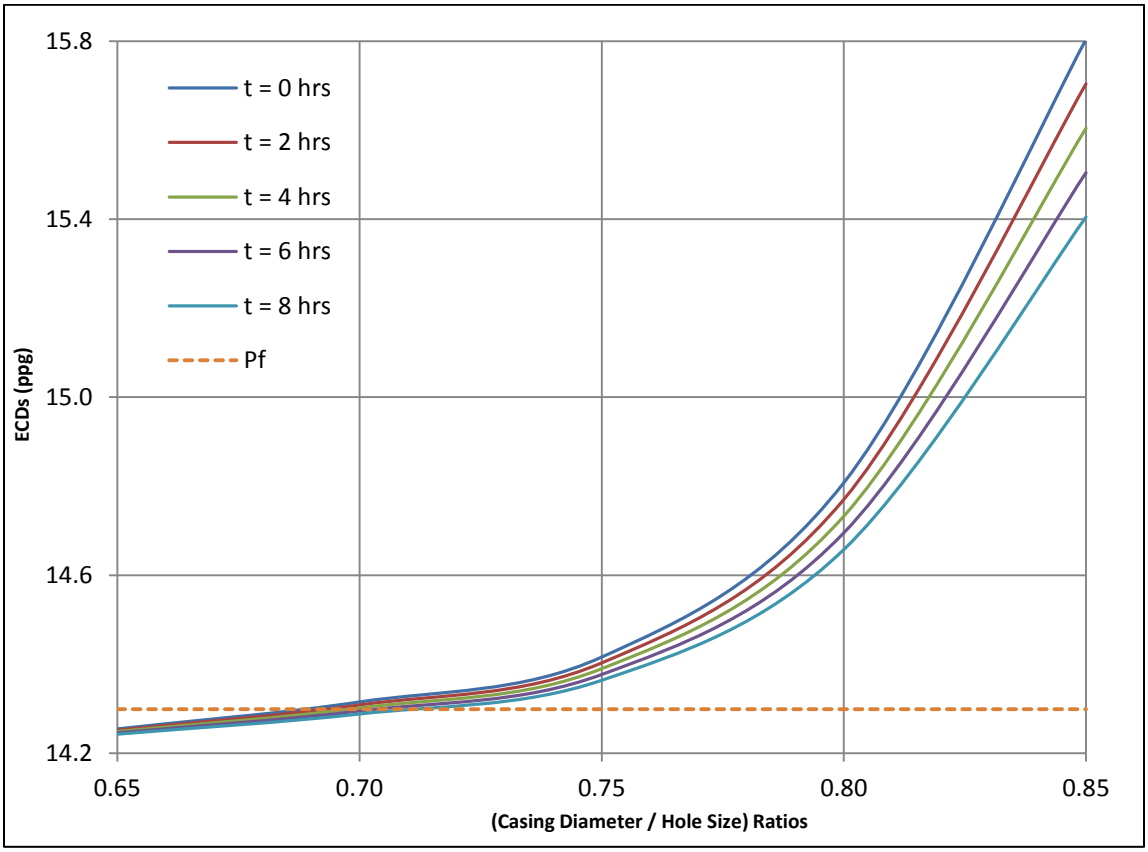

Fig. 58 – Effect of casing diameter / hole size ratios on ECDs with continued progress of drilling activity.

This plot shows that casing diameter / hole size ratios of 0.75 and beyond are very helpful in generating ECDs that are higher than the fracture initiation pressure P_f marked towards the bottom side of the graph. Ratios below 0.7 would not have resulted in any micro-fracture initiation due to ECDs. It would be desirable to plan a drilling program in

which ECDs are able to create and sustain a micro-fracture during the drilling operation. Very high ECDs for ratios beyond 0.85 would not be desirable as they may carry a risk of initiation and running away of micro-fractures even before they have had sufficient time to be plugged in due to very high pressures in the wellbore. This would lead to continued lost circulation and an uncontrolled fracture growth. The variation in ECDs with drilling time has also been shown to help us understand the subsequent changes in the drilling scenario in case an improvement in the fracture gradient has still not been realized after a few hours of casing while drilling operations.

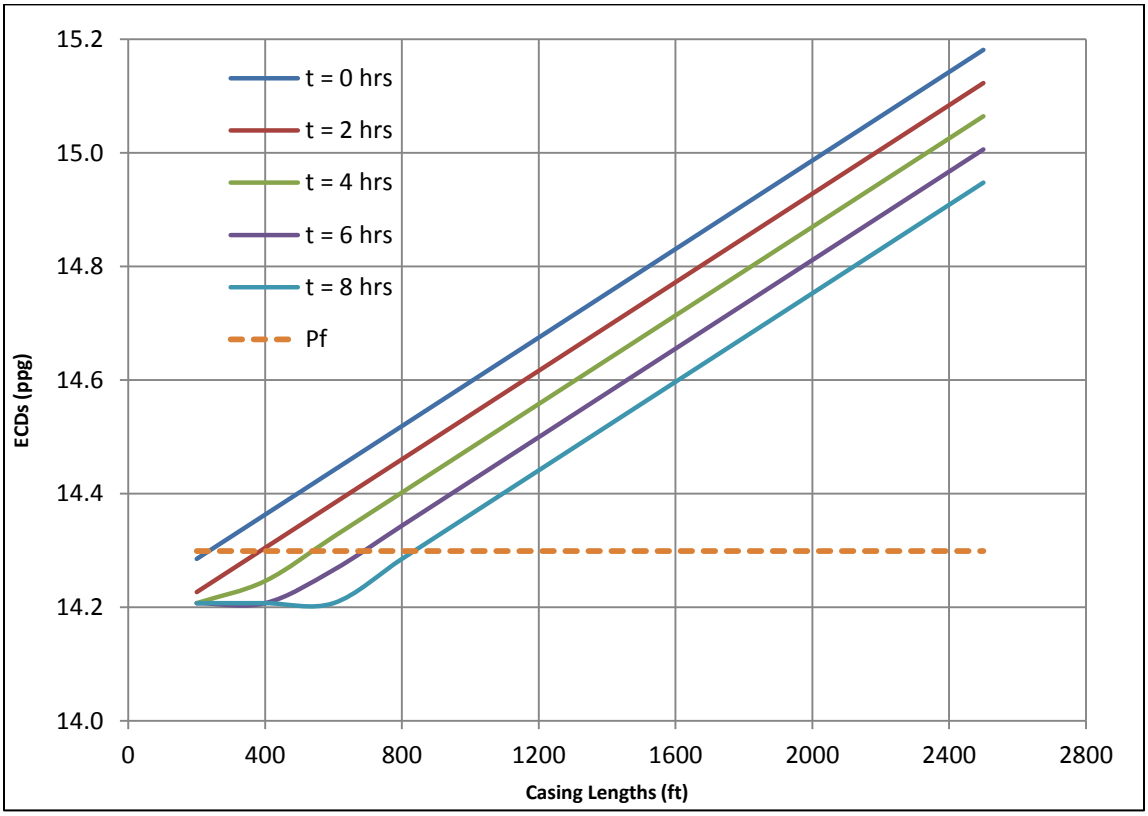

Fig. 59 – Variation of ECDs with casing lengths under continued progress of drilling activity.

Fig. 59 shows the variation of ECDs with different lengths of the casing string used to drill the wellbore at the depth of 6,400 ft (casing shoe). This plot shows that casing lengths of below 200 ft will not be able to generate any micro-fractures at that

depth. The variation with the duration of the drilling activity suggests that using 800 ft of casing would also not result in any micro-fractures after 8hrs of operation, if the desired improvement in the fracture gradient has yet not been attained. Fig. 58 and Fig. 59 also suggest that the increase in ECDs due to casing sizes is exponential while that due to the casing length is just linear and hence may not be lead to very high undesirable ECDs.

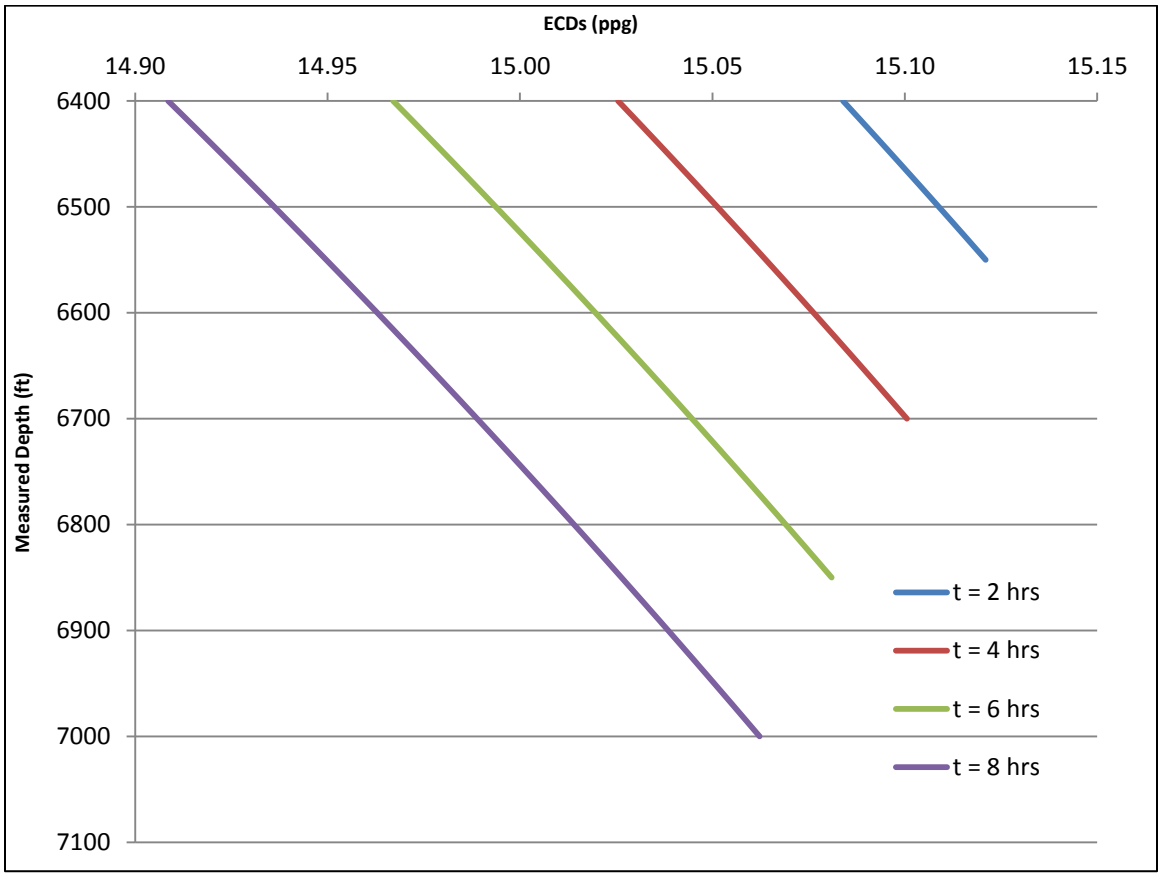

Fig. 60 – Variation of ECDs with depth under continued progress of drilling activity.

In addition, Fig. 60 shows the variation of ECDs with depth during the progress of the planned casing while drilling operation. The variation in micro-fracture widths and the resultant change in particle size distribution due to a change in ECDs can be easily evaluated using the models presented in the previous section. Higher ECDs would result in larger fracture widths and hence require larger sized particles to plug the generated micro-fractures.

6.6 Effect of Formation Properties

The formation properties like Young's modulus, Poisson's ratio and fracture toughness play a very significant role in designing an optimum casing while drilling program to effectively realize the benefits of the smear effect through plugging of micro-fractures. The Young's modulus of the formation plays an important role in determining the fracture geometry. Different formations having different Young's moduli will generate different widths for the micro-fractures even under the same underlying stress fields and operating conditions. Varying fracture widths will require their own appropriate particle size distribution designed for the casing while drilling program for the smear effect to be successful. Fig. 61 below shows the variation in fracture widths generated due to the variation of Young's modulus of the formation.

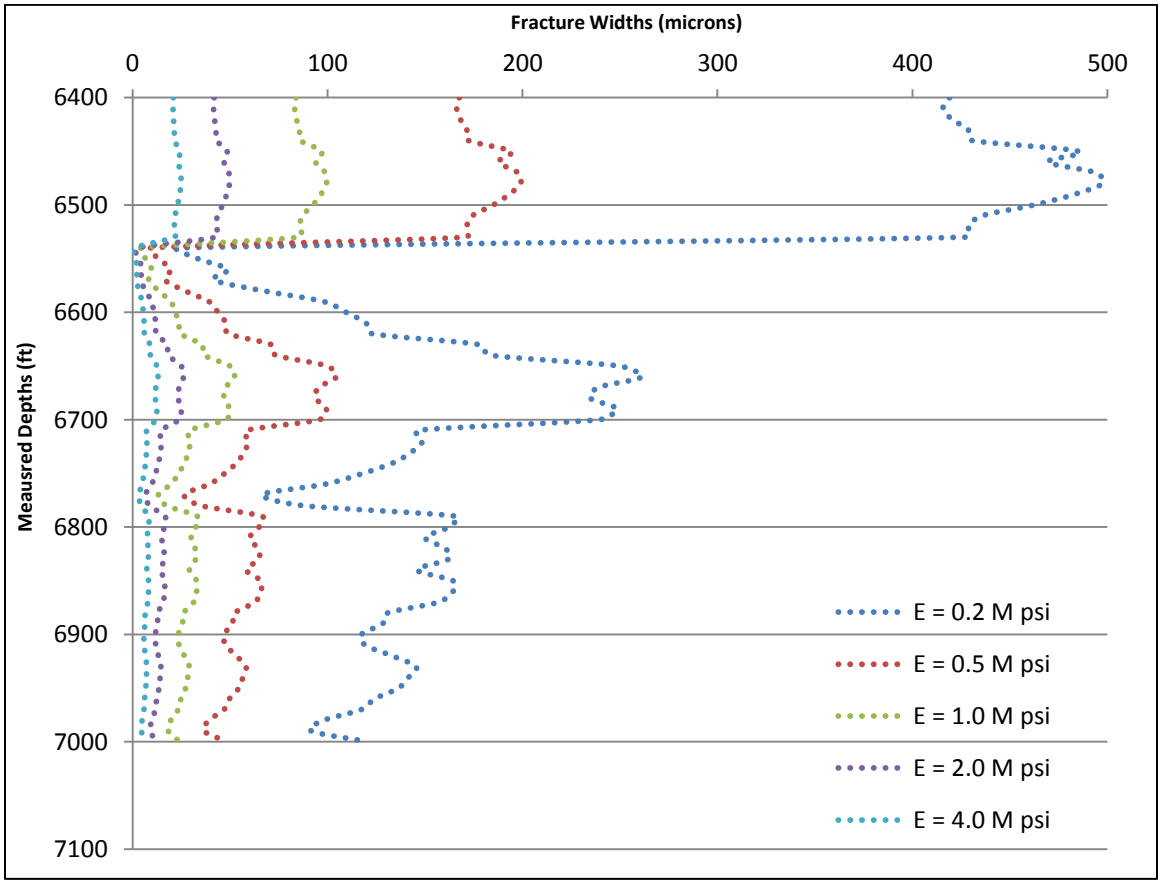

Fig. 61 – Variation of fracture widths with Young's modulus.

This plot shows that we need a wider range of particle sizes to plug fractures if the Young's modulus of the formation is low. However, as the Young's modulus increases, the variation in particle sizes decreases and becomes almost uniform for the entire fracture. Fig. 62 shows the variation in the improvement of the fracture gradient that may be obtained for varying fracture toughness of the formation. Higher fracture toughness would result larger increase in the fracture gradient upon the plugging of micro-fractures during the casing while drilling operation.

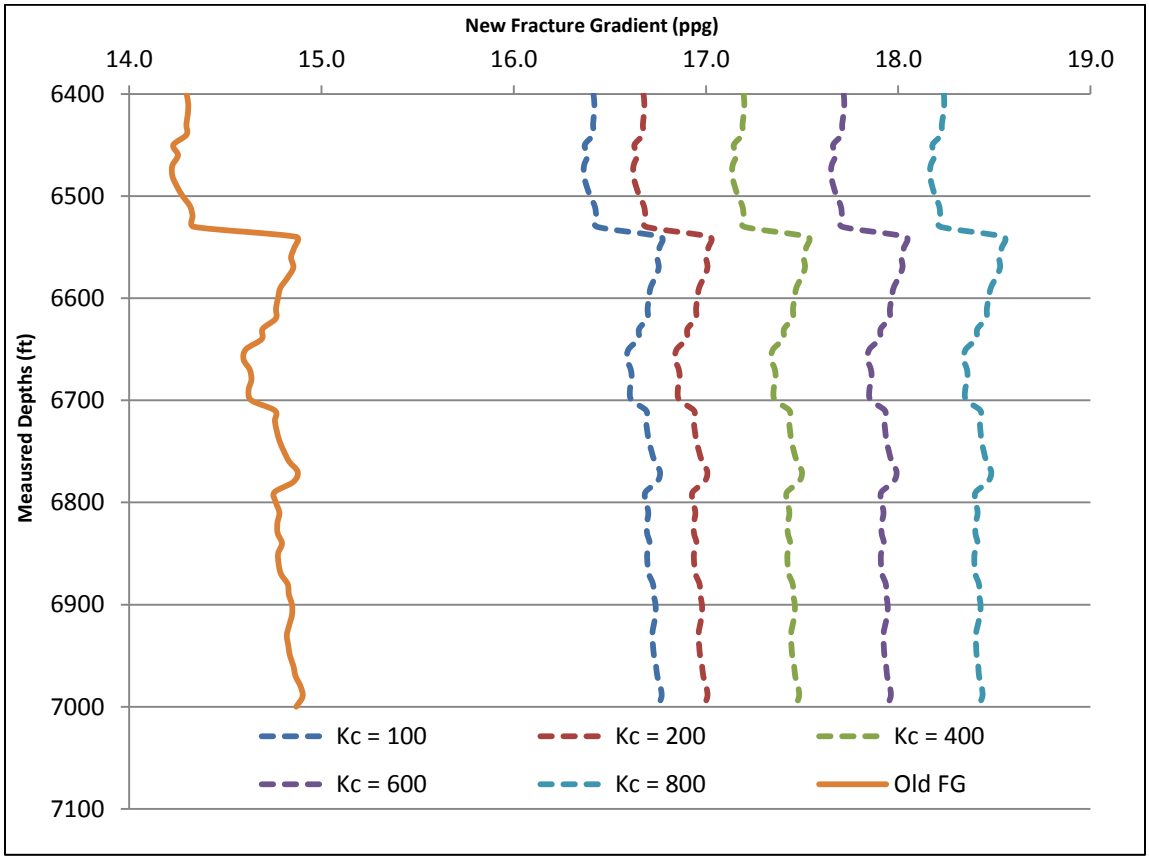

Fig. 62 – Variation of improvement in the fracture gradient with fracture toughness of the formation.

The Poisson's ratio of the formation affects the fracture initiation pressure as well as the fracture geometry of the created micro-fractures. The variation of fracture widths has been analyzed and it was found that the Poisson's ratio is not a very significant parameter governing the width distribution as compared to the Young's modulus. The

study to analyze the effect of Poisson's ratio on the fracture initiation pressure has been shown in Fig. 63 below. In this case as well, formations with lower values of Poisson's ratio show only a marginal increase in the fracture initiation pressure while higher Poisson's ratio have slightly lower pressures.

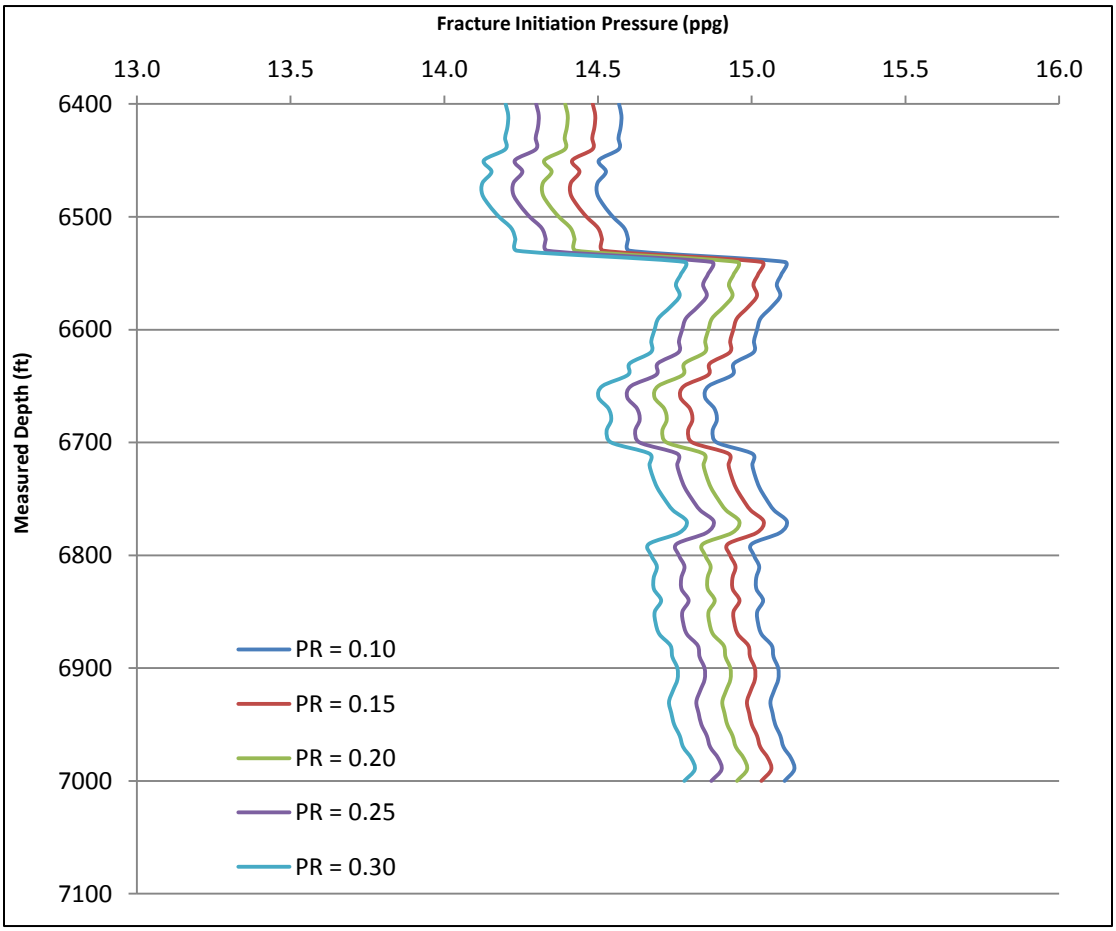

Fig. 63 – Variation of fracture initiation pressure with Poisson's ratios.

6.7 Effect of Operating Parameters

The operating parameters like mud flow rate and the mud weight of the drilling fluid also play a very significant role in the initiation of micro-fractures due to higher ECDs in casing while drilling operation. Fig. 64 below shows the variation of ECD at the casing shoe depth of 6,400 ft due to an increase in the mud flow rate. It shows that the pressure in the annulus increases significantly beyond a certain value of the flow rate.

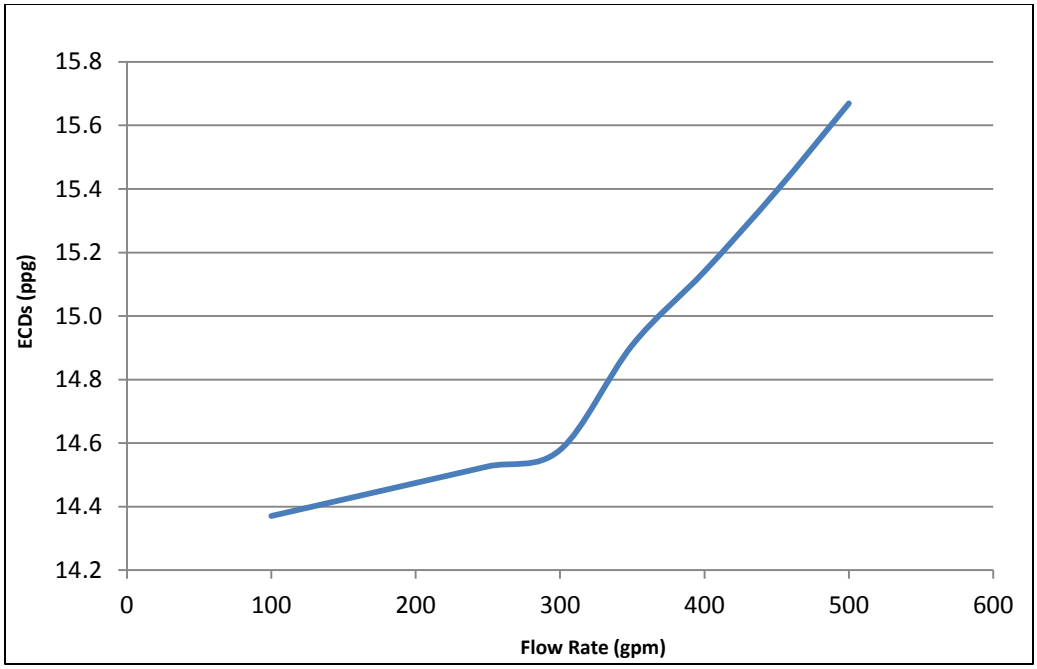

Fig. 64 – Variation of ECDs with flow rate at the casing shoe depth of 6,400 ft.

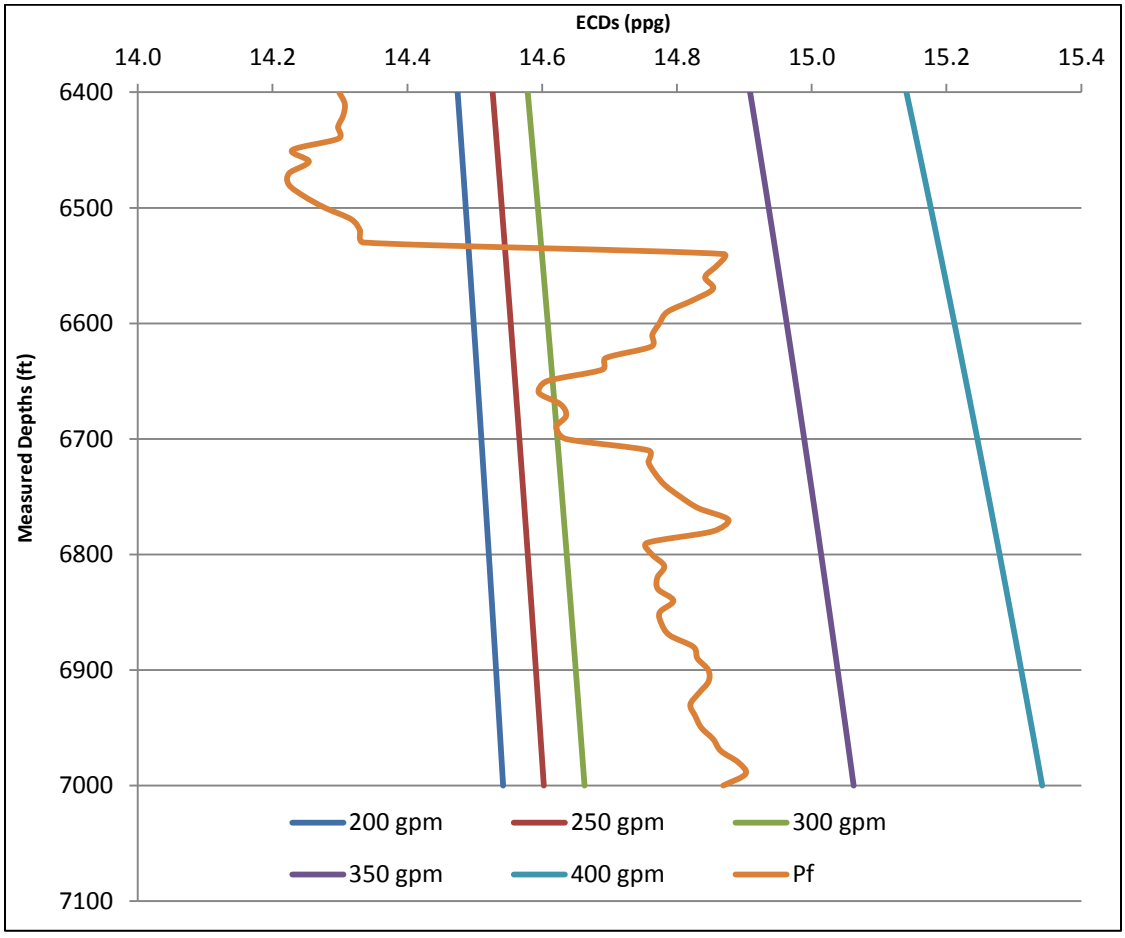

Fig. 65 – Variation of ECDs with flow rate along the entire open hole section.

Fig. 65 shows that lower flow rate values may not be sufficient enough to initiate micro-fractures at the borehole wall along the entire open hole section for the case under consideration. Hence, an optimum design for the flow rate of the drilling fluid is essential to take advantages of the smear effect mechanism.

The drilling fluid mud weight increases the ECDs linearly in the annulus of the casing string at any given depth. Fig. 66 below shows the variation of ECDs along the well with changing mud weights. It also shows the pore and fracture pressures. Lower mud weights result in insufficient pressures in the wellbore to initiate fractures. This plot helps us select the optimum mud weight so that it is successful in initiating micro-fractures to help improve the fracture by the smear effect mechanism.

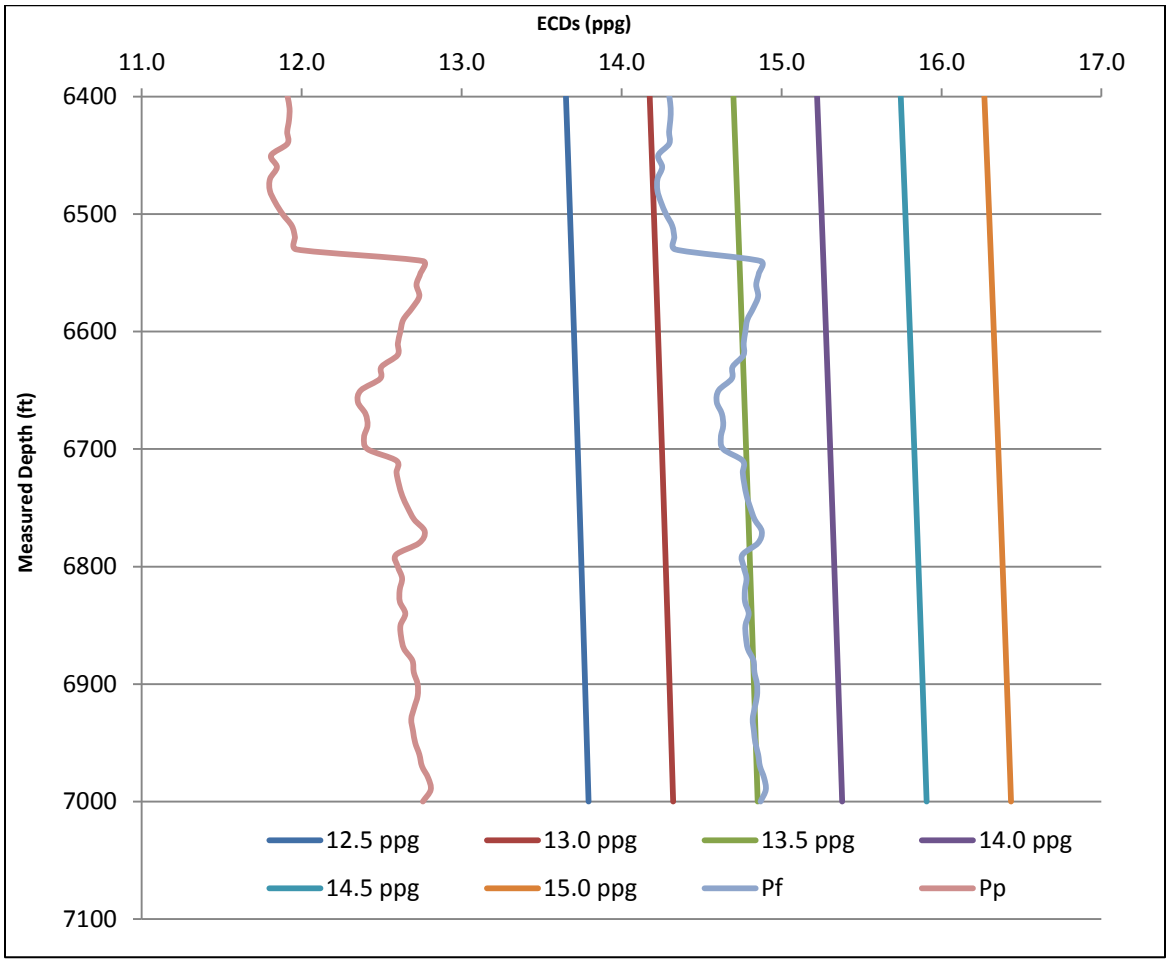

Fig. 66 – Variation of ECDs with mud weight along the entire open hole section.

Very high values of flow rate and mud weight are also not advisable during a casing while drilling operation as they might create pressures in the wellbore sufficient to break-open the fractures that had already been plugged before at the mouth by the cuttings and additional lost circulation materials. Very high pressures may also result in an uncontrolled fracture extension which if happens may cause significant losses of the drilling fluid and leads to losing control over the well.

In addition, flow rates and mud weight affect the widths of the micro-fractures being initiated resulting in wider fractures at higher pressures in the wellbore. They affect the particle size distribution essential for the success of a casing while drilling program and need to be carefully taken into consideration during the planning phase to effectively utilize the smear effect.

CHAPTER 7

CONCLUSIONS & RECOMMENDATIONS

7.1 Summary

- A mathematical model has been proposed to analyze the effect of pipe friction on downhole temperatures of the drilling fluid for deviated, horizontal and extended-reach wells.
- Heat generated from wellbore friction was quantified and incorporated in a steady-state heat transfer model to solve for the temperature profiles.
- The maximum temperatures downhole were estimated to be at a certain depth above the bottomhole in the annulus of the drill string.
- Drilling fluid properties like heat capacity, specific gravity, inlet temperatures as well as operating parameters like mud flow rate and rotational speed of the drill string were found to significantly affect fluid temperatures in the annulus.
- An increase in temperature of about 50°F has been estimated for the deviated well at the starting depth of drilling operations from Fig. 35.
- An increase in downhole temperatures of about 10°F has been estimated due to drill pipe and wall friction for the horizontal well from Fig. 39.
- An analytical model has then been proposed to estimate the heat generated downhole as a result of the continuous contact of the casing string with the wellbore wall in a casing while drilling operation.
- This heat loss has been incorporated in the heat transfer model presented earlier to understand the effect on increase in temperature of the drilling fluid.

- The effect of wellbore temperatures on the fracture gradient has then been presented to help understand its contribution to the smear effect mechanism.
- Improvement in wellbore strengthening achieved due to temperatures has been shown for incremental depths, duration of the drilling activity, varying mud flow rates and changing rotational speeds of the casing string.
- The smear effect mechanism was further investigated to understand the effect of initiation of micro-fractures due to high ECDs and their subsequent plugging by the casing and wellbore wall contact.
- An analytical model has been studied to determine the scenarios that result in initiation of micro-fractures at the wellbore wall and those respective fracture geometries have been predicted using existing models.
- A mathematical formulation has then been presented to estimate the increase in the fracture gradient due to the plugging of these generated micro-fractures at the fracture mouth.
- An analysis of casing size and length, formation properties and operational parameters has also been presented to help plan better future casing while drilling operations that aim to effectively realize the benefits of the smear effect.

7.2 Conclusions

- The wellbore and pipe friction as well as the heat transfer model will prove to be particularly useful for drilling of deviated, horizontal and extended-reach wells as it incorporates the effect of the increase in downhole temperatures owing to mechanical friction.

- An accurate estimation of the maximum temperatures of the drilling fluid encountered downhole during the planning phase of the drilling program will help us maintain a better control on fluid properties and undesired temperatures that may lead to tool failures.
- Wellbore temperatures resulted in only a marginal increase in the fracture gradient due to the smear effect in a casing while drilling operation.
- The effect of plugging of micro-fractures seems to be the plausible reason leading to an improvement in the fracture gradient of the formation due to the smear effect mechanism.

7.3 Future Work & Recommendations

- Numerical studies may be conducted to understand the effect of varying fluid properties on downhole temperatures during a complex drilling operation.
- Wellbore friction should be accounted for during the planning phase of the drilling operation as it plays an important role on downhole fluid temperatures.
- The effect of the other contributors like plugging of pore spaces and thin mud cake on improving the fracture gradient by the smear effect should be studied.
- A casing while drilling operation to realize the benefits of the smear effect should be planned aiming to successfully initiate micro-fractures due to ECDs and should focus on plugging those fractures using the most appropriate particle size distribution based on the fracture widths.
- A study to understand the phenomena of plugging of micro-fractures by drilled cuttings and lost circulation materials should also be conducted to improve the chances of success of the smear effect phenomenon.

REFERENCES

Aadnoy, B.S. and Belayneh, M. 2009, "A New Fracture Model That Includes Load History, Temperature, and Poisson's Effects," *SPE Drilling & Completion*, Vol. 24, No. 3, 452–455, September.

Aadnoy, B.S. and Djurhuus, J. 2008, "Theory and Application of New Generalized Model for Torque and Drag," Paper IADC/SPE 114684 presented at the IADC/SPE Asia Pacific Drilling Technology Conference and Exhibition, Jakarta, Indonesia, 25–27 August.

Addis, M.A., Cauley, M.B. and Kuyken, C. 2001, "Brent In-Fill Drilling Program: Lost Circulation Associated With Drilling Depleted Reservoirs," Paper SPE/IADC 67741 presented at SPE/IADC Drilling Conference, Amsterdam, The Netherlands, 27 February–1 March.

Alberty, M.W. and McLean, M.R. 2004, "A Physical Model for Stress Cage," Paper SPE 90493 presented at the SPE Annual Technical Conference and Exhibition, Houston, Texas, 26–29 September.

Azar, J.J. and Samuel, R. 2007, Drilling Engineering, Pennwell Publishers.

Barrett, S., Cassanelli, J.P., Manescu, G., Vasquez, G. and Growcock, F. 2010, "Wellbore Strengthening – Where Field Application Meets Theory," Paper SPE 139167 presented at the SPE Latin American and Caribbean Petroleum Engineering Conference, Lima, Peru, 1–3 December.

Diaz, H., Miska, S., Takach, N. and Yu, M. 2004, "Modeling of ECD in Casing Drilling Operations and Comparison with Experimental and Field Data," Paper IADC/SPE 87149 presented at the IADC/SPE Drilling Conference, Dallas, Texas, 2–4 March.

Gil, I., Roegiers, J.-C. and Moos, D. 2006, "Wellbore Cooling as a Means to Permanently Increase Fracture Gradient," Paper SPE 103256 presented at the SPE Annual Technical Conference and Exhibition, San Antonio, Texas, 24–27 September.

Gonzalez, M.E., Bloys, J.B., Lofton., J.E., Pepin, G.P., Schmidt, J.H., Naquin, C.J., Ellis, S.T. and Laursen, P.E. 2004, "Increasing Effective Fracture Gradients by Managing Wellbore Temperatures." Paper IADC/SPE 87217 presented at the IADC/SPE Drilling Conference, Dallas, Texas, 2–4 March.

Hettema, M.H.H., Bostrom, B. and Lund, T. 2004, "Analysis of Lost Circulation during Drilling in Cooled Formations," Paper SPE 90442 presented at the SPE Annual Technical Conference and Exhibition, Houston, Texas, 26–29 September.

Holmes, C.S. and Swift, S.C. 1970, "Calculation of Circulating Mud Temperatures," *Journal of Petroleum Technology*, Vol. 22, No.6, 670–674, June.

Iyoho, A.W., Rask, J.H., Wieseneck, J.B. and Grant, L.S. 2009, "Comprehensive Drilling Model Analyzes BHT Parameters," Paper SPE 124142 presented at the SPE Annual Technical Conference and Exhibition, New Orleans, Louisiana, 4–7 October.

Jansen, J.D. 1992, "Whirl and Chaotic Motion of Stabilized Drill Collars," *SPE Drilling Engineering*, Vol. 7, No.2, 107–114, June.

Johancsik, C.A., Friesen, D.B., and Dawson, R. 1984, "Torque and Drag in Directional Wells – Prediction and Measurement," *Journal of Petroleum Technology*, Vol. 36, No.6, 987–992, June.

Kabir, C.S., Hasan, A.R., Kouba, G.E. and Ameen, M.M. 1996, "Determining Circulating Fluid Temperature in Drilling, Workover, and Well-Control Operations," *SPE Drilling & Completions*, Vol. 11, No.2, 74–79, June.

Karimi, M., Petrie, S., Moellendick, E. and Holt, C. 2011, "A Review of Casing Drilling Advantages to Reduce Lost Circulation, Improve Wellbore Stability, Augment Wellbore Strengthening, and Mitigate Drilling-induced Formation Damage," Paper SPE/IADC 148564 presented at the SPE/IADC Middle East Drilling Technology Conference and Exhibition, Muscat, Oman, 24–26 October.

Karimi, M., Ghalambor, A., Montgomery, M. and Moellendick, E. 2011, "Formation Damage and Fluid Loss Reduction Due to Plastering Effect of Casing Drilling," Paper SPE 143656 presented at the SPE European Formation Damage Conference, Noordwijk, The Netherlands, 7–10 June.

Karimi, M., Moellendick, E. and Holt, C. 2011, "Plastering Effect of Casing Drilling; A Qualitative Analysis of Pipe Size Contribution," Paper SPE 147102 presented at the SPE Annual Technical Conference and Exhibition, Denver, Colorado, 30 October–2 November.

Kumar, A., Savari, S., Whitfill, D.L. and Jamison, D.E. 2010, "Wellbore Strengthening: The Less Studied Properties of Lost-Circulation Materials," Paper SPE 133484 presented at the SPE Annual Technical Conference and Exhibition, Florence, Italy, 19–22 September.

Loloi, M., Zaki, K.S., Zhai, Z. and Abou-Sayed, A. 2010, "Borehole Strengthening and Injector Plugging – The Common Geomechanics Thread," Paper SPE 128589 presented at the SPE North Africa Technical Conference and Exhibition, Cairo, Egypt, 14–17 February.

Marshall, D.W. and Bentsen, R.G. 1982, "A Computer Model to Determine the Temperature Distributions in a Wellbore," *Journal of Canadian Petroleum Technology,* Vol. 21, No. 1, 63–75, January–February.

Moellendick, E. and Karimi, M. 2011, "How Casing Drilling Improves Wellbore Stability," Paper AADE-11-NTCE-64 presented at the AADE National Technical Conference and Exhibition, Houston, Texas, 12–14 April.

Morita, N. and Fuh, G. 2011, "Parametric Analysis of Wellbore Strengthening Methods from Basic Rock mechanics," Paper SPE 145765 presented at the SPE Annual Technical Conference and Exhibition, Denver, Colorado, 30 October–2 November.

Oort, E., Friedheim, J., Pierce, T. and Lee, J. 2009, "Avoiding Losses in Depleted and Weak Zones by Constantly Strengthening Wellbores," Paper SPE 125093 presented at the SPE Annual Technical Conference and Exhibition, New Orleans, Louisiana, 4–7 October.

Radwan, A. and Karimi, M. 2011, "Feasibility Study of Casing Drilling Application in HPHT Environments; A Review of Challenges, Benefits and Limitations," Paper 148433 presented at the SPE/IADC Middle East Drilling Technology Conference and Exhibition, Muscat, Oman, 24–26 October.

Salehi, S. and Nygaard, R. 2011, "Evaluation of New Drilling Approach for Widening Operational Window: Implications for Wellbore Strengthening," Paper SPE 140753 presented at the SPE Production and Operations Symposium, Oklahoma City, Oklahoma, 27–29 March.

Samuel, R. 2007, Downhole Drilling Tools – Theory and Practice for Students and Engineers, Gulf Publishing.

Schoeppel, R.J. and Bennett, R.E. 1971, "Numerical Simulation of Borehole and Formation Temperature Distributions While Drilling to Total Depth," Paper SPE

3364 presented at the 46th Annual Fall Meeting of the Society of Petroleum Engineers of AIME, New Orleans, Louisiana, 3–6 October.

Stroud, D.R.H., Lines, L.A. and Minett-Smith, D.J. 2011, "Analytical and Experimental Backward Whirl Simulations for Rotary Steerable Bottom Hole Assemblies," Paper SPE/IADC 140011 presented at the SPE/IADC Drilling Conference and Exhibition, Amsterdam, The Netherlands, 1–3 March.

Tang, L. and Luo, P. 1998, "The Effect of Thermal Stress on Wellbore Stability," Paper SPE 39505 presented at the SPE India Oil and Gas Conference and Exhibition, New Delhi, India, 17–19 February.

Vandiver, J.K., Nicholson, J.W. and Shyu, R. 1990, "Case Studies of the Bending Vibration and Whirling Motion of Drill Collars," *SPE Drilling Engineering*, Vol. 5, No. 4, 282–290, December.

Wang, H., Towler, B.F. and Soliman, M.Y. 2007, "Near Wellbore Stress Analysis and Wellbore Strengthening for Drilling Depleted Formations," Paper SPE 102719 presented at the SPE Rocky Mountain Oil & Gas Technology Symposium, Denver, Colorado, 16–18 April.

Watts, R.D., Greener, M.R., McKeever, S., Scott, P.D. and Beardmore, D. 2010, "Particle Size Distribution Improves Casing-While-Drilling Wellbore Strengthening Results," Paper IADC/SPE 128913 presented at the IADC/SPE Drilling Conference and Exhibition, New Orleans, Louisiana, 2–4 February.

Whitfill, D. 2008, "Lost Circulation Material Selection, Particle Size Distribution and Fracture Modeling with Fracture Simulation Software," Paper IADC/SPE 115039 presented at the IADC/SPE Asia Pacific Drilling Technology Conference and Exhibition, Jakarta, Indonesia, 25–27 August.

APPENDIX A

A-1

Reynolds number for Bingham Plastic drilling fluid to estimate turbulence criteria:

In Drill Pipe – $$N_{Re} = \frac{928\rho v_p(2r_i)}{\mu_p}, \quad \text{(A-1)}$$

In Annulus – $$N_{Re} = \frac{757\rho v_a(2r_w - 2r_o)}{\mu_p}. \quad \text{(A-2)}$$

Frictional pressure losses for Bingham Plastic drilling fluid in Laminar Flow:

In Drill Pipe – $$\left(\frac{dp_{fric}}{dz}\right) = \frac{\mu_p v_p}{1500(2r_i)^2} + \frac{\tau_y}{225(2r_i)}\left(\frac{psi}{ft}\right), \quad \text{(A-3)}$$

$$v_p = \frac{q}{2.448(2r_i)^2}\ ft/sec, \quad \text{(A-4)}$$

In Annulus – $$\left(\frac{dp_{fric}}{dz}\right) = \frac{\mu_p v_a}{1000(2r_w - 2r_o)^2} + \frac{\tau_y}{200(2r_w - 2r_o)}\left(\frac{psi}{ft}\right), \quad \text{(A-5)}$$

$$v_a = \frac{q}{2.448(2r_w - 2r_o)^2}\ ft/sec, \quad \text{(A-6)}$$

where μ_p is the plastic viscosity and τ_y is the yield stress.

Frictional pressure losses for Bingham Plastic drilling fluid in Turbulent Flow:

In Drill Pipe – $$\left(\frac{dp_{fric}}{dz}\right) = \frac{\rho^{0.75} {v_p}^{1.75} \mu_p^{0.25}}{1800\ (2r_i)^{1.25}}\left(\frac{psi}{ft}\right), \quad \text{(A-7)}$$

In Annulus – $$\left(\frac{dp_{fric}}{dz}\right) = \frac{\rho^{0.75} {v_a}^{1.75} \mu_p^{0.25}}{1396\ (2r_w - 2r_o)^{1.25}}\left(\frac{psi}{ft}\right), \quad \text{(A-8)}$$

Bit Pressure Drop – $$p_b = \frac{8.311\times10^{-5}\rho q^2}{C_d^2 A_n^2}\ (psi), \quad \text{(A-9)}$$

where C_d is the nozzle discharge coefficient and A_n is the total nozzle area.

A-2

Hubert and Willis' estimation of horizontal stresses:

$$\sigma_{11} = \frac{1}{3}(\sigma_{ob} - p_o), \quad \text{(A-10)}$$

$$\sigma_{22} = \frac{1}{2}(\sigma_{ob} - p_o), \quad \text{(A-11)}$$

where σ_{ob} is the effective overburden stress.

APPENDIX B

B-1

Bingham Plastic Mud		Rpm	100
Mud Specific Gravity	1.7	Drill Collar OD (in.)	6
Fan VG Reading at 600	55	Drill Collar ID (in.)	3.5
Fan VG reading at 300	35	Drill Collar Length (ft)	400
Minimum Annular Velocity (ft/min)	100	Drill Collar Wt. (lb/ft)	100.8
Plastic Viscosity (cp)	20	Nozzle size	13-13-13
Yield stress (lb/100 ft^2)	15	Cd	0.95
Inlet temperature at drill pipe (K)	300	KOD (ft)	5000
Co-efficient of friction in open hole	0.3	Length tangent section (ft)	10000
Surface temperature (°C)	15.3	Length radius section (ft)	2000
Geothermal gradient (°C/m)	0.0173	Angle of inclination (°)	80
Open hole (in.)	7.875	Heat capacity pipe/collar (J/kg.K)	400
Drill pipe OD (in.)	4.25	Heat capacity drilling fluid (J/kg.K)	1600
Drill pipe ID (in.)	3.5	Therm. cond. pipe/collar (W/m.K)	43.75
Drill pipe Wt. (lb/ft)	40	Therm. cond. drilling fluid (W/m/.K)	1.75

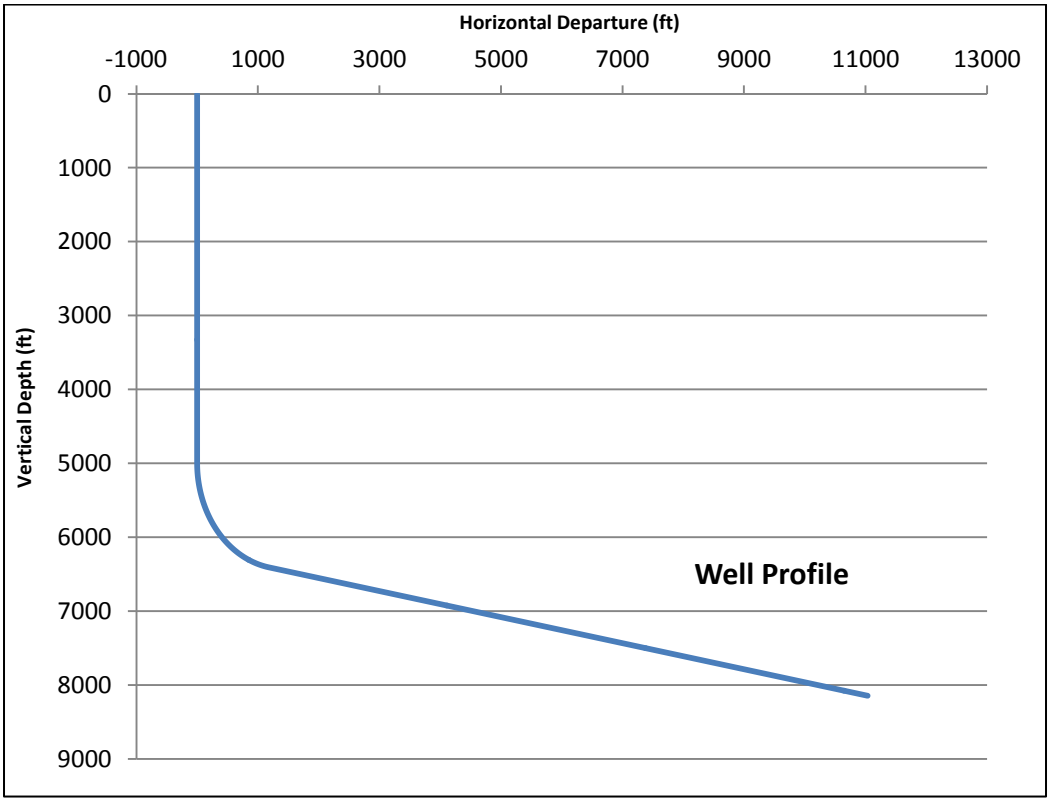

Fig. 67 – Well profile for Appendix B-1.

B-2

Bingham Plastic Mud		Surface temperature (°C)	15
Mud Specific Gravity	1.2	Geothermal gradient (°C/m)	0.025
Fan VG Reading at 600	55	Open hole (in.)	8.5
Fan VG reading at 300	35	Drill pipe OD (in.)	5
Plastic Viscosity (cp)	20	Drill pipe ID (in.)	3
Yield stress (lb/100 ft^2)	15	Drill pipe Wt. (lb/ft)	40
Inlet temperature at drill pipe (K)	300	Drill Collar OD (in.)	6.5
Co-efficient of friction in open hole	0.35	Drill Collar ID (in.)	2.81

Drill Collar Length (ft)	520	Cd	0.95
Drill Collar Wt. (lb/ft)	100.8	Heat capacity pipe/collar (J/kg.K)	400
Bit TFA (sq. in.)	1.2	Therm. cond. pipe/collar (W/m.K)	43.7

B-3

Bingham Plastic Mud		Drill pipe OD (in.)	5
Mud Specific Gravity	1.68	Drill pipe ID (in.)	3
Fan VG Reading at 600	55	Drill pipe Wt. (lb/ft)	40
Fan VG reading at 300	35	Drill Collar OD (in.)	6.5
Plastic Viscosity (cp)	20	Drill Collar ID (in.)	2.81
Yield stress (lb/100 ft^2)	15	Drill Collar Length (ft)	520
Inlet temperature at drill pipe (K)	295	Drill Collar Wt. (lb/ft)	100.8
Co-efficient of friction in open hole	0.3	Bit TFA (sq. in.)	1.2
Surface temperature (°C)	15	Cd	0.95
Geothermal gradient (°C/m)	0.02	Heat capacity pipe/collar (J/kg.K)	400
Open hole (in.)	8.5	Therm. cond. pipe/collar (W/m.K)	43.75

B-4

Bingham Plastic Mud		Casing String Length (ft)	750
Mud Density (ppg)	10	Casing String Wt. (lb/ft)	26
Fan VG Reading at 600	55	Casing String ID (in.)	6.276
Fan VG reading at 300	35	BHA OD (in.)	6.0
Plastic Viscosity (cp)	20	BHA ID (in.)	5.0
Yield stress (lb/100 ft^2)	15	BHA Length (ft)	70
Inlet temperature at drill pipe (K)	290	BHA Wt. (lb/ft)	30
Therm. cond. of mud (W/m.K)	1.75	Bit TFA (sq. in.)	1.2
Co-efficient of friction in open hole	0.3	Cd	0.95
Surface temperature (°C)	20	Geothermal gradient (°C/m)	0.025
Open hole (in.)	8.75	Heat capacity of mud (J/kg.K)	1200
Drill pipe OD (in.)	5.0	Heat capacity pipe/casing (J/kg.K)	400
Drill pipe ID (in.)	4.0	Therm. cond. pipe/casing (W/m.K)	43.75
Drill pipe Wt. (lb/ft)	25.6	Flow Rate (gpm)	250
Casing String OD (in.)	7.0	RPM	75.0

B-5

Bingham Plastic Mud		Drill pipe OD (in.)	5.0
Mud Density (ppg)	12	Drill pipe ID (in.)	4.0
Fan VG Reading at 600	55	Drill pipe Wt. (lb/ft)	25.6
Fan VG reading at 300	35	Casing String OD (in.)	7.625
Plastic Viscosity (cp)	20	Casing String ID (in.)	6.375
Yield stress (lb/100 ft^2)	15	Casing String Length (ft)	840
Inlet temperature at drill pipe (K)	300	Casing String Wt. (lb/ft)	47.1
Therm. cond. of mud (W/m.K)	1.75	Bit TFA (sq. in.)	1.2
Heat capacity of mud (J/kg.K)	1200	Cd	0.95
Co-efficient of friction in open hole	0.3	Heat capacity pipe/casing (J/kg.K)	400
Surface temperature (°C)	20	Therm. cond. pipe/casing (W/m.K)	43.75
Geothermal gradient (°C/m)	0.025	Flow Rate (gpm)	200
Open hole (in.)	8.875	RPM	90.0

B-6

Bingham Plastic Mud		Inlet temperature at drill pipe (K)	285
Mud Density (ppg)	10	Therm. cond. of mud (W/m.K)	1.75
Fan VG Reading at 600	55	Heat capacity of mud (J/kg.K)	1200
Fan VG reading at 300	35	Co-efficient of friction in open hole	0.3
Plastic Viscosity (cp)	20	Surface temperature (°C)	25
Yield stress (lb/100 ft^2)	15	Geothermal gradient (°C/m)	0.025

Open hole (in.)	8.75	Casing String Wt. (lb/ft)	29
KOD (ft)	1775	BHA OD (in.)	6.0
Build length (ft)	1200	BHA ID (in.)	5.0
Initial Length of Tangent Section (ft)	700	BHA Length (ft)	70
Total build angle (deg.)	67	BHA Wt. (lb/ft)	30
Drill pipe OD (in.)	5.0	Bit TFA (sq. in.)	1.2
Drill pipe ID (in.)	4.0	Cd	0.95
Drill pipe Wt. (lb/ft)	25.6	Heat capacity pipe/casing (J/kg.K)	400
Casing String OD (in.)	7.0	Therm. cond. pipe/casing (W/m.K)	43.75
Casing String ID (in.)	6.184	Flow Rate (gpm)	400
Casing String Length (ft)	610	RPM	60.0

B-7

Bingham Plastic Mud		Initial Length of Tangent Section (ft)	700
Mud Density (ppg)	12	Total build angle (deg.)	45.0
Fan VG Reading at 600	55	Drill pipe OD (in.)	5.0
Fan VG reading at 300	35	Drill pipe ID (in.)	4.0
Plastic Viscosity (cp)	20	Drill pipe Wt. (lb/ft)	25.6
Yield stress (lb/100 ft^2)	15	Casing String OD (in.)	7.625
Inlet temperature at drill pipe (K)	295	Casing String ID (in.)	6.625
Therm. cond. of mud (W/m.K)	1.75	Casing String Length (ft)	690
Heat capacity of mud (J/kg.K)	4200	Casing String Wt. (lb/ft)	39
Co-efficient of friction in open hole	0.3	Bit TFA (sq. in.)	1.2
Surface temperature (°C)	15	Cd	0.95
Geothermal gradient (°C/m)	0.02	Heat capacity pipe/casing (J/kg.K)	400
Open hole (in.)	8.5	Therm. cond. pipe/casing (W/m.K)	43.75
KOD (ft)	8050	Flow Rate (gpm)	225
Build length (ft)	1500	RPM	65.0

B-8

Elastic Mod. for Sandstone (GPa)	15	TVD (ft)	9185
Coeff. of Thermal Expan. (/°C)	0.000005	Poisson's Ratio	0.25

B-9

Bingham Plastic Mud		Casing String OD (in.)	7.625
Mud Density (ppg)	10	Casing String ID (in.)	6.375
Fan VG Reading at 600	55	Casing String Length (ft)	2400
Fan VG reading at 300	35	Casing String Wt. (lb/ft)	47.1
Plastic Viscosity (cp)	20	Bit TFA (sq. in.)	1.2
Yield stress (lb/100 ft^2)	15	Cd	0.95
Inlet temperature at drill pipe (K)	300	Heat capacity pipe/casing (J/kg.K)	400
Therm. cond. of mud (W/m.K)	1.75	Therm. cond. pipe/casing (W/m.K)	43.75
Heat capacity of mud (J/kg.K)	1200	Flow Rate (gpm)	350
Co-efficient of friction in open hole	0.3	RPM	90.0
Surface temperature (°C)	30	Elastic Mod. for Sandstone (GPa)	15
Geothermal gradient (°C/m)	0.025	Coeff. of Thermal Expan. (/°C)	0.000005
Open hole (in.)	8.875	Poisson's Ratio	0.25
Drill pipe OD (in.)	5.0	ROP (ft/hr)	75
Drill pipe ID (in.)	4.0	Length of Stand (ft)	90
Drill pipe Wt. (lb/ft)	25.6	Number of Stands Drilled	25

B-10

Bingham Plastic Mud		Plastic Viscosity (cp)	20
Mud Density (ppg)	13.7	Yield stress (lb/100 ft^2)	15
Fan VG Reading at 600	55	Flow Rate (gpm)	350
Fan VG reading at 300	35	Open hole (in.)	8.5

Drill pipe OD (in.)	5.0	Rate of penetration (ft/hr)	75.0
Drill pipe ID (in.)	4.0	Overburden Gradient (psi/ft)	1.0
Casing String OD (in.)	7.0	Pore Pressure Gradient (psi/ft)	0.465
Casing String ID (in.)	6.276	Poisson's Ratio	0.25
Casing String Length (ft)	2400	Biot's Constant	0.7
Casing diameter / Hole size	0.82	Tensile Strength (psi)	0
Cased Depth (ft)	6400	Young's Modulus (M psi)	1.0
Open Hole Section (ft)	600	Fracture Toughness (psi√in)	200
Drilled Depth (ft)	7000	Kick Margin (ppg)	0.5
Length of Micro-fractures (in.)	0.5	Trip Margin (ppg)	0.5